Petrology of the micaceous Koidu and Tongo - Tonguma kimberlites, Man Craton, Sierra Leone

By: Anton Viljoen

VLJANT002

A dissertation submitted for the fulfilment of the degree of

Master of Science

Department of Geological Sciences

University of Cape Town

South Africa

Supervisor: Dr. Geoffrey H. Howarth

January 2022

Plagiarism declaration

I, ANTON VILJOEN, hereby declare that the work presented herein is my own. I know that plagiarism is wrong. Plagiarism is to use another's work and claiming it as one's own.

I have used the Harvard convention for citation and referencing. Each contribution to this thesis, from the works of other people has been attributed, and cited and has been referenced. This thesis is my own work.

Signed by candidate

Date: 01/01/2022

Acknowledgements

I would like to thank NRF-CIMERA for the research funding. Without this organization, I would not of had the opportunity to complete this research. I would subsequently like to thank my supervisor, Geoffrey Howarth for his support, expertise, constructive criticism, and guidance throughout the research process. I would also like to thank Dr. Christian Reinke for his assistance and guidance while using the electron microprobe at the University of Johannesburg.

For all references to the supplementary online material (SOM) refer to the following link: https://drive.google.com/drive/folders/1WsNgMQN1Ir6upNHSV7tFXT4YC9CYYacH?usp=sharing

Abstract

Sierra Leone contains two Jurassic-aged diamondiferous volcanic clusters, namely Koidu and Tongo-Tonguma (hereafter referred to as Tongo), consisting of eruptive pipes at Koidu and NE-SW trending dikes at both Koidu and Tongo. Petrographically, the diamondiferous rocks from both clusters have features of both micaceous kimberlites and unevolved Kaapvaal lamproite, making classification ambiguous. To successfully classify and constrain the petrogenesis of these rocks, a combination of detailed petrography, and phlogopite, spinel and olivine chemistry is used in this study.

The Koidu rocks are predominantly macrocrystic in texture, whereas the Tongo rocks can broadly be separated into macrocrystic and aphanitic varieties. Olivine is present as macrocrysts and microcrysts, while phlogopite is occasionally present as macrocrysts and abundantly present as groundmass microcrysts (33 vol.% average). Other groundmass minerals include spinel, perovskite, apatite, and calcite set in a base of serpentine possibly containing secondary carbonate. These characteristic features can be present in both micaceous kimberlites and unevolved Kaapvaal lamproites, making classification based on petrography ambiguous.

Phlogopite and spinel have similar compositional trends for both Koidu and Tongo, comparable to trends observed for archetypal kimberlites rather than lamproites. This in combination with previously studied trace element geochemistry and isotopic compositions from rocks within the Tongo cluster, indicate characteristics of an archetypal kimberlite. The overall phlogopite abundances further indicate that these rocks are micaceous kimberlites.

Olivine core compositions are divided into Mg-rich (Fo >89) and Fe-rich (Fo <89) endmembers, with Koidu and Tongo cores being dominantly Mg-rich with fewer Fe-rich cores. The overall olivine core compositions range between Fo 84.7 to 94.5 for Koidu and between 83.2 to 94.6 for Tongo. The Mg-rich olivine cores often contain intensely resorbed margins and no groundmass inclusions, consistent with a xenocrystic origin, whereas the Fe-rich population have resorbed margins to a lesser extent and are interpreted to be derived from a Cr-poor megacryst suite. Olivine rim compositions have Fo contents which are relatively homogenous, with compositional overlaps observed between Tongo and Koidu. Olivine rims often contain mineral inclusions of groundmass spinels and are interpreted as having crystallized from a magma.

Previous models have suggested that olivine chemistry and groundmass mineralogy in world-wide diamondiferous rocks can be used to constrain their origin and evolution. However, the Koidu-Tongo rocks are the first example where multiple kimberlite clusters do not align with these models. The Koidu-Tongo rocks are highly micaceous and contain Mg-rich olivine core-rim compositions and correspond with Kaapvaal lamproites and so an alternative model has been suggested where the rocks are likely derived from the asthenosphere, like a typical kimberlite, but assimilated phlogopite-rich material in the SCLM.

Contents

List of figures

List of tables

Chapter 1: Introduction

1.1. Opening remarks

After the discovery of diamondiferous kimberlites in South Africa at the end of the nineteenth century, Percy Wagner published two influential studies (Wagner, 1928, 1914), wherein two distinctive types of kimberlites were identified. These two types were known as "basaltic" and "micaceous" kimberlites and were classified based primarily on macroscopic observations. Smith (1983) later identified distinct geochemical differences between these "basaltic" and "micaceous" kimberlites and the terms Group I and Group II were given to the respective kimberlites. Numerous studies (Dawson, 1987; Fraser, 1987; Fraser et al., 1985; Fraser and Hawkesworth, 1992; Mitchell, 1994; Mitchell and Meyer, 1989; Skinner, 1989; Skinner et al., 1994; Tainton and Browning, 1991; Tainton and McKenzie, 1994; Tainton, 1992) revealed that Group I and Group II kimberlites were mineralogically and geochemically distinct from each other and that Group II kimberlites were more similar to lamproites. This further led Mitchell (1995) to suggest the revival of the term "orangeite", first introduced by Wagner (1928), as a reclassification of Group II kimberlites.

Kimberlites are thought to be derived from a common asthenospheric reservoir worldwide and share trace element and isotope characterisitics whereas the major elements are controlled by melt-SCLM interactions (Giuliani et al., 2020). In contrast, lamproites and orangeites are generally believed to originate from melting in the SCLM (Giuliani et al., 2015; Mitchell, 1995). However, now it is becoming apparent that some lamproites, i.e., in India are derived from the kimberlite source but assimilate highly metasomatised SCLM material and turn into lamproites (Shaikh et al., 2016).

The Man craton is host to kimberlites that are highly micaceous and appear mineralogically similar to lamproites (Skinner et al., 2004; Taylor et al., 1994). They occur as several Jurassic-aged clusters located in Sierra Leone, Liberia and Guinea and an additional Neoproterozoic age cluster (Weasua) in Liberia (Andrews-Jones, 1968; Haggerty, 1982; Skinner et al., 2004). These kimberlites share petrographic characteristics with orangeites, including abundant phlogopite and the presence of tetraferriphlogopite, while having bulk rock geochemical characteristics comparable to archetypal kimberlites (e.g., Mathafeng, 2021; Skinner et al., 2004; Taylor et al., 1994; Tompkins and Haggerty, 1984). A recent study by Howarth and Giuliani (2020) on the kimberlites from the Tongo cluster (Sierra Leone) and the lamproites of the Weasua cluster (Liberia) has revealed similar conclusions. The rocks from Tongo were classified as micaceous kimberlites due the high phlogopite abundances and having unusual phlogopite compositions with concurrent increases in Al_2O_3 and FeO or decreasing Al_2O_3 with increasing Fe_2O_3

(tetraferriphlogopite). The rocks from Weasua were classified as lamproites due to the presence of primary diopside and phlogopite compositional trends similar to lamproites and orangeites. However, olivine core chemistry from both locations reveal a similar petrogenetic history. Thus, these diamondiferous rocks are not easily classified as simply archetypal kimberlite or orangeite/ lamproite. Further, there is a growing body of evidence showing that kimberlites and lamproites occur together in cratonic regions and can even be derived from the same source but with different assimilation histories in the SCLM (Howarth and Giuliani, 2020; Shaikh et al., 2019, 2016).

1.2. Aim and scope

This study investigates the diamondiferous Jurassic-aged phlogopite-rich rocks of the Koidu and Tongo-Tonguma clusters from Sierra Leone. These rocks contain elevated phlogopite abundances compared to previously studied archetypal kimberlites and even compared to other phlogopite-rich kimberlites from worldwide occurrences. Further, these rocks share mineralogical characteristics that align with previously studied orangeites and so delineating a petrogenesis for these rocks would assist in understanding the nature of these rock types. The motivation behind the current work is to put these rocks into context with similar rocks worldwide, determine a classification and delineate a petrogenetic history. In particular, to test the hypothesis that SCLM assimilation, constrained by olivine chemistry and phlogopite abundance, controls the major element composition of the kimberlite melt erupting at the surface. The primary goals of the current study are to: 1) Use detailed petrographic observation in conjunction with phlogopite and spinel chemistry to classify and contrast both Koidu and Tongo clusters with worldwide kimberlite and lamproite data; 2) Determine the origin of the ubiquitous zoned olivine grains derived from Koidu and Tongo by contrasting olivine zone compositions between the two clusters and with worldwide kimberlite and lamproite data; and 3) Testing of the hypothesis of olivine rim vs. phlogopite abundance to track melt-SCLM interactions.

1.3. Significance

Kimberlites, orangeites and lamproites are the primary hosts to diamonds and so understanding these deposits has economic significance to the diamond industry. Further, during the previous decades of studying these rock types, the nomenclature and classification of these rocks have frequently been incorrectly applied, often evolving from previous studies. This study tries to set certain terms straight and eliminate outdated terms (e.g. archetypal kimberlites as opposed to

Group I kimberlites). This study also has implications for our current understanding of melt-SCLM interactions and ultimately how kimberlites are different from lamproites and why.

1.4.Outline

Chapter 2 (Background) begins with a summary of the history of kimberlite deposits from the first discovery up until modern day understanding of these deposits and their different varieties. This is followed by a detailed overview of similar diamondiferous rocks worldwide compared to the current study including archetypal kimberlites, orangeites and lamproites. The significance of olivine is then introduced and highlights how it can be used as a tool for delineating the petrogenesis of diamondiferous rocks. Previous work on the West African kimberlites (including the regional geology) is then further discussed and compared to these worldwide diamondiferous rocks. Chapter 3 (Methodology) explains where the samples were derived from, and the analytical procedures used to study the rocks. Chapter 4 (Results) presents the petrography and mineral chemistry of the representative samples of the Koidu and Tongo clusters from the West African Man craton. Chapter 5 (Discussion) discusses the data, with previous studies being contrasted. Moreover, a new petrogenetic model is proposed to explain the nature of the rocks. Finally, Chapter 6 (Conclusion) presents the main conclusions of the study.

Chapter 2: Background

2.1. Introduction

The first diamondiferous kimberlites were discovered in central South Africa on the farms of Bultfontein, Dorstfontein (also known as Dutoitspan), Koffiefontein and Jagersfontein between the period of October 1869 and July 1870. The diamonds were found in small quarries in muddy material adjacent to cylindrical depressions filled with shallow water, known in South Africa at the time as "pans". In May 1871, significant diamond recoveries were made on the farm of Vooruitzigt, leading to the discovery of three other diamond-rich deposits in the area. Subsequently, this led to the establishment of four major diamond mines and the town of Kimberley. Roberts (1976), Lenzen (1980), and Wilson (1982) describe the development of the town and story behind the early discoveries in more detail.

Initially, it was thought that the diamonds were of alluvial origin, but further investigation saw that the diamonds were hosted within a highly altered and decomposed rock. The diamond-bearing material near the surface was locally termed "yellow ground" and transitioned, with increasing depth, to more competent "blue ground". This blue ground was later interpreted to be an altered igneous rock and the primary diamond source, concluding that these diamond deposits could not be of alluvial origin.

Only in 1887, did the diamond-bearing rock receive a petrographic name after Henry Carvill Lewis stressed the unique nature and character of the rock at the British Association for the Advancement of Science in Manchester. It was described by Lewis (1888) as a porphyritic mica-bearing peridotite and was thought to be a type of volcanic breccia. It was subsequently termed kimberlite (derived from Kimberley) based on the type locality nomenclature rules at the time.

By the end of the 19th century the geological characteristics of kimberlites were better understood, and many other kimberlites were discovered throughout South Africa. These discoveries were specifically located in what previously was the Transvaal (presently Gauteng, Mpumalanga, Limpopo and the eastern Northwest Province), the Orange Free State (presently the Free State) and the Cape province (presently the Western Cape, Northern Cape and Eastern Cape). After these discoveries any igneous rock containing diamonds worldwide were referred to as a kimberlite by prospectors and subsequently by geologists. In many parts of the world, this practice has been ongoing for many decades (Mitchell, 1995). For example, some Australian petrologists have referred to the diamond bearing Aries pipe as a "micaceous kimberlite" (Downes et al., 2007) and some Russian petrologists have referred to diamond-bearing deposits occurring on the eastern flanks of the Anabar Shield as "kimberlites" (Kornilova et al., 1983), whereas they are more accurately classified as lamproite and melilitite respectively.

The first comprehensive summary of the kimberlite occurrences in South Africa was published in 1914 by Percy Wagner called "The Diamond Fields of South Africa". Some important petrological observations were made, and the work was extremely influential. Wagner (1914) based his terminology of diamond-bearing volcanic and hypabyssal rocks primarily on the macroscopic appearance of the rock. He proposed that there were two distinctive types of kimberlites, a "basaltic" and a "micaceous" kimberlite, with the only similarity between the two being the presence of diamond and olivine macrocrysts. The fundamental differences between the two varieties of "kimberlites" were recognized by Wagner (1928) and he believed there was concise evidence in supporting the reclassification of the one variety as a new rock type. The micaceous kimberlite was referred to as an orangeite during a study by Wagner (1928) on the Lion Hill Dyke.

In a study done by Smith (1983), it was demonstrated that monticellite calcite serpentine kimberlite and phlogopite kimberlite, petrographically selected by E. Michael W. Skinner (previously De Beers), had distinctive differences in their Sr and Nd isotopic compositions. These were termed Group I and Group II kimberlites on this basis, equating to the "basaltic" and "micaceous" kimberlites of Wagner (1914), respectively. Smith (1983) proposed that Group I kimberlites were derived from an asthenospheric mantle source and that Group II kimberlites were derived from a lithospheric mantle source.

These isotopic studies further led to Smith et al. (1985) and Skinner (1989, 1986) to separating Group I and Group II kimberlites based on differences in their whole rock geochemistry, isotopic character, xenoliths and megacrysts, mantle-derived xenocrysts, petrography, age and distribution patterns. Skinner (1989) noted that Group II kimberlites are unique to South Africa, whereas Group I kimberlites are found worldwide. Group II kimberlites also seem to be older in southern Africa compared to Group I kimberlites in the same geographic regions (Mitchell, 1995; Skinner et al., 1994; Smith et al., 1985).

Based on numerous studies and interest in characterizing the geochemistry and mineralogy of Group II kimberlites, it has become evident that these rocks are geochemically and mineralogically distinct from Group I kimberlites (Dawson, 1987; Fraser, 1987; Fraser et al., 1985; Fraser and Hawkesworth, 1992; Mitchell, 1994; Mitchell and Meyer, 1989; Skinner, 1989; Skinner et al., 1994; Tainton and Browning, 1991; Tainton and McKenzie, 1994; Tainton, 1992). These studies essentially indicated that Group II kimberlites have similar and closer affinities to lamproites as opposed to Group I kimberlites. Based on this Mitchell (1994, 1991) suggested that Group I and Group II kimberlites are derived from separate parental magmas. He also suggested that Group II kimberlites are not a variety of kimberlite and that they belong to a completely different petrological lineage compared to Group I kimberlites. This led Mitchell (1995) to suggest

the revival of the term “orangeite” first introduced by Wagner (1928) to be designated as the new name as opposed to Group II kimberlites (Mitchell, 1995).

Due to diamondiferous rocks sharing certain mineralogical and geochemical characteristics, the misclassification of these rocks has been common throughout previous decades. The most notable example is the Aries pipe from Western Australia. The Aries pipe consists of primary richterite, diopside and sanidine, however, contains geochemical characteristics more associated with the distinct Koidu kimberlites from the Man craton which are unlike archetypal kimberlite or orangeite (Edwards et al., 1992; Taylor et al., 1994). According to Scott Smith et al. (2013), the mineral assemblage of Aries is diagnostic of a lamproite and not a kimberlite and should be classified as an olivine lamproite as opposed to a kimberlite.

Recent progress within the field has led to clarification on certain terms and to eliminate names and classifications that are outdated or incorrect in terms of standard igneous petrology (Scott Smith et al., 2013). For example, orangeites are petrographically and geochemically more like lamproites as opposed to kimberlites. Petrographic similarities include the presence of tetraferriphlogopite, diopside, sanidine, richterite, spinel, apatite, and perovskite (Mitchell, 1995; Mitchell and Bergman, 1991). Geochemical similarities include sharing similar bulk-rock compositions and isotopic systematics (Pearson et al., 2019). Despite these similarities, some authors still prefer the term “Group II kimberlites” (e.g. Nkere et al., 2021; Ramokgaba et al., 2021), while others prefer to use the term “orangeite” (e.g., Compton-Jones et al., 2021). Due to the similarities in mineralogy and geochemistry, Pearson et al. (2019) referred to orangeites as a carbonate-rich sub-variety of lamproites, derived from a broadly similar source region. As a result, the suggestion was given to change the term “orangeite” to “carbonate-rich olivine lamproite”. However, not all orangeites contain carbonate and so this name is also technically incorrect. The name “Kaapvaal lamproite” was suggested by Scott Smith et al. (2018), as orangeites are believed to be characteristic and unique to the Kaapvaal craton but still a sub-category of lamproites. Within the current study Group I kimberlites will be referred to as “archetypal kimberlites” and Group II kimberlites as Kaapvaal lamproites.

In the next sections, the characteristics of archetypal kimberlites, Kaapvaal lamproites and lamproites will be discussed. Further, these characteristics will be contrasted with West African kimberlites and the importance of olivine as a tool for understanding kimberlite petrogenesis will be highlighted.

2.2. Archetypal kimberlites

2.2.1. Definition

Kimberlites are silica undersaturated, potassic, volatile-rich (CO_2 and H_2O) rocks produced by partial melting in the asthenosphere which have been interpreted to reflect variable degrees of assimilation in the subcontinental lithospheric mantle (SCLM) (Giuliani et al., 2020; Mitchell, 1995). They are typically characterized by an inequigranular texture consisting of macrocrysts (>0.5mm) of olivine, phlogopite, clinopyroxene, garnet and/ or ilmenite. The groundmass mineral assemblage consists of microcrysts (<0.5mm) of olivine, phlogopite, spinel, perovskite, monticellite, apatite and calcite. This mineral assemblage is then often further set in a late-stage serpentine and/ or carbonate (Clement et al., 1984; Mitchell et al., 2019). Kimberlites are further referred to as "archetypal kimberlites" in this study, following the terminology suggested by Mitchell, (1995).

2.2.2. Mineral chemistry

a) Phlogopite

Kimberlite phlogopites are diagnostically elevated in Al_2O_3 and have low TiO_2 and FeOT. Kimberlite phlogopites are defined by Al_2O_3 ranging from 13-21 wt%, TiO_2 ranging from 0-3wt% and FeOT ranging from 0-5 wt% (Figure 1) (Mitchell, 1995). Zoning within kimberlite groundmass phlogopite can range from patchy and discontinuous zoning to continuous zoning. Groundmass phlogopite often also ranges in composition between the two end members of the phlogopite – kinoshitalite solid solution series, whereas microcrystal mica is generally phlogopite. Phlogopite within kimberlite generally have compositional trends with increasing Al and Ba and decreasing Fe, Ti and Si, whereas phlogopite within Kaapvaal lamproites/ lamproites are similar but differ in having a decrease in Al and an increase in Fe (Mitchell et al., 2019).

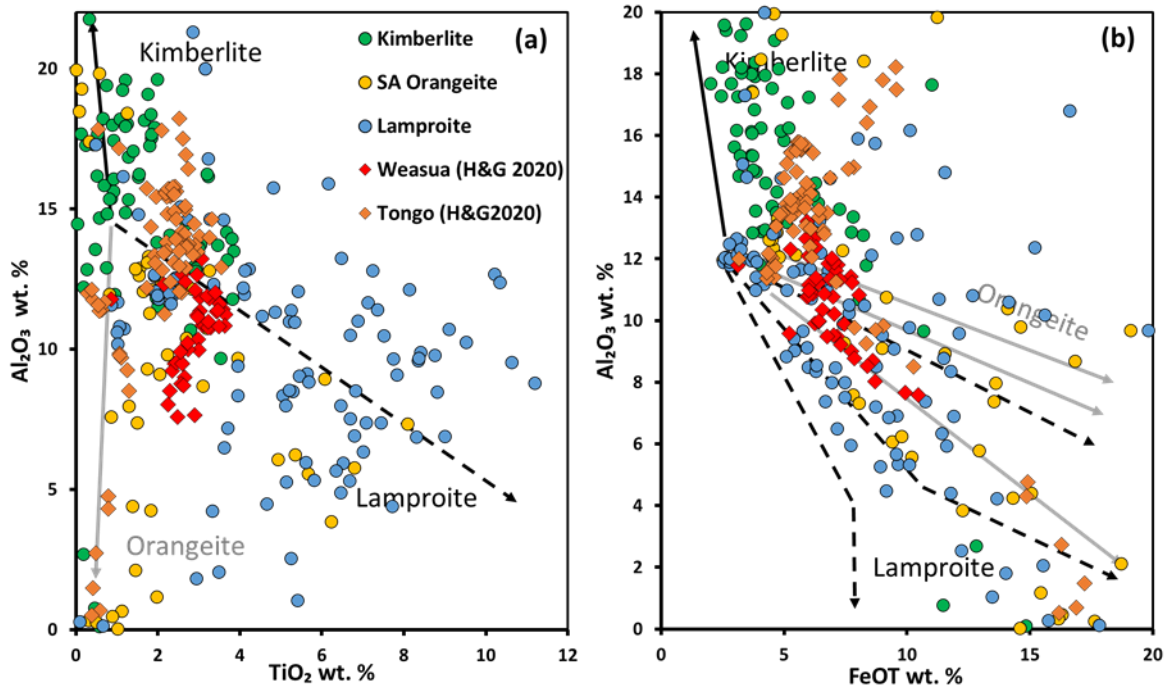

Figure 1: (a) Al_2O_3 wt % vs TiO_2 wt % for phlogopite core and rim analyses from Mitchell and Bergman (1991), Mitchell (1995), and Howarth and Giuliani (2020) plotted on a Al_2O_3 wt % vs TiO_2 wt % phlogopite classification diagram. (b) Al_2O_3 wt % vs FeO(t) wt % for phlogopite analyses from Mitchell and Bergman (1991), Mitchell (1995), and Howarth and Giuliani (2020) plotted on a Al_2O_3 wt % vs FeO(t) wt % phlogopite classification diagram.

b) Spinel

Kimberlitic spinels have been observed and described as an evolution from a chromium-rich spinel (TIMAC) to magnesio-ulvospinel-magnetite (MUM) (Figure 2) (Mitchell, 1986). On a Cr/(Cr+Al) vs $Fe^{2+}/(Fe^{2+}+Mg)$ diagram, the spinel has an initial elevated Cr/(Cr+Al) and evolves to a low Cr/(Cr+Al) with a relatively constant $Fe^{2+}/(Fe^{2+}+Mg)$ throughout the evolution of the spinel. On a $Fe^{3+}/(Fe^{3+}+Al+Cr)$ vs $Fe^{2+}/(Fe^{2+}+Mg)$ diagram, the spinel often has a low $Fe^{3+}/(Fe^{3+}+Al+Cr)$ concentration and evolves to a higher concentration of $Fe^{3+}/(Fe^{3+}+Al+Cr)$ with a relatively contant $Fe^{2+}/(Fe^{2+}+Mg)$ throughout the evolution of the spinel. This spinel evolution is known as trend 1 on the Cr/(Cr+Al) vs $Fe^{2+}/(Fe^{2+}+Mg)$ diagram and the $Fe^{3+}/(Fe^{3+}+Al+Cr)$ vs $Fe^{2+}/(Fe^{2+}+Mg)$ diagram (Mitchell, 1995).

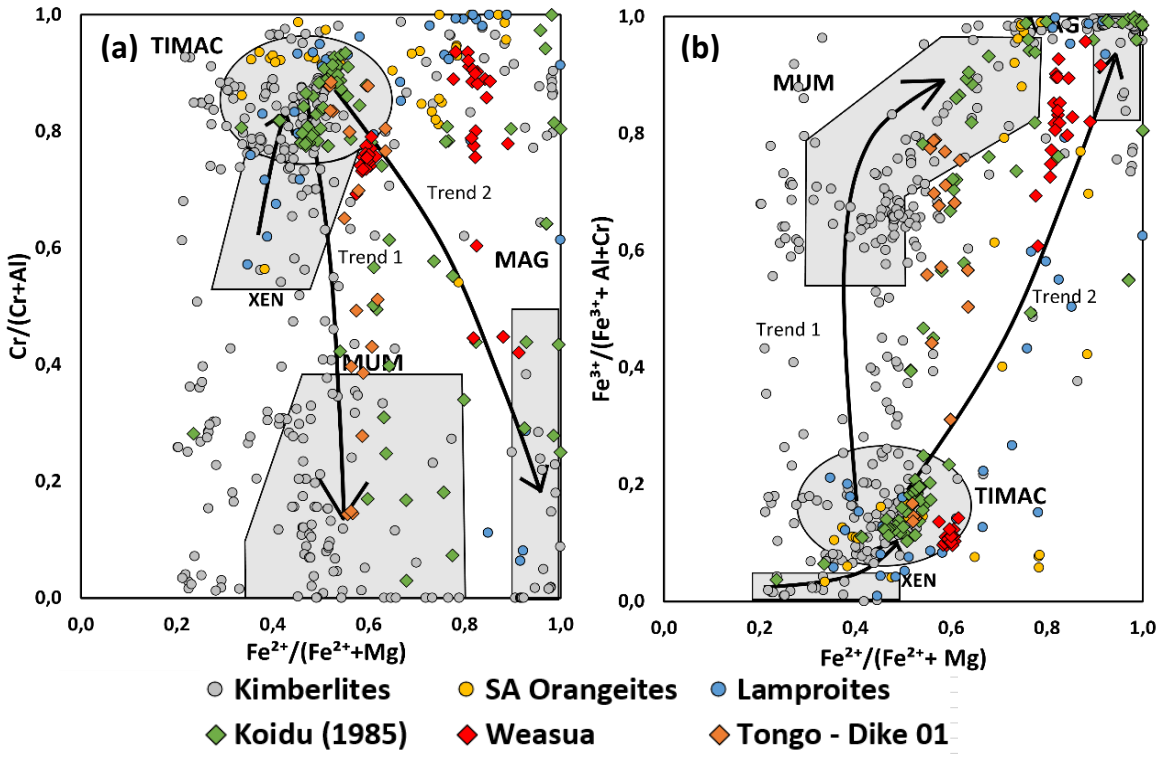

Figure 2: (a) Cr/(Cr+Al) vs $Fe^{2+}/(Fe^{2+}+Mg)$ for spinel core and rim analyses from Roeder and Schulze (2008), Tompkins and Haggerty (1985), and Howarth and Giuliani (2020). (b) $Fe^{3+}/(Fe^{3+}+Al+Cr)$ vs $Fe^{2+}/(Fe^{2+}+Mg)$ for spinel analyses from Roeder and Shulze (2008), Tompkins and Haggerty (1985), and Howarth and Giuliani (2020). Acronyms: TIMAC - chromium-rich spinel; MUM - magnesio-ulvospinel-magnetite; MAG – magnetite; XEN – xenocrystic spinel.

2.2.3. Geochemistry

Archetypal kimberlites typically have a wide range in major element compositions and are enriched in compatible and incompatible trace elements (Mitchell, 1986; Smith et al., 1985). They are potassic (<0.5 wt% Na_2O; ≤1.0 wt% K_2O), undersaturated ultrabasic rocks (25.0-35.0 wt.% SiO_2; 21.0-34.0 wt.% MgO), enriched in H_2O (≥5.0 wt%) and CO_2 (~10.0 wt%) and are deficient in Al_2O_3 (1.0-5.0 wt%) (Becker and Le Roex, 2006; Mitchell, 1986). Their low phlogopite abundance reflects the low bulk rock K_2O (<1.0 wt.%) content, while the abundance of Ti-spinels and perovskite is reflected in their elevated TiO_2 (1.0 to 5.0 wt.%) content. Their CaO content ranges between 7.0 to 17.0 wt.% and the Fe_2O_3 content ranges between 8.5 to 17.0 wt.% (Table 1) (Becker and Le Roex, 2006). Further, archetypal kimberlites have a linear chondrite normalized REE distribution, enriched in light REE and lack an Eu anomalies (Becker and Le Roex, 2006; Mitchell, 1995).

Table 1: Whole rock geochemistry averages for West African kimberlites, Archetypal kimberlites, Kaapvaal lamproites and Finland kimberlites.

	West African kimberlites		Archetypal Kimberlites		Kaapvaal lamproites (Orangeite)		Finland kimberlites	
	Average	SD	Average	SD	Average	SD	Average	SD
SiO2 (wt.%)	28.20	3.9	26.15	2.7	33.89	4.8	34,13	4,4
TiO2 (wt.%)	1.71	0.3	2.58	0.7	1.77	1.5	2,01	0,6
Al2O3 (wt.%)	4.08	1.0	2.76	0.45	3.76	2,00	4,24	1,1
Fe2O3 (wt.%)	10.23	1.7	10.72	1.2	8.76	0.6	10,22	1,1
MnO (wt.%)	0.19	0.01	0.19	0.03	0.18	0.05	0,20	0,1
MgO (wt.%)	21.01	1.0	25.2	2.1	23.15	4.2	25,38	3,6
CaO (wt.%)	12.47	1.8	13.26	2.2	9.96	2,00	8,84	3,9
Na2O (wt.%)	0.18	0.02	0.16	0.14	0.25	0.24	0,43	0,4
K2O (wt.%)	3.03	0.5	0.83	0.46	3.63	1.4	1,63	1,1
P2O5 (wt.%)	1.65	0.6	2.04	1.2	1.85	0.8	0,47	0,1
SO3 (wt.%)	0.19	0.1	0.17	0.15	0.21	0.16	0,11	0,1
Cr2O3 (wt.%)	0.20	0.01	0.18	0.04	0.23	0.09	-	-
NiO (wt.%)	0.09	0.0	0.11	0.03	0.14	0.06	-	-
H2O- (wt.%)	1.46	0.4	0.66	0.27	1.34	1.7	9,57	1,5
LOI (wt.%)	14.56	2.5	14.71	1.9	10.75	3.8	12,55	3,1
Sum (wt.%)	99.27	0.1	99.71	0.2	99.41	0.4	99,98	1,2
Cu (ppm)	35.20	14.2	95.9	60,00	42.9	14,00	96,2	32,4
Ni (ppm)	608.24	141.7	935,00	235,00	977,00	298,00	820,2	269,2
Nb (ppm)	365.03	50.4	239,00	147,00	165,00	88,00	181,6	43,2
Zr (ppm)	210.32	76.2	371,00	98,00	399,00	194,00	81,6	19,5
Y (ppm)	18.77	6.6	20.5	6,00	20.9	9,00	10,3	3,2
Sr (ppm)	1808.31	381.1	1295,00	444,00	1869,00	671,00	656,9	300,9
La (ppm)	363.12	25.43	150,00	16.5	194.6	17.2	118,1	38,2
Gd (ppm)	15.87	4.2	11.84	2.2	8.74	3.5	5,0	1,4
Yb (ppm)	1.016	0.06	1.088	0.01	0.93	0.02	0,7	0,2
Rb (ppm)	160.91	14.8	47.1	25,00	151,00	57,00	88,1	54,1
U (ppm)	17.41	6.0	5.76	4,00	6.14	3,00	3,4	0,9
Th (ppm)	36.22	5.3	24.3	18,00	40.3	27,00	17,3	5,5
Pb (ppm)	12.81	3.1	10.4	5,00	33.3	12,00	7,8	3,1
Co (ppm)	78.25	9.2	89.1	9,00	74.7	9,00	70,9	18,3
Cr (ppm)	1508.97	101.3	1508,00	481,00	2096,00	449,00	1278,7	304,4
V (ppm)	191.71	42.6	155,00	46,00	112,00	46,00	138,4	43,4
Ba (ppm)	2787.20	728.9	1380,00	876,00	3799,00	1503,00	1502,7	612,4
(87Sr/86Sr)i	0,703950	-	0,704401	0,0008	0,707800	5,3611	-	-
(143Nd/144Nd)i	0,512531	0,00001	0,512630	0,0003	0,511901	0,0005	-	-

West African kimberlites data from Mathafeng (2021), Archetypal kimberlites from Becker and le Roux (2006), Kaapvaal lamproites from Becker and le Roux (2006) and Finland kimberlites from Dalton et al. (2020).

The initial division between archetypal kimberlite and Kaapvaal lamproite was determined by Smith (1983), who measured the composition of radiogenic isotopes Sr and Nd of the two respective rock types. This confirmed that the two rock types were derived from distinct magma types. Relative to bulk earth, kimberlites have depleted Sr-Nd signatures with initial $^{87}Sr/^{86}Sr$ ratios between 0.7026 and 0.7049 (Woodhead et al., 2009) and initial $^{143}Nd/^{144}Nd$ ratios between 0.5120 and 0.5128 (Figure 3) (Nowell et al., 2004). The epsilon parameter can be used to compare differences between CHUR (chondritic uniform reservoir; DePaolo and Wasserburg, 1976) and the $^{143}Nd/^{144}Nd$ ratios. The ε values can thus be positive or negative and means the magmas were formed from a depleted mantle source or an enriched mantle source respectively

(Wilson, 1989). Mitchell (1995) determined that kimberlites have a εNd value range from 0.31 to 3.17 indicating magma formation from a depleted mantle source. Kimberlites also have strongly negative ΔεHf (-1.2 to -10.1) values, determined from their distinctive Hf-Nd isotopic signatures which trend below the mantle array (Nowell et al., 2004). Nowell et al. (1999) proposed that in order to deviate from the mantle array, the ΔεHf component in kimberlites must be ancient (>1.0 Ga).

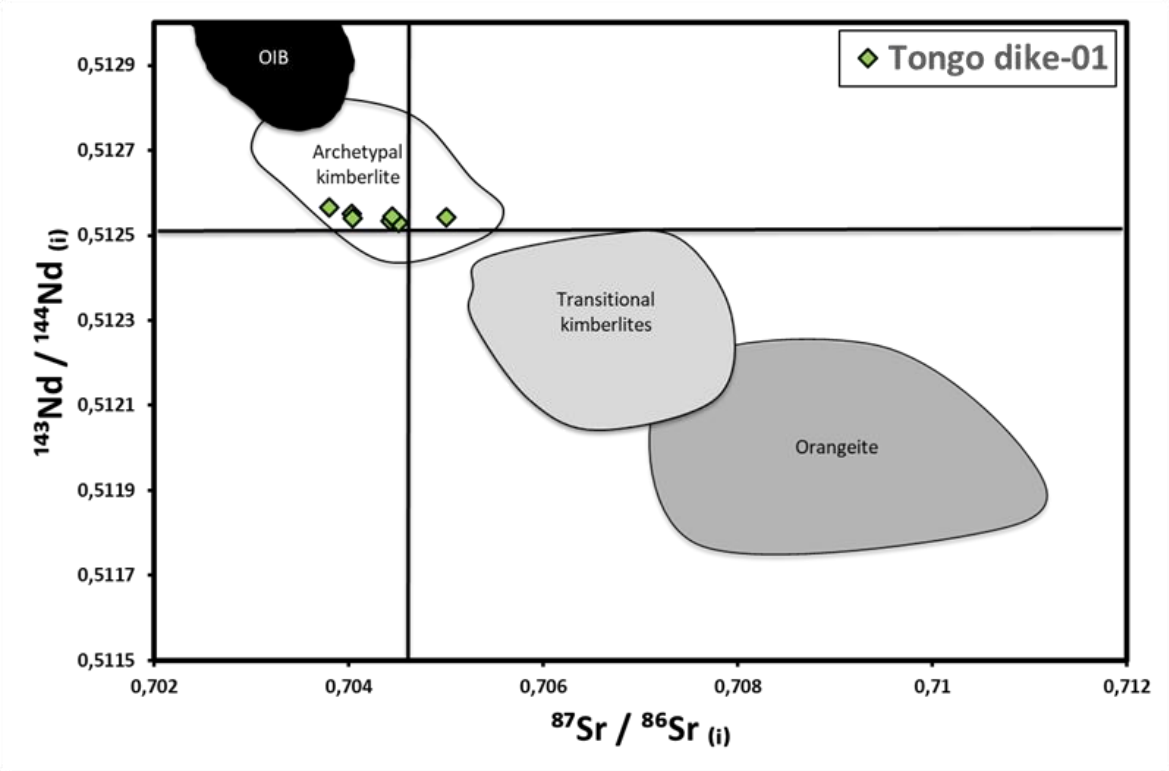

Figure 3: Variation plot of initial $^{143}Nd/^{144}Nd$ vs $^{87}Sr/^{86}Sr$ isotope ratios for representative data fields for ocean island basalts (OIB), kimberlites, transitional kimberlites, orangeites and West African kimberlites. The Tongo dike-01 data is from Mathafeng (2021). The orangeite, kimberlite and transitional kimberlite data fields are derived from Smith, 1983; Fraser & Hawkesworth, 1992; Tainton, 1992; Clark, 1994; Nowell et al., 1999, 2004; Coe, 2004; Becker & le Roex, 2006. The South Atlantic OIB data field was derived from O'Nions & Pankhurst, 1974; O'Nions et al., 1977; le Roex, 1985; le Roex et al., 1990

2.2.4. Petrogenesis

Recent studies on radiogenic isotopes have demonstrated that archetypal kimberlites are derived from geochemically similar homogeneous source region reservoirs. Further, It was proposed that this homogenous reservoir has evolved in isolation for ±2.5 billion years and consists of an isotopic composition that is characteristic of a pristine and uniform mantle source. This source was then contaminated around 200 million years ago by subduction related exogenetic material and subsequent kimberlite magmatism occurring after this event reveal radiogenic isotopic signatures (high $^{206}Pb/^{204}Pb$; negative ΔεHf) indicative of such an event (Woodhead et al., 2019). Studies on incompatible trace elements have similarly revealed that archetypal kimberlite magmas are derived from a common mantle component (Giuliani et al.,

2020). On the basis of these combined lines of evidence, it was inferred that this common kimberlite source region. is located in the convective mantle. Trace element compositions of Cretaceous-Eocene Canadian, Brazilian and southern African kimberlites indicate a limited influence of subduction related exogentetic material on the source region. Mantle-like oxygen isotope compositions of olivine in these kimberlites are also consistent with this finding (Giuliani et al., 2020). Giuliani et al. (2020) further proposed a linear correlation between olivine core and rim forsterite (Fo) content and that this correlation can only be achieved if a primary kimberlite melt has a similar Mg# and subsequent major element compositions before interacting with the lithospheric mantle. The study ultimately suggested that the degree of lithospheric mantle assimilation determines the surface composition of a kimberlite.

2.3. Kaapvaal lamproites (aka orangeites or Group II kimberlites)

2.3.1. Definition

Kaapvaal lamproites (previously Group II kimberlite) are a suite of volatile-rich (H_2O-rich dominantly) ultrapotassic peralkaline rocks of the lamproite clan. They are characterized by the presence of macrocrystic and microcrystic phlogopite and typically consist of additional groundmass tetraferriphlogopite. Olivine is always present as euhedral microcrysts and or rounded anhedral macrocrysts. Kaapvaal lamproites are divided into an “evolved” and “unevolved” category based on mineralogy (Mitchell, 1995). The primary mineral assemblage of the groundmass includes diopside, various spinels, ranging from Mg-chromite to Ti-magnetite, perovskite (Sr- and REE- rich), apatite (Sr-rich), Mn-ilmenite, Nb-rutile, phosphates (REE-rich) and hollandite Group minerals. This primary mineral assemblage is set within a mesostasis which may consist of one or more of the following: calcite, dolomite, and other rare earth carbonates and serpentine (Mitchell, 1995). Unevolved Kaapvaal lamproites can appear to have a similar mineralogy to archetypal kimberlites, however, are generally distinguished by the presence of phlogopite evolution to tetraferriphlogopite and often (but not always) containing primary diopside. In contrast, evolved Kaapvaal lamproites are distinguished from archetypal kimberlites by the presence of additional sanidine, titanian aegirine, and potassium richterite. Further, geochemical signatures are additionally used to distinguish archetypal kimberlites from Kaapvaal lamproites, with the former having high TiO_2 and low K_2O and lower Th/Nb, Ba/Nb, and La/Nb ratios. Additionally, archetypal kimberlites have a near chondritic to super-chondritic Sr-Nd-Hf isotope compositions compared to more enriched isotope compositions found within Kaapvaal lamproites (Becker and Le Roex, 2006; Coe et al., 2008; Le Roex et al., 2003; Mitchell, 1995; Nowell et al., 2004; Smith, 1983; Woodhead et al., 2019).

2.3.2. Mineral chemistry

a) Phlogopite

Cores of Kaapvaal lamproite phlogopites are characterized by Al_2O_3 ranging from 0-13 wt%, TiO_2 ranging from 0-3wt% and FeOT ranging from 5-19 wt% (Figure 1) (Mitchell, 1995). With respect to Al-Fe evolutionary trends, Kaapvaal lamproite and lamproite micas share some compositional similarities. The initial unevolved phenocrystal mica composition is similar on the Al-Fe diagrams, however local post-emplacement crystallization conditions determine the evolution of the trends. Kaapvaal lamproite micas evolve towards a decreasing or constant Ti content with increasing Al, are generally poor overall in TiO_2 (1-3 wt %) and evolve towards tetraferriphlogopite (Mitchell, 1995). However, Kaapvaal lamproites bearing richterite and sanadine contain micas with Al-Ti evolutionary trends similar to those found in lamproites, as seen in Kaapvaal lamproite micas from Voorspoed, Postmasburg, Besterskraal and Sover North (Mitchell, 1995).

Kaapvaal lamproite micas have low Na (typically ~0.5 wt% Na2O) and F (typically ~1.0 wt%) compared to lamproite micas, which can be used to distinguish between the two. Additionally, Kaapvaal lamproite micas have complex zoning and reverse zoning textures which do not occur in lamproite micas (Mitchell, 1995).

b) Spinel

Kaapvaal lamproite and lamproitic spinels commonly share similarities in spinel chemistry and have been observed and described as an evolution from a chromium-rich spinel (TIMAC) to a magnetite (MAG) (Figure 2) (Mitchell, 1986). On a Cr/(Cr+Al) vs $Fe^{2+}/(Fe^{2+}+Mg)$ diagram, the spinel has an initial elevated Cr/(Cr+Al) composition and a moderate $Fe^{2+}/(Fe^{2+}+Mg)$ composition. The evolution then follows a decrease in Cr/(Cr+Al) and an increase in $Fe^{2+}/(Fe^{2+}+Mg)$. On a $Fe^{3+}/(Fe^{3+}+Al+Cr)$ vs $Fe^{2+}/(Fe^{2+}+Mg)$ diagram, the spinel often has a low $Fe^{3+}/(Fe^{3+}+Al+Cr)$ composition with a moderate $Fe^{2+}/(Fe^{2+}+Mg)$ composition. The evolution then follows an increase in both $Fe^{3+}/(Fe^{3+}+Al+Cr)$ and $Fe^{2+}/(Fe^{2+}+Mg)$. This spinel evolution is known as trend 2 on the Cr/(Cr+Al) vs $Fe^{2+}/(Fe^{2+}+Mg)$ diagram and $Fe^{3+}/(Fe^{3+}+Al+Cr)$ vs $Fe^{2+}/(Fe^{2+}+Mg)$ diagram (Mitchell, 1986).

2.3.3. Geochemistry

Kaapvaal lamproites are a suite of volatile-rich (H_2O-rich dominantly) ultrapotassic peralkaline rocks, ranging from an unevolved to an evolved endmember. The evolved Kaapvaal lamproite is rich in SiO_2 (41-47 wt.%) due to the presence of richterite and K-feldspar. They are rich in Al_2O_3 (4.0 to 8.0 wt.%) and depleted in MgO (14.0 to 28.0 wt.%) (Mitchell, 1995). Evolved Kaapvaal lamproites are thought to have been derived from a mineralogically different source or a low pressure differentiates of Kaapvaal lamproites (Mitchell, 1995). Unevolved Kaapvaal lamproites have overall lower SiO_2 (27.0 – 43.0 wt.%) contents, lower Al_2O_3 (0.90 to 6.0 wt.%) contents and MgO contents between 10.0 to 40.0 wt.% (Table 1) (Becker and Le Roex, 2006; Mitchell, 1995).

Despite the two endmembers, Kaapvaal lamproites are overall distinct from archetypal kimberlites in having much higher K_2O/ TiO_2 ratios (>2 compared to <1), due to their mica rich nature. Their ultrapotassic nature is reflected by higher (>3) Na_2O/ K_2O ratios. Their CaO content ranges from 3.0 to 24.0 wt.%, Fe_2O_3 content ranges from 5.7 to 10.0 wt.% and CO_2 content ranging from 0.2 to 14.0 wt.% (Mitchell, 1995). Further, Kaapvaal lamproites are extremely fractionated in LREE relative to HREE (Mitchell, 1995).

Relative to bulk earth, Kaapvaal lamproites have enriched Sr-Nd signatures with initial $^{87}Sr/^{86}Sr$ ratios between 0.7068 and 0.7088 (Woodhead et al., 2009) and initial $^{143}Nd/^{144}Nd$ ratios between 0.5119 and 0.5121 (Figure 3) (Becker and Le Roex, 2006; Nowell et al., 2004). Kaapvaal lamproites have a εNd value range from -6.2 to -13.4 indicating magma formation from an enriched mantle source. Kaapvaal lamproites also have less rediogenic ΔεHf (3.6 to -2.6) compositions, which trend close to the mantle Hf-Nd array (Nowell et al., 2004).

2.3.4. Petrogenesis

Kaapvaal lamproite magmas are are inferred to have been derived from an enriched source with high Rb-Sr and low U/Pb and Nd/Sm ratios (Smith, 1983). The melt is believed to be developed within the subcontinental lithospheric mantle (SCLM) from the partial melting of metasomatised mantle material (M. Giuliani et al., 2015; Mitchell, 1995). The metasomatised mantle material is thought to be a mica-amphibole-rutile-ilmenite-diopside (MARID) or a phlogopite-ilmenite-clinopyroxene (PIC) in composition (M. Giuliani et al., 2015). In contrast, Dawson and Smith (1977) envisage that the MARID suite are cumulates which crystallized from a magma of kimberlitic affinities, based on compelling petrographic evidence. The various stages of Kaapvaal lamproite magmatism was introduced by Mitchell (1995) and includes: 1) The mantle source development; 2) The source undergoing partial melting; 3) The magma evolution and contamination from the mantle until emplacement; 4) Post emplacement crystallization.

2.4. Lamproites

2.4.1. Definition

Lamproites are peralkaline ultrapotassic rocks that exhibit an extremely wide range of mineral assemblages dependent on the source locality of where they occur. Lamproites refer to a clan of rocks as opposed to any specific rock variety. As a group lamproites are now characterized by the presence of phlogopite, tetraferriphlogopite, richterite, leucite, diopside, sanadine, priderite, jeppeite, davanite, wadeite and shcherbakovite. Additional characteristics include the absence of primary carbonate and the occasional occurrence of olivine, spinel, apatite and perovskite (Mitchell and Bergman, 1991).

2.4.2. Geochemistry

Lamproites are ultrapotassic ($K_2O/Na_2O > 3$) magnesian rocks enriched in H_2O ($\geq$5.0 wt%) and lack CO_2 (Mitchell and Bergman, 1991; Scott-Smith and Skinner, 1982). Three broad varieties have been defined by Mitchell and Bergman (1991) and can be separated into an olivine lamproite, madupitic lamproite and a phlogopite lamproite.

Olivine/ madupitic lamproites have the following major element compositional ranges: SiO_2 from 40.0 to 51.0 wt.%, TiO_2 from 1.0 to 5.0 wt.%, Al_2O_3 from 3.0 to 9.0 wt.%, FeOT from 5.0 to 9.0 wt.%, CaO from 4.0 to 13.0 wt.%, MgO from 12.0 to 28 wt.%, Na_2O below 2.0 wt.%, K_2O between 7.0 to 13.0 wt.%, P_2O_5 from 1.0 to 3.0 wt.% and H_2O from 1.0 to 3.0 wt.% (Mitchell and Bergman, 1991).

Phlogopite lamproites have the following major element compositional ranges: SiO_2 from 50.0 to 60.0 wt.%, TiO_2 from 1.0 to 7.0 wt.%, Al_2O_3 from 7.0 to 12.0 wt.%, FeOT from 3.0 to 7.0 wt.%, CaO from 2.0 to 7.0 wt.%, MgO from 3.0 to 12 wt.%, Na_2O below 2.0 wt.%, K_2O between 7.0 to 13.0 wt.%, P_2O_5 from 1.0 to 3.0 wt.% and H_2O from 1.0 to 3.0 wt.% (Mitchell and Bergman, 1991).

Compatible elements compositions vary between individual lamproites and can vary considerably depending on the element. Incompatible elements in lamproites include Ba-Sr, Zr-Hf, Nb-Ta, Th-U, REE and Y and vary considerably between locations.

Overall relative to bulk earth, lamproites have enriched Sr-Nd isotopic signatures, however, specific ranges are highly dependent on the associated lamproite. For example, Murcia-Almeria and West Kimberley provinces are more enriched in radiogenic Sr than the Greenland and North American lamproites. Lamproites overall have εNd values ranging from -7.3 to -25.9 indicating magma formation from an enriched mantle source (Mitchell and Bergman, 1991).

2.4.3. Petrogenesis

Lamproite magmatism has been ascribed to partial melting, under reduced H_2O-rich volatile conditions, of a lithospheric harzburgitic source that has undergone ancient enrichment. It is inferred that olivine lamproite compositions do not represent the composition of their parental magmas and are hybrid rocks (Mitchell and Bergman, 1991). The long-term development of the source region is required to undergo multiple events of ancient metasomatic enrichment as a pre-requisite to produce lamproite melts from partial melting. In contrast to archetypal kimberlites, this precludes lamproites from occurring near continental craton margins where mobile belts are located. Archetypal kimberlites are derived from a deeper source and thus can be emplaced in cratons and mobile belts. The geographical overlap between lamproites and archetypal kimberlites observed occasionally is thus possible. However, evidence has suggested that lamproites could have a source derived from the asthenosphere, which is supported by the finding of majorite as an inclusion in a diamond derived from the Helam lamproite (McKenna et al., 2003).

2.5. Olivine: a tool for constraining the petrogenesis of kimberlites

Olivine is a primary mineral constituent of a kimberlite magma (Mitchell, 2008) and occurs as both macrocrysts (>0.5 cm) and microcrysts (<0.5 cm) (Clement et al., 1984). Olivine macrocrysts are zoned, containing distinct cores and rims. Olivine cores are often irregular in shape, do not contain inclusions of groundmass phases, have grain boundaries that are sharp or gradational and commonly have an undulose extinction (Arndt et al., 2010; Bussweiler et al., 2015; Giuliani, 2018). Occasionally these core shapes can have embayed margins, indicating resorption of the original xenocrystic grain in a foreign melt. These textures are generally interpreted to reflect a xenocrystic origin of the cores (Giuliani, 2018; Kamenetsky et al., 2009; Mitchell, 2008). The surrounding rim zone often contains inclusions of groundmass minerals (e.g. spinel and perovskite). Further, NiO contents decrease and CaO + MnO contents increases from inner rim to outer rim consistent with fractional crystallisation of olivine and are indications of crystallization from the kimberlite melt (Arndt et al., 2010; Brett et al., 2009; Bussweiler et al., 2015; Cordier et al., 2015; Fedortchouk and Canil, 2004; Giuliani, 2018; Giuliani et al., 2017; Howarth and Giuliani, 2020; Howarth and Gross, 2019; Howarth and Taylor, 2016; Kamenetsky et al., 2008; Lim et al., 2018; Moore and Costin, 2016; Pilbeam et al., 2013; Shaikh et al., 2019, 2018; Sobolev et al., 2018, 2015).

Olivine core and rim compositions were compiled from kimberlites, Kaapvaal lamproites and lamproites from cratons worldwide and are displayed in Figure 4 and Figure 5, respectively. Olivine core chemistry is generally separated into Mg-rich and Fe-rich end members (e.g., Giuliani, 2018). The Mg-rich endmember is interpreted to be derived from the disaggregation of peridotite xenoliths and ranges from Fo 89 to Fo 94, whereas the Fe-rich endmember is related to the disaggregation of megacrysts and ranges from Fo 78 to Fo 89 (Moore, 1988; Moore and Costin, 2016; Giuliani, 2018; and references therein).

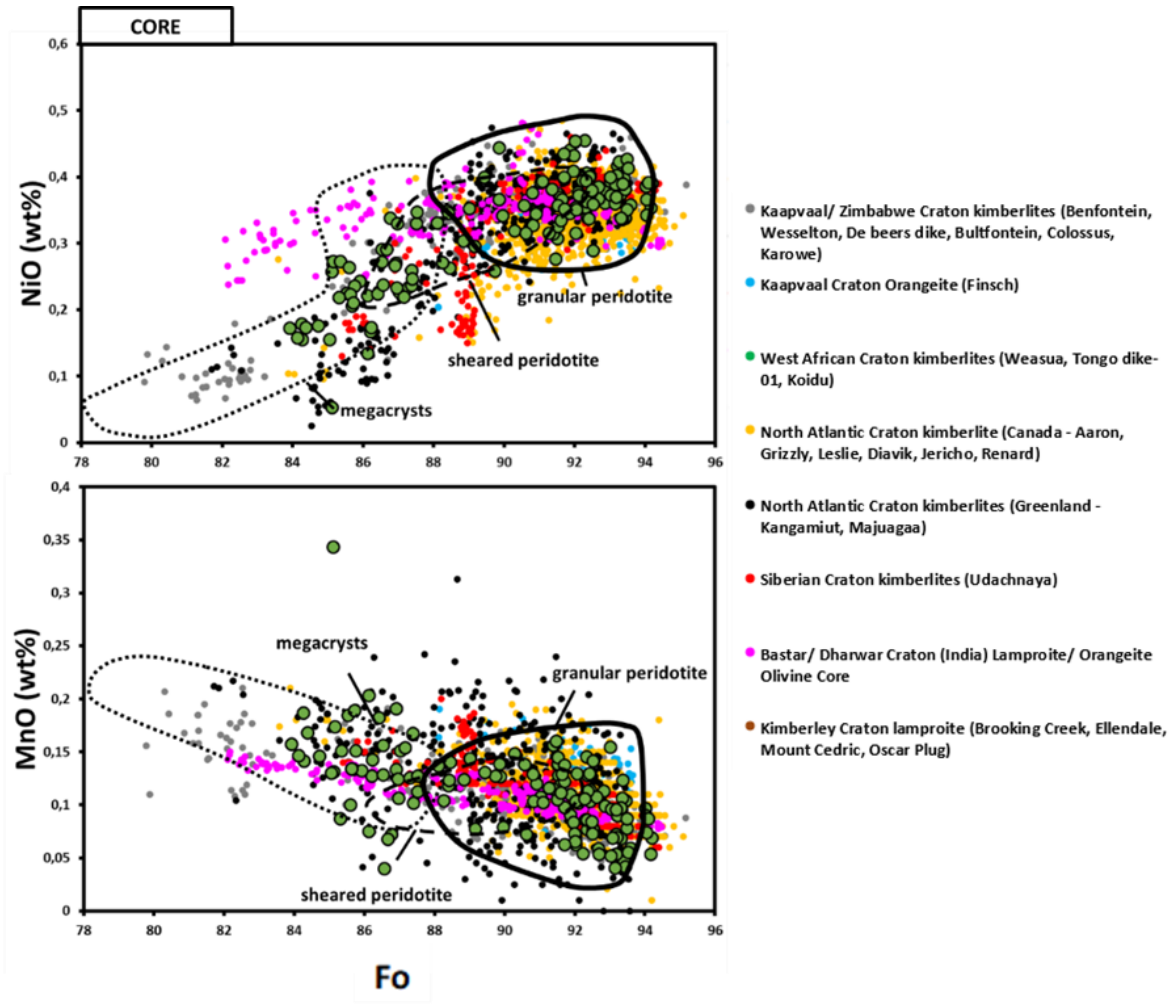

Figure 4: NiO wt %vs Fo and MnO wt % vs Fo for olivine core EPMA data from kimberlites/ orangeites and Lamproites worldwide. Source of data: Giuliani (2018), Howarth and Nembambula (2021), Howarth & Giuliani (2020), Shaikh et al (2019) and Jacques & Foley (2018).

Internal zones are occasionally observed in olivine's internal structure, occurring between the core and rim. Internal zones were first thought to have originated from diffusional equilibration or from the interaction of early kimberlitic melts in the mantle with the xenocrystic core (Pilbeam et al., 2013). The diffusional equilibrium theory was challenged by Cordier et al. (2015) after concluding that elements with similar diffusivity in olivine, e.g. Mg/ Fe and Ni, behave inconsistently. This was later re-interpreted by Giuliani and Foley (2016), suggesting that the

internal zones represented an early liquidus olivine that crystallized simultaneously or after orthopyroxene assimilation during ascent. Cordier et al. (2015) further suggested the internal zones formed in the mantle during metasomatism of the magmatic conduit. This was supported by Howarth and Taylor (2016) in their study of the Benfontein olivine internal zones, which displayed Cr and Ni values higher than the core and rim zones. This suggests that internal zone crystallization occurs before kimberlite ascent and after assimilation of orthopyroxene in the upper lithospheric mantle.

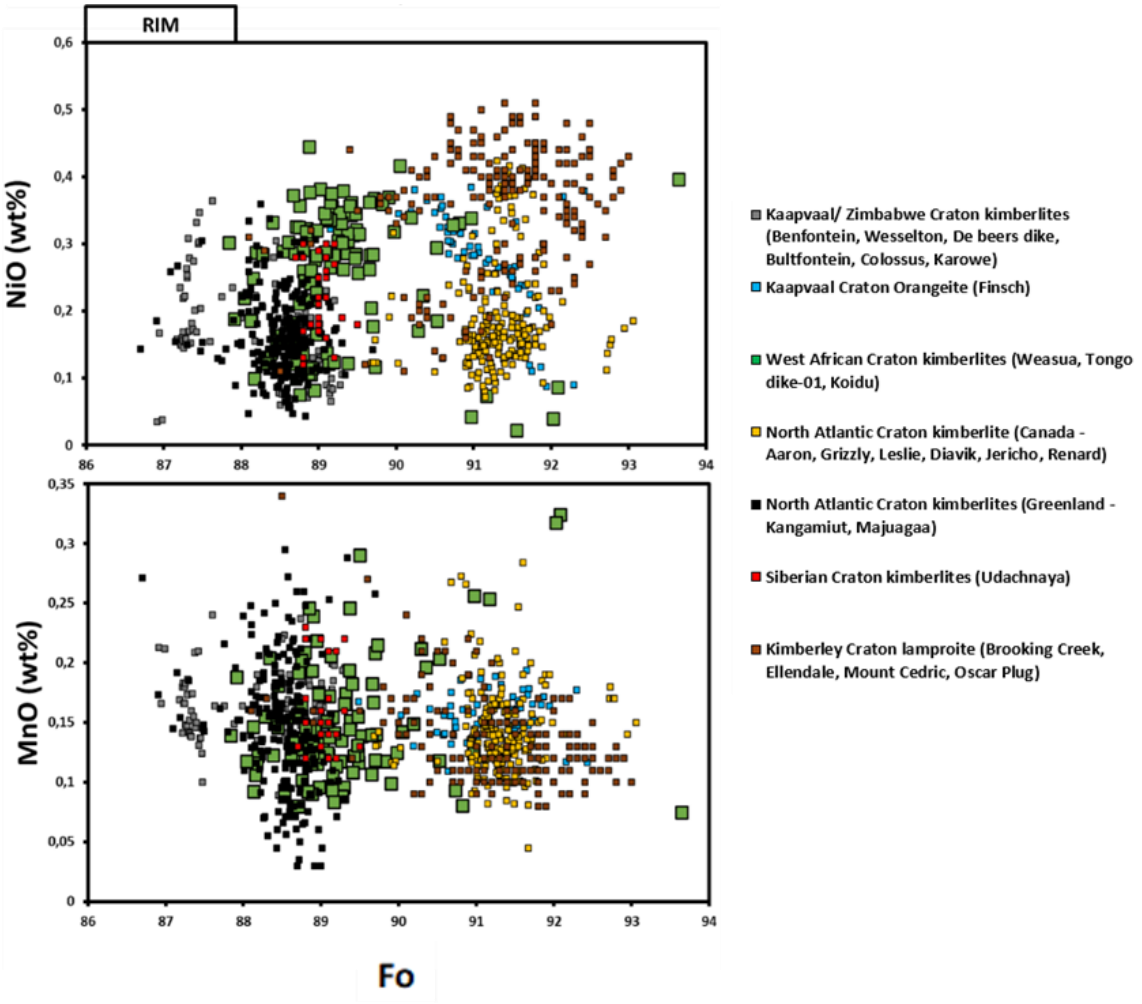

Figure 5: NiO wt %vs Fo and MnO wt % vs Fo for olivine rim EPMA data from kimberlites/ orangeites and Lamproites worldwide. Source of data: Giuliani (2018), Howarth and Nembambula (2021), Howarth & Giuliani (2020), Shaikh et al (2019) and Jacques & Foley (2018).

Rind zones fringe the olivine grains and often contain inclusions of late-stage groundmass minerals such as phlogopite and calcite, indicating a late-stage magmatic origin (Lim et al., 2018). Previous studies showed that rinds have higher Fo, Mn and Ca and lower Ni contents compared to olivine rims (Bussweiler et al., 2015; Fedortchouk and Canil, 2004; Howarth and Taylor, 2016; Lim et al., 2018). The increase in Fo in the rind zones was ascribed tothe crystallization from a residual melt at high oxygen fugacity conditions. The Fo enrichment can be compared to other

late-stage magmatic phases (spinel, monticellite and ilmenite). The early crystallization of Mn and Ca-poor and Ni-rich phases (olivine rims, spinel, ilmenite, rutile), results in the Mn and Ca enrichment and Ni depletion observed in the olivine rind zones (Bussweiler et al., 2015).

Giuliani et al. (2020) further proposed a linear positive correlation between olivine core and rim Fo.This correlation can only be achieved if a primary kimberlite melt has a similar Mg# to the magma in equilibrium with the olivine rim before interacting with the lithospheric mantle. The study ultimately suggested that the degree of lithospheric mantle assimilation determines the surface composition of a kimberlite. A similar model was proposed by Lim et al. (2018), who, compared phlogopite and oxide abundances in kimberlites to their corresponding olivine rim compositions. They concluded that a linear negative correlation exists between the two components and the model ultimately suggests that the degree of SCLM metasomatism undergone prior to kimberlite genesis determines the surface expression of any given kimberlite. Both these models will be used to contrast the groundmass mineralogy and abundances and olivine compositions in the Koidu and Tongo rocks.

2.6. West African kimberlites

2.6.1. Regional Geology

During the Mesozoic when the Atlantic Ocean was being formed by rifting of the Precambrian craton, two localized cratons were formed, the Man craton in West Africa and the Guyana craton in South America. The Man craton is made up of three age provinces, the Leonean (3.0 Ga), the Liberian (2.7 Ga) and the Eburnian (2.0 Ga), with some debate regarding the separation of the Leonean and the Liberian provinces. The Leonean/ Liberian provinces are made up of typical granite-greenstone terrains found worldwide. The majority (65%) of the outcrop area is made up of older tonalite-trondhjemite-granodiorite-gneisses (2.9 Ga). Younger granites (2.8-2.7 Ga) have intruded the margins of the associated greenstone belts. A much younger Pan-African age province, consisting of upper Proterozoic to mid Cambrian sedimentary rocks and Triassic-Jurassic basic intrusives, defines a tectonic event at 550 Ma in the coastal belt of Sierra Leone and Liberia (Skinner et al., 2004). The extensive coverage of these rock types is testified by the presence of these rock types as xenoliths in the Sierra Leone kimberlites (Hubbard, 1983).

West African diamondiferous rocks occur as several Jurassic-aged (135 – 155 Ma) clusters in Sierra Leone, Liberia and Guinea and as Neoproterozoic-aged (~800 Ma) clusters in Liberia (Andrews-Jones, 1968; Haggerty, 1982; Skinner et al., 2004). Within these regions they are emplaced as small pipes and prolific dike systems (Haggerty, 2017; Howarth and Giuliani, 2020; Skinner et al., 2004; Taylor et al., 1994). Two prolific dike trends are observed in the area, known

as the Sierra Leone trend and Liberian trend (Haggerty, 2017). The Sierra Leone trend includes the Jurassic-aged kimberlite dikes in Guinea (Droujba 153 Ma) and Sierra Leone (Koidu 146 Ma and Tongo 140 Ma; Figure 6) and are all ENE-WSW trending. The Liberian trend are NE-SW trending and includes the Mano Godua, Camp alpha, Kumgbo and Weasua dikes all located in Liberia (Haggerty, 2017). Due to the limited presence of diatreme-facies compared to hypabyssal-facies, these kimberlites are interpreted to have been eroded down (as much as 1-2 km) to the root-zone since the start of the Jurassic (Skinner et al., 2004).

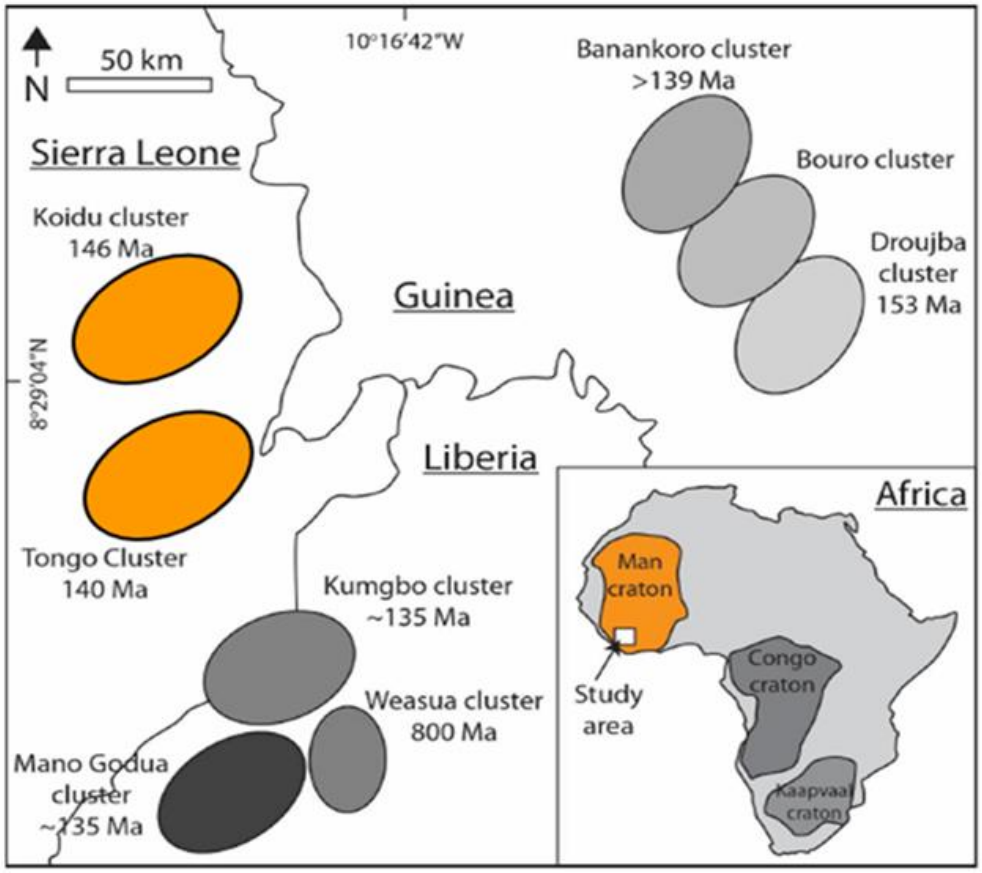

Figure 6: Map showing the approximate locations of kimberlite clusters in Sierra Leone, Guinea, and Liberia including the Tongo and Weasua clusters. Adapted after Skinner et al. (2004).

Within the Koidu kimberlite cluster, pipes K1 and K2, and a series of sub-parallel vertical dikes and adjoining blows make up the kimberlite population (Moss et al., 2012). These pipes and dikes have known resources and have already been mined in the past by Koidu (Ltd) owned by Octea mining company (Octea limited, 2014). The Tongo (also known as Tongo-Tonguma) kimberlite cluster are comprised primarily of four prospective vertical dikes which all have indicated resources namely, Kundu, Lando, Pandebu and Tongo dike-01 (Howarth and Giuliani, 2020). Additional dike prospects are known in the area, namely, Tongo dike-02, Tongo dike-03, Tongo dike-04, Tongo-Johnson, Seleima, Panguma and Peyima, which currently are all in the early phases of exploration (Newfield resources limited, 2019).

2.6.2. Mineralogy

Diamondiferous rocks from the Sierra Leone trend are characterised by a groundmass consisting of phlogopite, olivine, spinel, apatite, perovskite and occasional monticellite set in a base of serpentine and carbonate (calcite and dolomite). Relative to archetypal kimberlites, the Jurassic-aged West African rocks have high abundances of phlogopite and share petrographic characteristics with Kaapvaal lamproites (e.g., Howarth and Giuliani, 2020; Skinner et al., 2004; Taylor et al., 1994; Tompkins and Haggerty, 1984).

The Liberian trend consists of three main mineralogical varieties. The first variety (Weasua) consists of macrocrysts of olivine in a groundmass of phlogopite, olivine, diopside, spinel, apatite and perovskite set in a base of serpentine and occasional calcite and is classified as a lamproite (Howarth and Giuliani, 2020). The second variety (also Weasua) is classified as archetypal kimberlites and consists of macrocrysts of olivine in a groundmass of phlogopite, olivine, apatite and perovskite set in a base of serpentine and occasional calcite (Skinner et al., 2004). This variety has considerably lower phlogopite abundances compared to diamondiferous rocks from the Sierra Leone trend. The third variety (Camp Alpha) is also classified as an archetypal kimberlites and consists of macrocrysts of olivine in a groundmass with variable concentrations of ilmenite, serpentine, chlorite, phlogopite, and xenocrystic garnet with kelyphitic rims (Haggerty, 2017).

2.6.3. Classification based on phlogopite and spinel chemistry

Phlogopite and spinel core and rim compositions from the Jurassic (Tongo and Koidu) and Neoproterozoic (Weasua) diamondiferous rocks from the Howarth and Giuliani (2020) and Tompkins and Haggerty (1985) study were taken as representative samples of the West African kimberlites and compared to the kimberlite, lamproite and Kaapvaal lamproite phlogopite and spinel compositions on Figure 1 & Figure 2. Groundmass phlogopite cores from Tongo display an enrichment in Al_2O_3 and are similar to those seen in archetypal kimberlites (Howarth and Giuliani, 2020). Sympathetic increases in FeO and Al_2O_3 is further observed in the Tongo micas, which is unlike kimberlites or lamproites (Howarth and Giuliani, 2020). An evolution toward tetraferriphlogopite is observed in the Tongo phlogopite rim analyses characterised by an enrichment in FeO and occurs commonly in Kaapvaal lamproites and occasionally in archetypal kimberlites (Howarth and Giuliani, 2020). The Weasua phlogopite compositions contain a lamproitic trend of Al_2O_3 depletion and Fe_2O_3 enrichment (Howarth and Giuliani, 2020).

Spinel trends observed from Tongo consist of an evolution from a chromium-rich (TIMAC) spinel to a magnesio-ulvospinel-magnetite (MUM), which is a diagnostic characteristic of a kimberlitic

spinel (Howarth and Giuliani, 2020). Koidu spinels are also kimberlitic (Tompkins and Haggerty, 1985) with a similar evolution from TIMAC to MUM seen in the Tongo spinels. Spinel trends observed from Weasua consist of an evolution from TIMAC spinel to a magnetite (MAG), which is characteristic of a lamproitic spinel (Howarth and Giuliani, 2020).

2.6.4. Geochemistry

Previous geochemical data was collected from Haggerty (2017), Mathafeng (2021), Skinner et al., (2004) and Taylor et al. (1994) from the Jurassic-aged Koidu and Tongo rocks and from the Neoproterozoic-aged rocks from the Camp Alpha and Weasua region. This data was further compared to other kimberlite, Kaapvaal lamproite and lamproite data worldwide by Mathafeng (2021). Estimates of parental melts for Tongo are K_2O-rich (>3 wt.%) reflecting their micaceous nature and more similar to Kaapvaal lamproites than archetypal kimberlites (Mathafeng, 2021). Major element distributions reveal the rocks to have characteristics of both Kaapvaal lamproite and archetypal kimberlite (Mathafeng, 2021). For example, the average SiO_2 and CaO contents are ~28.2 wt.% and ~12.5 wt.% respectively and are characteristic of archetypal kimberlite. Whereas the average K_2O and Al_2O_3 contents are 3.03 wt.% and 4.08 wt.% respectively and are characteristic of an Kaapvaal lamproite (Table 1). Trace element distributions reveal the Tongo rocks to have characteristics of archetypal kimberlites (Mathafeng, 2021), with Th/Nb < 0.14; Ce/Pb > 22; La/Nb < 1.1 and Ba/Nb < 12. However, the Nb/La and Ce/Sr trace element ratios from Koidu share characteristics from the Aries lamproite (Taylor et al., 1994). Isotopic signatures from the Tongo rocks are also characteristic of archetypal kimberlites and have $^{143}Nd/^{144}Nd$ (i) ratios ranging between 0.5125 and 0.5126, while the $^{87}Sr/^{86}Sr$ (i) ratios range between 0.7038 and 0.7058 (Figure 3) (Mathafeng, 2021).

Chapter 3: Methodology

3.1. Sample selection

The Tongo samples analysed in this study were sections of drill core, received from Newfields resources (Ltd) and were drilled during the exploration phases of the Tongo-Tonguma project. The area consists of several prospective dikes (Figure 7) and a total of 28 samples were obtained from four of these dikes, namely, Kundu (n=4), Lando (n=8), Pandebu (n=1) and Tongo-dike 01 (n=15). These samples were further sectioned and examined. A total of six representative samples were then selected for mineral chemistry analyses, with two chosen from Kundu (TG11-039A and TG11-048), three from Lando (TG12-176, TG12-189 and TG12-190) and one from Pandebu (TG11-049). The Tongo-dike 01 samples were only petrographically examined and not analysed for mineral chemistry as this was previously done by Howarth and Giuliani (2020).
The Koidu samples analysed in this study were thin sections from the collection of Mike Skinner. The Koidu area consists of two kimberlite pipes and several proximal dikes, but, it is not known where the samples were collected from. A total of six samples were sectioned and used for petrographic observations. Based on these petrographical observations two representative samples (Y5770 and Y5774) were further analysed for mineral chemistry.

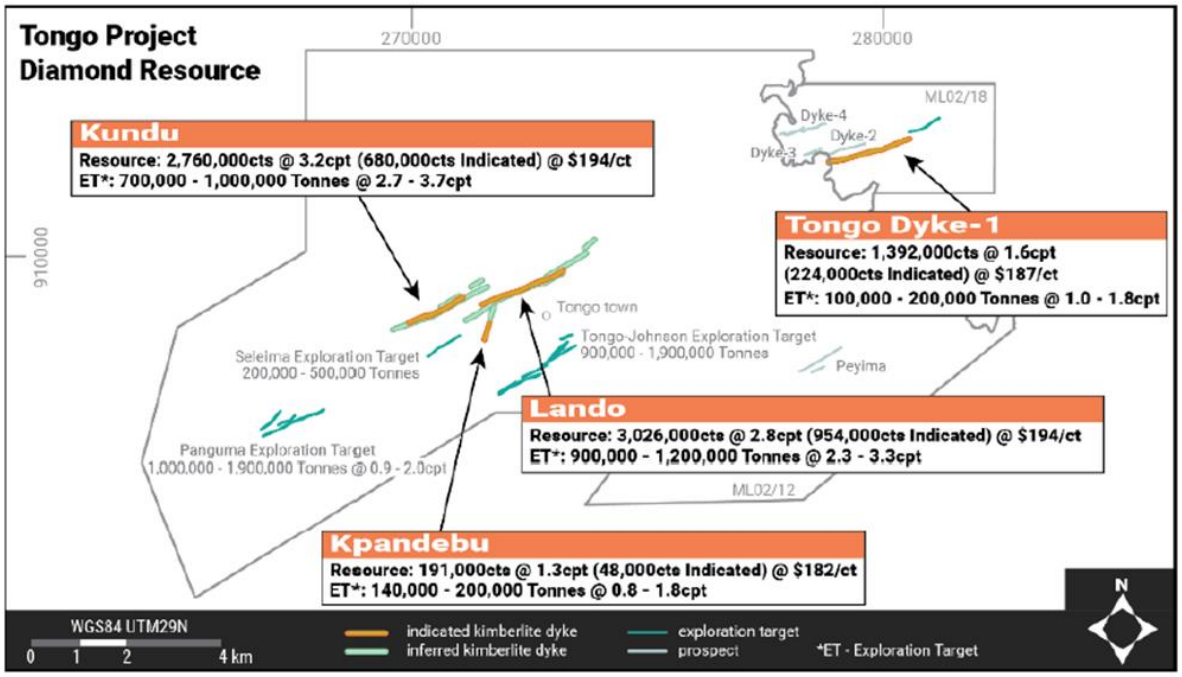

Figure 7: Distribution of the kimberlite dikes located at the Tongo kimberlite cluster (Newfields Resources Limited, 2019).

3.2. Electron microprobe

Electron probe micro analyses (EPMA) of olivine and spinel were conducted at the University of Johannesburg using a Cameca SX-100 microprobe analyser. The analyses were conducted with four wavelength dispersive spectrometers (WDS), with an accelerating voltage of 15 kV, beam

current of 20 nA, and on peak counting times of 30 sec for Na, Mg, Al, Si, K, Ti, Cr, Mn, Fe, Ca, Ni. Natural and synthetic standards include jadeite (Na), olivine (Mg), almandine (Al), diopside (Si), orthoclase (K), wollastonite (Ca), TiO_2 (Ti), Cr_2O_3 (Cr), rhodonite (Mn), hematite (Fe) and NiO (Ni).

The analysis of phlogopite was also done at the University of Johannesburg using a Cameca SX-100 microprobe analyser. The analyses were conducted with four wavelength dispersive spectrometers (WDS), with an accelerating voltage of 15 kV, beam current of 20 nA, and counting times were set to 10-50 s (depending on the element) for F, Cl, Ca, Ba, Mg, Al, Si, K, Ti, Cr, Mn, Fe, Ni. Natural and synthetic standards fluorite (F), NaCl (Cl), wollastonite (Ca), barite (Ba), olivine (Mg), almandine (Al), diopside (Si), orthoclase (K), TiO_2 (Ti), Cr_2O_3 (Cr), rhodonite (Mn), hematite (Fe) and NiO (Ni).

3.3. EPMA cation and spinel FeO and Fe_2O_3 wt.% calculations

The data obtained from the EPMA is presented in oxide weight percent. The following steps are then used to convert this data into the number of cations that are in the final mineral formula:

1. Convert oxide wt.% into molecular proportion of each oxide. This is done by dividing the wt. % of each oxide by the molecular weight of the oxide. This gives the molecular proportion of each oxide.
2. Multiply the molecular proportion for each oxide by the # of oxygen atoms present in each oxide. This gives the O atomic proportion.
3. Sum the O atomic proportion column.
4. Divide the known total # of oxygen (O) atoms per unit cell in the mineral by the sum of the O atomic proportion. This operation gives you a normalization factor.
5. Next, normalize the O atomic proportions from each oxide by multiplying each entry by this normalization factor. This gives the number of anions based on the known number in the mineral formula.
6. Determine the number of cations associated with the oxygens by dividing the number of anions determined in step 5 by the number of oxygens in the reported oxide. The number you obtain is the number of cations that are in the final mineral formula.

FeO obtained from the EPMA is given as a total, which includes both Fe^{2+} and Fe^{3+} cations. To calculate the FeO and Fe_2O_3 as separate oxide weight percentages, the following steps are followed:

A. Based on the mineral chemistry of spinel, the total charge needs to add up to 8 once the total cations have been calculated in step 6 above.

B. If a spinel grain has a variation of Fe^{2+} and Fe^{3+} within the grain, the total charge will be less than 8. The difference in charge, will be the total cation for Fe^{3+}.

C. To calculate the actual cation value for Fe^{2+}, the cation total calculated for Fe^{3+} (step B) needs to be subtracted from the total cation FeO (both Fe^{2+} and Fe^{3+}) calculated in step 5 above.

D. Once the cations are calculated for Fe^{2+} and Fe^{3+}, the corresponding oxide weight percentages need to be calculated.

E. To calculate the new oxide weight percentage for FeO, multiply the molar mass of FeO by Fe^{2+} cation value (step C)/ (Fe^{2+} cation value (step C) + Fe^{3+} cation value (step B)).

F. To calculate the new oxide weight percentage for Fe_2O_3, multiply the molar mass of FeO by Fe^{3+} cation value (step B)/ (Fe^{3+} cation value (step B) + Fe^{2+} cation value (step C)) (1). Then divide the molar mass of Fe_2O_3 by 2*molar mass of FeO (2). Then multiply (1) by (2).

Chapter 4: Results

4.1. Petrography

All samples in this study were selected based on their hypabyssal texture and pyroclastic textured samples were avoided. Modal abundances were calculated using the point count method, with 300 points counted per thin section.

The samples from the Tongo-Tonguma kimberlite cluster are described based on the dike phase from where they were sampled and based on petrographic similarities.

At the end of each description an economic interest rating is allocated based on spinel sizes and olivine abundances. Spinel size represents the time it took for spinel grains in a kimberlite to grow in a magma at low pressures at temperatures >575°C (i.e. the smaller, the better). Sampled diamonds within a kimberlite at a prolonged amount of time at low pressures and temperatures >575^{0}C will thus be detrimental for diamond preservation. Moreover, diamonds are xenocrystic and so olivine macrocrysts are used as a proxy for the amount of xenocrystic material the kimberlite has sampled from the mantle (i.e. the higher the abundance, the better). Therefore, the following criteria from Scott-Smith et al. (2018) has been used to determine economic interest:

- High interest - *>25% macrocryst modal abundance; Spinel grain size <0,07mm.*
- Moderate interest - *~25% macrocryst modal abundance; Spinel grain size >0,07 & < 0,15mm.*
- Low interest - *<25% macrocrysts modal abundance; Spinel grain size >0,15mm.*

4.1.1. Koidu kimberlite (Koidu cluster)

The samples (S0125, S0124, Y5770, Y5774, Y5776 and Y5772) from the Koidu kimberlite cluster are described as a whole, due to the few samples obtained from the area (six) and having no clear petrographic distinction between the samples. The samples from Koidu are all relatively fresh, except sample Y5772, which has olivine grains that are all serpentinized.

The samples are macrocrystic (Figure 8 ab), predominantly consisting of olivine macrocrysts (26-57 vol.%) and two samples (Y5770 and Y5774) containing additional minor phlogopite macrocrysts. Olivine macrocrysts are generally anhedral and subrounded, range in size from 0.5mm to 16mm, and occasionally fragmented/broken. Some olivine macrocrysts are polycrystalline around the margins (Figure 8 c). One sample (Y5770) contains olivine macrocrysts which has a slight preferred orientation, resembling a flow texture. Phlogopite macrocrysts are light brown to colourless, range in length from 0.5 to ~1mm, and are prismatic

with rounded edges. Several garnet macrocrysts were found in one sample (S0125) ranging from 0.5 to 1.5mm in size with occasional kelyphite rims and one larger garnet grain 7mm in size found in sample Y5776.

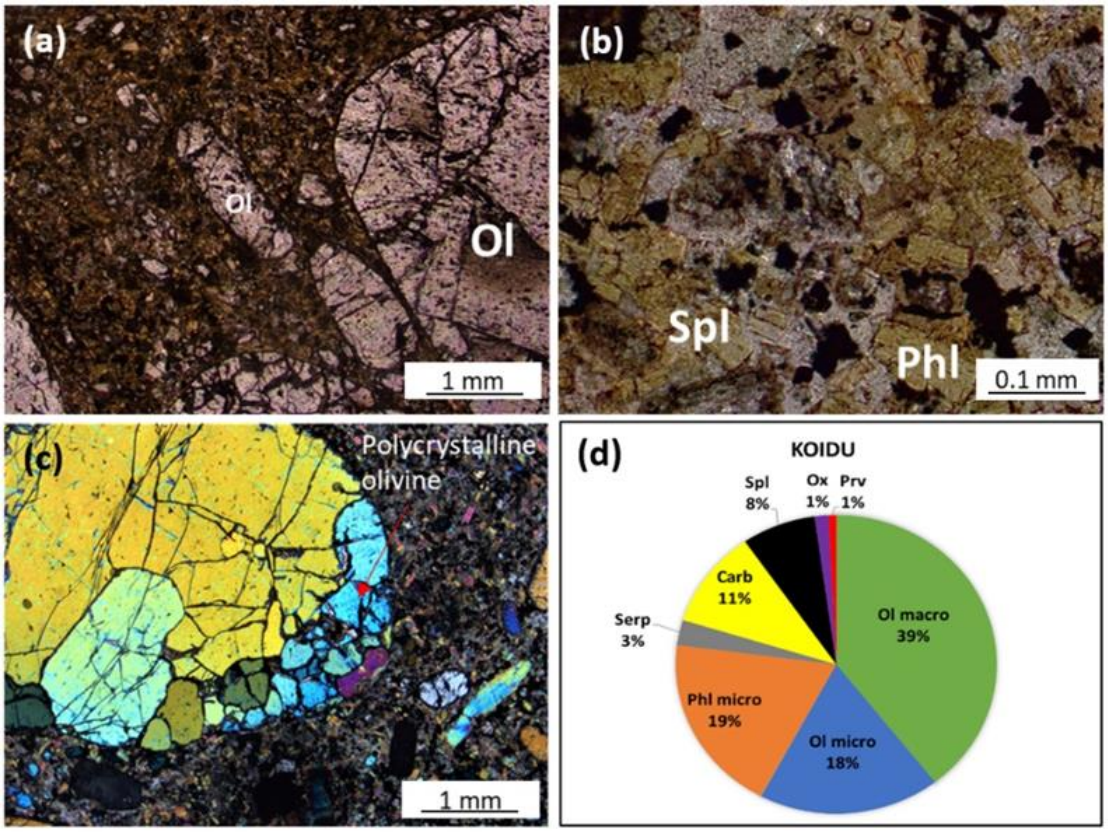

Figure 8: (a) & (b) Photomicrographs under plane polarized light (PPL) of representative samples for Koidu (sample Y5770). (c) Photomicrographs of polycrystalline olivine macrocryst from sample Y5770 (XPL). (d) A pie chart comparison of the various mineral components within the Koidu samples.

The groundmass consists of olivine microcrysts (<0.5 mm), calcite, phlogopite, serpentine, spinel and perovskite (Table 2) (Figure 8 d). Apatite laths are also present in trace amounts in sample Y5774 only. Olivine microcrysts make up 13-24 vol.% of the total modal abundance, are sub-rounded to rounded in shape and are partially altered. Calcite occurs as interstitial material in varying abundances (1-21 vol.%). The calcite contains inclusions of phlogopite, spinel, perovskite and occasionally apatite. Phlogopite occurs as pale orange-brown lath-shaped grains varying in abundance from 14-26 vol.% and ranges in size from 0.05-0.5mm in length. These phlogopite laths often have dark brick red tetraferriphlogopite rims ±0.005-0.05 mm in width (Figure 5B). Serpentine is present in low abundances (1-5 vol.%) as interstitial material. Spinel occurs as euhedral opaque phases distributed in varying abundances (2-14 vol.%) throughout the samples and range in size from 0.03-0.1mm (<0.07mm avg). Atoll-textured spinel is observed in one sample (Y5772). Perovskite occurs as semi-opaque, high relief, dark brown grains and in relatively low abundances (trace-2 vol.%).

Table 2: Summary of mineralogy from the Koidu cluster.

Sample ID	Macrocrysts		Microcrysts		Groundmass
	Ol (vol.%)	Phl (vol.%)	Ol (vol. %)	Phl (vol.%)	
S0125	26	0	17	17	Cc, Spl, Serp, Ox, Prv
S0124	36	0	23	23	Spl, Cc, Serp, Ox
Y5770	57	5	13	15	Cc, Spl, Serp, Ox
Y5774	26	5	24	20	Cc, Spl, Serp, Ox
Y5776	41	1	19	26	Spl, Serp, Ox, Cc, Prv
Y5772	50	0	13	14	Cc, Serp, Spl, Prv, Ox, Ap

*Note: Cc=Calcite, Spl=Spinel, Serp=Serpentine, Ox=Oxides (opaque), Prv=Perovskite, Ap=Apatite

The rock is classified as an olivine macrocryst-rich micaceous coherent kimberlite. Petrographically it is rated as high interest due to the abundance (>25 vol.%) of olivine macrocrysts, the overall size of groundmass spinel (<0.07 mm), and the proven diamond grades from the Koidu kimberlites (Octea limited, 2014).

4.1.2. Kundu kimberlite dike (Tongo-Tonguma cluster)

The Kundu samples (TG11-039A, TG11-048, TG11-042, TG11-039B) are fresh, all containing unaltered olivine macrocrysts.

The samples are macrocrystic (Figure 9 ab), except for sample TG11-39B (only 5 vol.% macrocrysts). Phlogopite macrocrysts are present but are relatively fine-grained (~0.5-1mm) and rare (ranging from one per thin section to <1 vol.%). Olivine macrocrysts make up 5-24 vol.% of the overall abundance. They range in size from 0.5-8mm and are anhedral and rounded. Some olivine macrocrysts are polycrystalline around the margins. Phlogopite macrocrysts are light brown to colourless, range in length from 0.5mm to ~1mm and are prismatic with rounded edges.

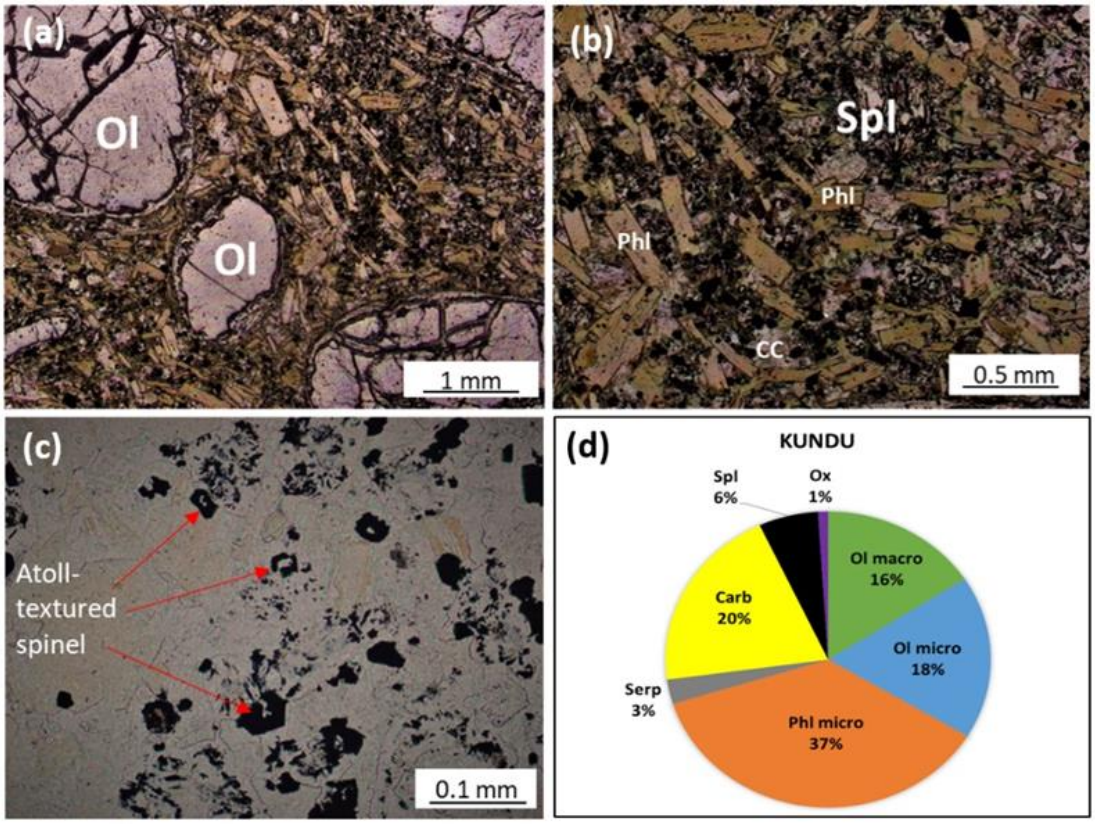

Figure 9: (a) & (b) Photomicrographs under plane polarized light (PPL) of representative samples for Kundu (sample TG11-048). (c) Photomicrographs of atoll textured spinel from sample TG11-048 (PPL). (d) A pie chart comparison of the various mineral components within the Kundu samples.

The groundmass consists of olivine microcrysts, phlogopite, calcite, serpentine, spinel and atoll-textured spinel (excluding sample TG11-039A) (Table 3) (Figure 9 d). The olivine microcrysts are unaltered, occur as rounded to sub-rounded grains and make up 10-28 vol.% of the samples. Phlogopite occurs as pale orange-brown lath-shaped grains varying in abundance from 30-45 vol.% and ranges in size from 0.05-0.5mm in length. Spinel inclusions can often be found within the phlogopite laths. The phlogopite laths often have a dark brick red tetraferriphlogopite rim which is 0.005 mm to 0.05 mm in width. Spinel occurs as euhedral opaque phases distributed in varying abundances (2-11 vol.%) throughout the samples and range in size from 0.01 to 0.06 mm. Atoll-textured spinel is relatively abundant compared to the other locations and is a diagnostic feature of the Kundu samples (Figure 9 c). Both TG11-039A and TG11-039B are samples from the same drill hole, however, TG11-039A does not contain atoll spinel and TG11-039B does. Calcite occurs as interstitial material in varying abundances (11-28 vol.%) and is overall anhedral with occasional 120/60 degree cleavage present in some grains. The calcite contains inclusions of phlogopite, spinel and perovskite. Serpentine is present in low abundances (1-7 vol.%) as interstitial material.

Table 3: Summary of mineralogy from the Kundu dike (Tongo cluster).

Sample ID	Macrocrysts		Microcrysts		Groundmass
	Ol (vol.%)	Phl (vol.%)	Ol (vol. %)	Phl (vol.%)	
TG11-039A	17	0	28	36	Cc, Spl, Ox, Serp
TG11-048	24	0	17	30	Cc, Spl, Serp, Ox
TG11-042	18	0	10	35	Cc, Serp, Spl, Ox
TG11-039B	5	0	17	45	Cc, Spl, Serp, Ox

*Note: Cc=Calcite, Spl=Spinel, Serp=Serpentine, Ox=Oxides (opaque), Prv=Perovskite, Ap=Apatite

The rocks are classified as macrocrystic to aphanitic micaceous coherent kimberlites. Petrographically they are of moderate interest due to the olivine macrocrysts lacking sufficient abundance (5-24 vol.%), however, on average still having >15 vol.% olivine macrocrysts and having sufficiently small (<0.07 mm) spinel grains.

4.1.3. Lando kimberlite dike (Tongo-Tonguma cluster)

The Lando samples (TG12-189, TG12-065, TG12-190 and TG11-004) are macrocrystic and fresh, containing unaltered olivines (Figure 10 ab). Phlogopite macrocrysts are present but are small (~0.5-1mm) and in trace amounts. Olivine macrocrysts are highly variable in abundance, with most ranging from 16-30 vol.%, range in size from 0.5-16mm, sub-rounded to sub-angular, and occasionally fragmented. Sample TG12-176 is an aphanitic variation with only 8 vol.% in olivine macrocrysts, while sample TG11-005 is a macrocrystic variation and contains up to 73 vol.% in olivine macrocrysts. The variability in olivine macrocryst abundance can possibly be a reflection of the degree of flow sorting within the Lando kimberlite dike. Two samples (TG12-189 and TG11-004) have olivine macrocrysts slightly aligned in a preferred orientation. Several olivine macrocrysts are polycrystalline near the margins of the grains. Phlogopite macrocrysts are light brown to colourless, range in length from 0.5mm to 1mm, are well sorted and are prismatic with rounded edges. Several garnet macrocrysts were observed, ranging in size from 1-3mm with one macrocryst containing a kelyphite rim. Several Ilmenite macrocrysts were also observed, all ~1mm in size.

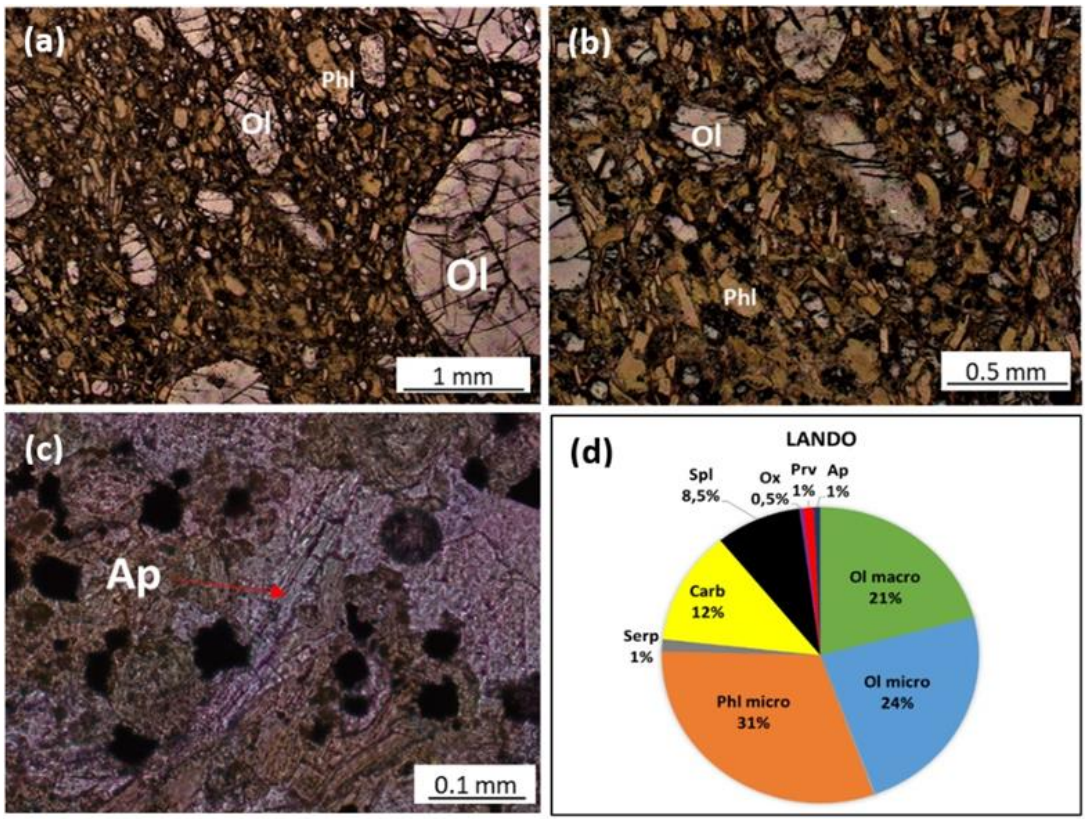

Figure 10: (a) & (b) Photomicrographs under plane polarized light (PPL) of representative samples for Lando (sample TG12-189). (c) Photomicrographs of a groundmass apatite lath from sample TG11-005 (PPL). (d) A pie chart comparison of the various mineral components within the Lando samples.

The groundmass consists of olivine microcrysts, phlogopite, calcite, serpentine, spinel, perovskite and rarely apatite (Table 4) (Figure 10 d). The olivine microcrysts are mostly unaltered, occur as rounded to sub-rounded grains and make up 15-35 vol.% of the samples. Phlogopite occurs as pale orange-brown lath-shaped grains varying in abundance from 29-33 vol.% and ranges in size from 0.05-0.5mm in length. Spinel inclusions can often be found within the phlogopite laths. These phlogopite laths often have a dark brick red tetraferriphlogopite rims which are 0.005 mm to 0.05 mm in width. Spinel occurs as euhedral opaque phases distributed in varying abundances (6-12 vol.%) throughout the samples and ranges in size from 0.01-0.08mm (<0.07 mm avg). Perovskite occurs as semi-opaque, high relief, dark brown grains and low abundances (trace-4 vol.%). One sample (TG11-004) contained 3 vol.% modal abundance of apatite occurring as elongated colorless laths within the groundmass and are 0.1-0.2 mm in length (Figure 10 c). The remaining samples contain no apatite or trace amounts. Calcite occurs as interstitial material in varying abundances (5-17 vol.%) and is overall anhedral. The calcite contains inclusions of phlogopite, spinel and perovskite. Serpentine is present in trace amounts and occasionally up to 2 vol.% as interstitial material.

Table 4: Summary of mineralogy from the Lando dike (Tongo cluster).

Sample ID	Macrocrysts		Microcrysts		Groundmass
	Ol (vol.%)	Phl (vol.%)	Ol (vol.%)	Phl (vol.%)	
TG12-189	19	0	23	30	Cc, Spl, Ox
TG12-065	16	0	24	31	Cc, Spl, Serp, Prv
TG11-020A	30	0	15	31	Cc, Spl, Serp
TG12-176	8	0	21	52	Cc, Spl, Prv, Serp
TG11-005	73	0	9	10	Spl, Cc, Serp, Ox, Prv
TG12-190	19	1	35	29	Spl, Cc, Prv, Serp, Ox
TG11-004	20	0	21	33	Cc, Spl, Ap, Serp, Prv

*Note: Cc=Calcite, Spl=Spinel, Serp=Serpentine, Ox=Oxides (opaque), Prv=Perovskite, Ap=Apatite

The rock is classified as a macrocrystic micaceous coherent kimberlite. Petrographically, it is of moderate to high interest due to the abundance (16-30 vol.%) of olivine macrocrysts (occasionally having >25% of olivine macrocrysts) and having spinel grains that are <0.07 mm in size.

4.1.4. Pandebu kimberlite dike (Tongo-Tonguma cluster)

Only one sample (TG11-049) was obtained from the Pandebu dike. The sample is moderately altered, with some olivine grains completely altered and others only partially altered (Figure 11 ab). The sample contains 11 vol.% olivine macrocrysts. Phlogopite macrocrysts are present in low abundances (<1 vol.%) and are between 0.5-1mm in size. The olivine macrocrysts are subrounded, well sorted and range in size from 0.5-8mm. One olivine macrocryst is polycrystalline.

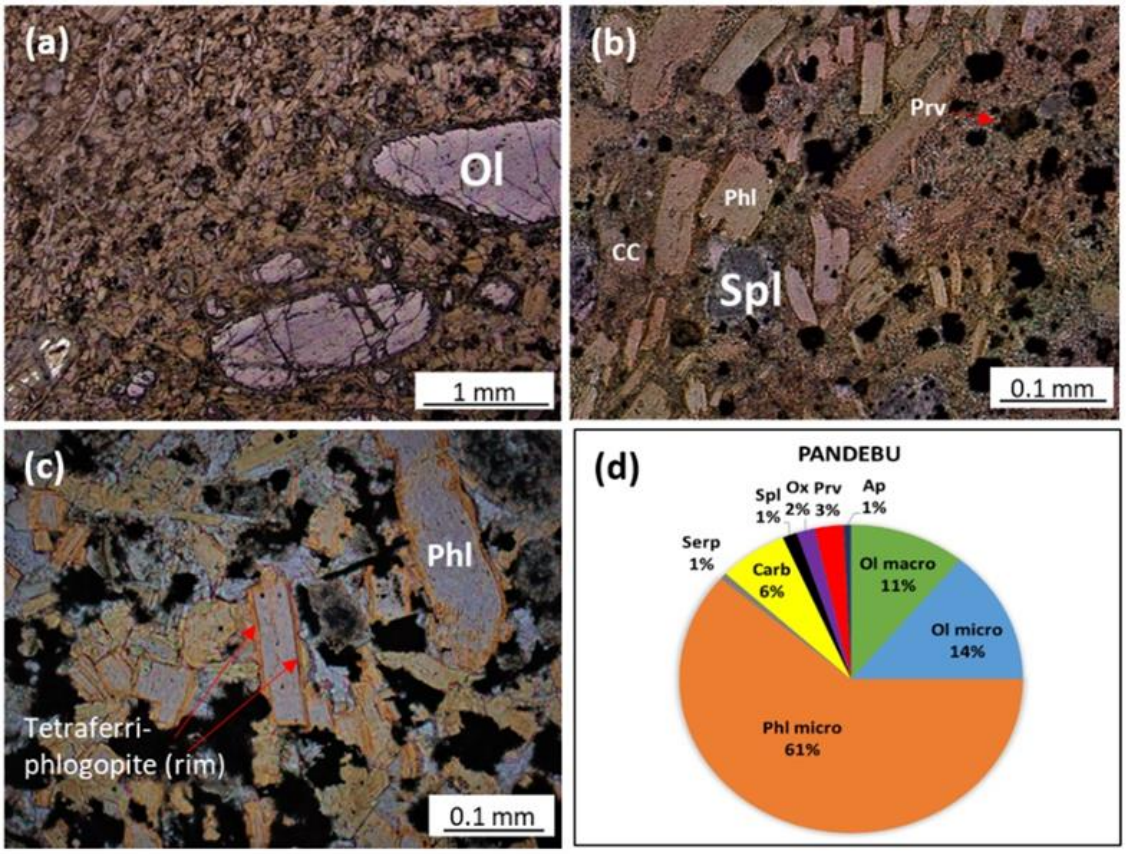

Figure 11: (a) & (b) Photomicrographs under plane polarized light (PPL) of sample TG11-049 from the Pandebu dike. (c) Photomicrographs of a groundmass phlogopite microcrysts from sample Y5770 (PPL). (d) A pie chart comparison of the various mineral components within the Pandebu samples.

The groundmass consists of olivine microcrysts, phlogopite, calcite, perovskite, serpentine, spinel and apatite (Table 5) (Figure 11 d). The olivine microcrysts occur as altered (serpentinized) rounded to sub-rounded grains and make up 14 vol% of the rock. Phlogopite occurs as pale orange-brown lath-shaped grains and makes up 60 vol.% and ranges in size from 0.05-0.5mm in length. These phlogopite laths often have a dark brick red tetraferriphlogopite rims which are 0.005-0.05 mm in width (Figure 11 c). Spinel, perovskite and other oxides can occasionally be found as inclusions within phlogopite laths but are found more frequently surrounding phlogopite laths or as inclusions in the interstitial calcite. An unidentified groundmass oxide occurs as ~0.1mm sized needle-like grains randomly distributed throughout the sample and overall makes up 2 vol.% of the modal abundance. Perovskite occurs as ~0.05mm sized semi-opaque to high relief dark brown grains and makes up 3 vol.% of the sample. Serpentine occurs mostly as trace amounts of interstitial material. Spinel is present in low abundance (1 vol.%) as opaque euhedral grains that range in size from 0.02-0.05mm throughout the sample. Apatite is present as trace amounts, occurs as laths within the groundmass and are 0.1-0.2mm in length. Calcite occurs as interstitial material and makes up 6 vol.% of the sample. The calcite contains inclusions of phlogopite, spinel and perovskite.

Table 5: Summary of mineralogy from the Pandebu dike (Tongo cluster).

Sample ID	Macrocrysts		Microcrysts		Groundmass
	Ol (vol.%)	Phl (vol.%)	Ol (vol.%)	Phl (vol.%)	
TG11-049	11	0	14	60	Cc, Prv, Ox, Spl, Ap, Serp

*Note: Cc=Calcite, Spl=Spinel, Serp=Serpentine, Ox=Oxides (opaque), Prv=Perovskite, Ap=Apatite

The rock is classified as an aphanitic micaceous coherent kimberlite. Petrographically, it is of low interest, due to the low abundance of olivine macrocrysts (11 vol.%).

4.1.5. Tongo kimberlite dike-01 (Tongo-Tonguma cluster)

There are several textural varieties of kimberlite within Tongo dike-01 and they are summarized separately below. The textural varieties mostly have the same essential groundmass mineralogy with olivine microcrysts, phlogopite, calcite, serpentine, spinel, and perovskite all present in various abundances. The descriptions below include macrocrystic features, the textural variety classification and economic importance. The groundmass mineralogy and abundances have been included in separate tables associated with each textural variety. For detailed descriptions of each variety, see Appendix B.

a) Aphanitic variation 1

The Aphanitic variation 1 is only comprised of one sample (TP0101). The sample is very fresh and contains olivines which are all unaltered (Figure 12 a). Olivine macrocrysts make up 5 vol.% (i.e., aphanitic). One 1.5mm in length phlogopite macrocryst lath was observed. The olivine macrocrysts ranges in size from 0.5-4mm and are sub-rounded. They are also aligned slightly in a preferred orientation. The phlogopite macrocryst is light brown and is 2mm in length and is prismatic with rounded edges. The distinctive feature of this variation is the high olivine microcryst and spinel abundances (33 vol.% and 25 vol.% respectively). The rock is classified as an aphanitic olivine microcryst-rich, micaceous coherent kimberlite. Petrographically it is of low interest, due to the very low abundance of olivine macrocrysts (5 vol.%).

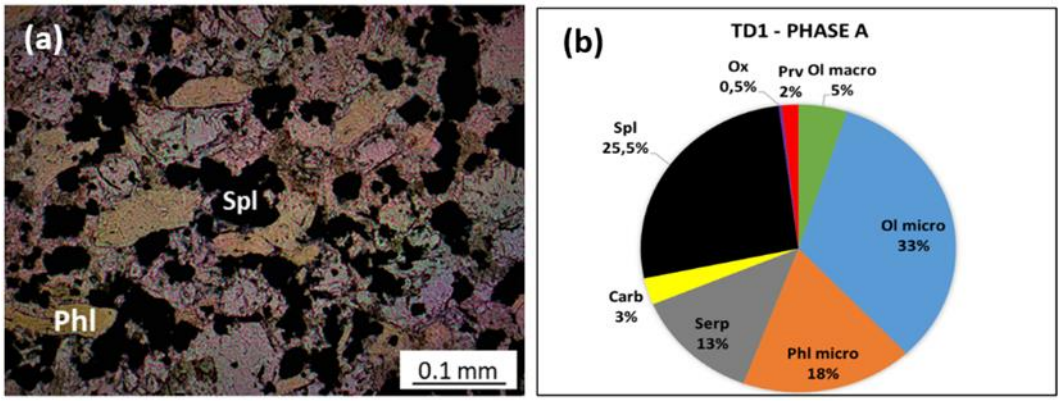

Figure 12: (a) Photomicrograph under plane polarized light (PPL) of sample TP0101 from Tongo dike-01 (phase A). (b) A pie chart comparison of the various mineral components within Phase A of the Tongo-dike 01 samples.

Table 6: Summary of mineralogy from the Aphanitic variation 1, Tongo-dike 01 (Tongo cluster).

Sample ID	Macrocrysts		Microcrysts		Groundmass
	Ol (vol.%)	Phl (vol.%)	Ol (vol. %)	Phl (vol.%)	
TP0101 A	5	0	33	18	Spl, Serp, Cc, Prv, Ox

*Note: Cc=Calcite, Spl=Spinel, Serp=Serpentine, Ox=Oxides (opaque), Prv=Perovskite, Ap=Apatite

b) Aphanitic to macrocrystic variation 1

The Aphanitic to macrocrystic variation 1 consists of three samples (TP0202, TP0812 and TP1014). These samples are relatively fresh, containing fresh unaltered olivine (Figure 13 a), except for sample TP1014, which has altered (serpentinized) olivine. Olivine macrocrysts make up 6-18 vol.% of the modal abundance. Phlogopite macrocrysts are present and more abundant (3 vol.% modal abundance) in TP0812 than the other two samples (trace amounts). The olivine macrocrysts range in size from 0.5-8mm and are sub-rounded. The phlogopite macrocrysts range in size from 0.5-3mm, are elongated, and occasionally rounded. One garnet macrocryst (2mm in size) with a kelyphite rim was also observed. The distinctive feature of this variation is the presence of phlogopite and olivine macrocrysts, however, in low abundances (1 vol.% and 12 vol.% respectively) and having elevated spinel abundances (10 vol.%). The rocks are classified as aphanitic to macrocrystic micaceous coherent kimberlites. Petrographically it is rated as moderate interest due to the lack of sufficient abundance of olivine macrocrysts (6-18 vol.%) but still having sufficiently small spinel grains (<0.07 mm). Sample TP0202, consisting of >15 vol.% olivine macrocrysts, might be of moderate to high interest.

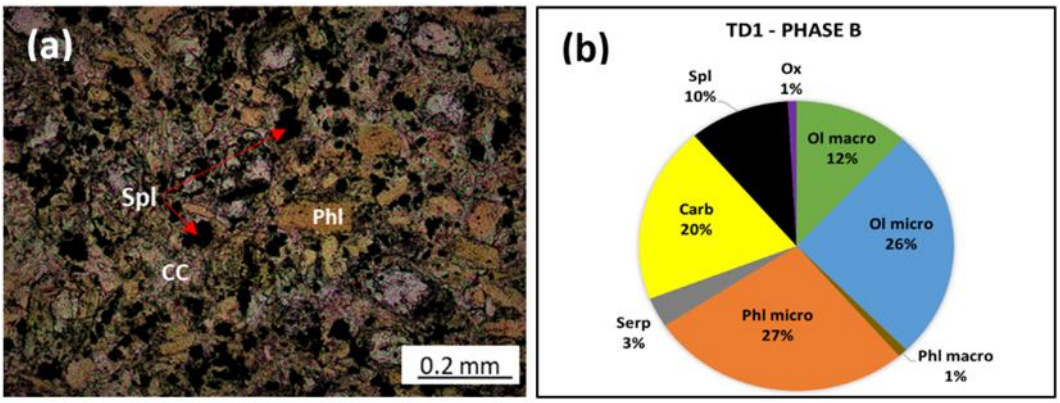

Figure 13: (a) Photomicrograph under plane polarized light (PPL) of sample TP0202 from Tongo dike-01 (phase B). (b) A pie chart comparison of the various mineral components within Phase B of the Tongo-dike 01 samples.

Table 7: Summary of mineralogy from the Aphanitic to macrocrystic variation 1, Tongo-dike 01 (Tongo cluster).

Sample ID	Macrocrysts		Microcrysts		Groundmass
	Ol (vol.%)	Phl (vol.%)	Ol (vol. %)	Phl (vol.%)	
TP0202 B	18	<1	29	21	Cc, Spl, Serp, Ox
TP0812 B	6	3	31	23	Cc, Spl, Serp
TP1014 B	12	<1	18	37	Cc, Spl, Serp, Ox, Prv

*Note: Cc=Calcite, Spl=Spinel, Serp=Serpentine, Ox=Oxides (opaque), Prv=Perovskite, Ap=Apatite

c) *Aphanitic to macrocrystic variation 2*

The Aphanitic to macrocrystic variation 2 consists out of three samples (TP0203, TP0204, TP0509). These samples are all altered, with fresh cores occasionally present (Figure 14 a). Olivine macrocrysts are present in two out of the three samples, with sample TP0203 not containing any olivine macrocrysts. The olivine macrocryst content for the two remaining samples are both 8 vol.%. The olivine macrocrysts present in the two samples range in size from 0.5-8mm, and sub-rounded. No phlogopite macrocrysts were observed. The distinctive feature of this variation is low total olivine abundance (17 vol.%) and the presence of apatite (5 vol.%). The rock is classified as an aphanitic to macrocrystic micaceous coherent kimberlite. Petrographically it is of low interest, due to the very low abundance of olivine macrocrysts (0-8 vol.%).

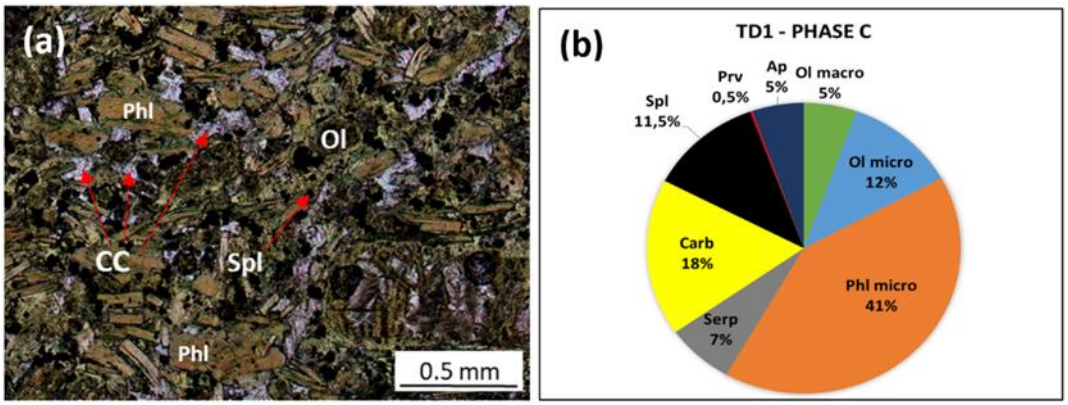

Figure 14: (a) Photomicrograph under plane polarized light (PPL) of sample TP0509 from Tongo dike-01 (phase C). (b) A pie chart comparison of the various mineral components within Phase C of the Tongo-dike 01 samples.

Table 8: Summary of mineralogy from the Aphanitic to macrocrystic variation 2, Tongo-dike 01 (Tongo cluster).

Sample ID	Macrocrysts		Microcrysts		Groundmass
	Ol (vol.%)	Phl (vol.%)	Ol (vol. %)	Phl (vol.%)	
TP0203 C	0	0	8	43	Cc, Ap, Spl, Serp, Prv
TP0204 C	8	0	17	39	Cc, Spl, Serp, Prv
TP0509 C	8	0	10	41	Spl, Cc, Serp, Ap

*Note: Cc=Calcite, Spl=Spinel, Serp=Serpentine, Ox=Oxides (opaque), Prv=Perovskite, Ap=Apatite

d) Aphanitic variation 2

The Aphanitic variation 2 consists out of two altered samples (TP0305, TP1115), containing no fresh olivines (Figure 15 a). The distinctive feature of this variation is the absence of macrocrystic material and the high calcite abundance (30 vol.%). The rock is classified as an aphanitic micaceous coherent kimberlite. Petrographically it is of low interest, due to the not containing any olivine macrocrysts.

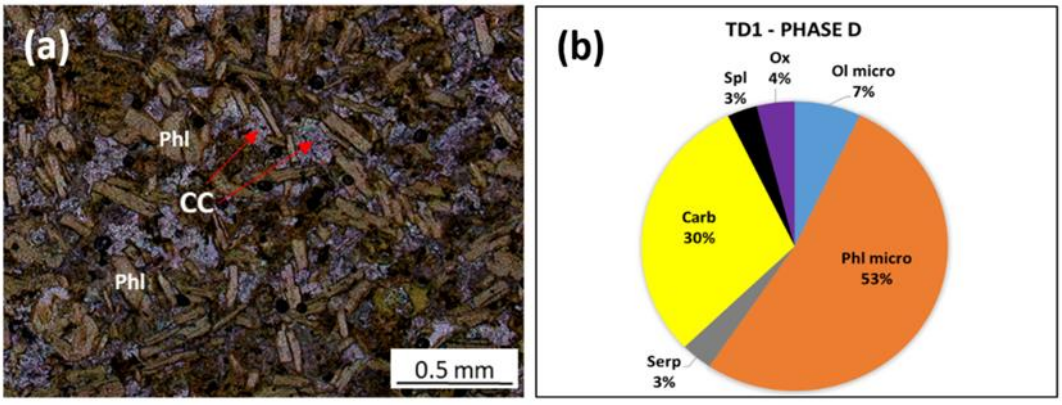

Figure 15: (a) Photomicrograph under plane polarized light (PPL) of sample TP0305 from Tongo dike-01 (phase D). (b) A pie chart comparison of the various mineral components within Phase D of the Tongo-dike 01 samples.

Table 9: Summary of mineralogy from the Aphanitic variation 2, Tongo-dike 01 (Tongo cluster).

Sample ID	Macrocrysts		Microcrysts		Groundmass
	Ol (vol.%)	Phl (vol.%)	Ol (vol. %)	Phl (vol.%)	
TP0305 D	0	0	9	54	Cc, Ox, Spl, Serp, Prv
TP1115 D	0	0	5	50	Cc, Spl, Serp, Spl, Ox

*Note: Cc=Calcite, Spl=Spinel, Serp=Serpentine, Ox=Oxides (opaque), Prv=Perovskite, Ap=Apatite

e) Aphanitic variation 3

The Aphanitic variation 3 consists of three samples (TP0306, TP0307, TP0408, TP0510). All the samples are altered with roughly all olivines serpentinized (Figure 16 a). Olivine macrocrysts make up 5-12 vol.% of the modal abundance. Phlogopite macrocrysts are present in one sample (TP0510) and make up roughly 5 vol.%. The olivine macrocrysts range in size from 0.5-8mm, and are sub-rounded. The phlogopite macrocrysts range in size from 0.5-7mm, are prismatic, and are occasionally rounded. The distinctive feature of this variation is the presence of phlogopite and olivine macrocrysts, however, in low abundance (1 vol.% and 7 vol.% respectively), the low olivine microcryst abundance (7 vol.%) and the presence of apatite (3 vol.%). The rock is classified as an aphanitic micaceous coherent kimberlite. Petrographically it is rated as low interest due to the low abundance of olivine macrocrysts.

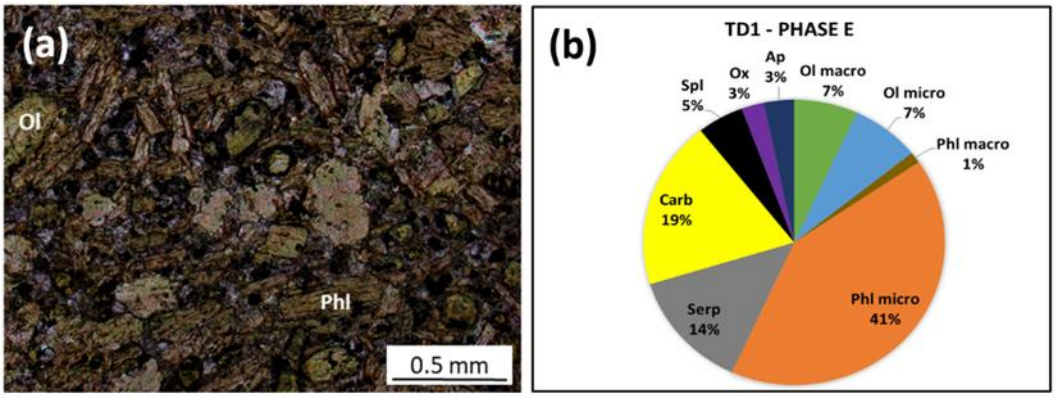

Figure 16: (a) Photomicrograph under plane polarized light (PPL) of sample TP0306 from Tongo dike-01 (phase E). (b) A pie chart comparison of the various mineral components within Phase E of the Tongo-dike 01 samples.

Table 10: Summary of mineralogy from Aphanitic variation 3, Tongo-dike 01 (Tongo cluster).

Sample ID	Macrocrysts		Microcrysts		Groundmass
	Ol (vol.%)	Phl (vol.%)	Ol (vol. %)	Phl (vol.%)	
TP0306 E	12	0	12	46	Cc, Spl, Serp, Ox, Ap
TP0307 E	8	0	0	40	Serp, Cc, Spl, Ox, Ap
TP0408 E	3	0	4	39	Cc, Serp, Ap, Ox, Spl
TP0510 E	5	5	14	41	Spl, Serp, Spl, Ap

*Note: Cc=Calcite, Spl=Spinel, Serp=Serpentine, Ox=Oxides (opaque), Prv=Perovskite, Ap=Apatite

f) Macrocrystic variation

The Macrocrystic variation is only made up of one diagnostic sample (TP1013). The sample is altered and contains olivines which have been altered to serpentine (Figure 17a). Olivine macrocrysts make up 20 vol.% of the sample. The olivine macrocrysts range in size from 0.5-16mm, is moderately sorted and sub-rounded to sub-angular. The distinctive feature of this variation is the olivine macrocryst abundance and size. The rock is classified as a macrocrystic micaceous coherent kimberlite. Petrographically it is rated as moderate to high interest due to the relatively abundant olivine macrocryst content (20 vol.%), and the sufficiently small size of groundmass spinels (<0.07mm).

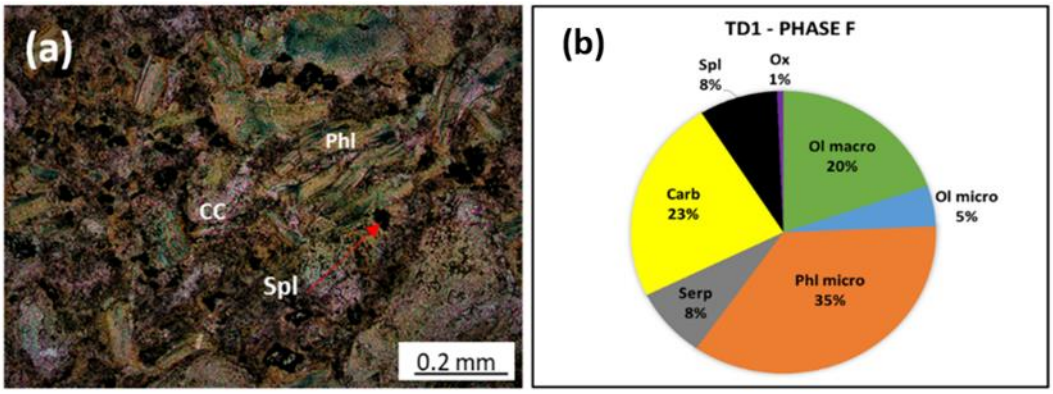

Figure 17: (a) Photomicrograph under plane polarized light (PPL) of sample TP1013 from Tongo dike-01 (phase F). (b) A pie chart comparison of the various mineral components within Phase F of the Tongo-dike 01 samples.

Table 11: Summary of mineralogy from the Macrocrystic variation, Tongo-dike 01 (Tongo cluster).

Sample ID	Macrocrysts		Microcrysts		Groundmass
	Ol (vol.%)	Phl (vol.%)	Ol (vol. %)	Phl (vol.%)	
TP1013 F	20	0	5	35	Cc, Spl, Serp, Ox

*Note: Cc=Calcite, Spl=Spinel, Serp=Serpentine, Ox=Oxides (opaque), Prv=Perovskite, Ap=Apatite

4.2. Mineral chemistry

4.2.1. Phlogopite groundmass chemistry

Groundmass phlogopite in samples from Koidu and Tongo have visually distinct core and rim zones in plane polarized light and backscatter electron (BSE) images (Figure 18 ab). As described in the petrography section, the phlogopite core occurs as pale orange-brown lath-shaped grains. These phlogopite grains occasionally have dark brick red rims. These distinct core and rim zones are not present in all samples.

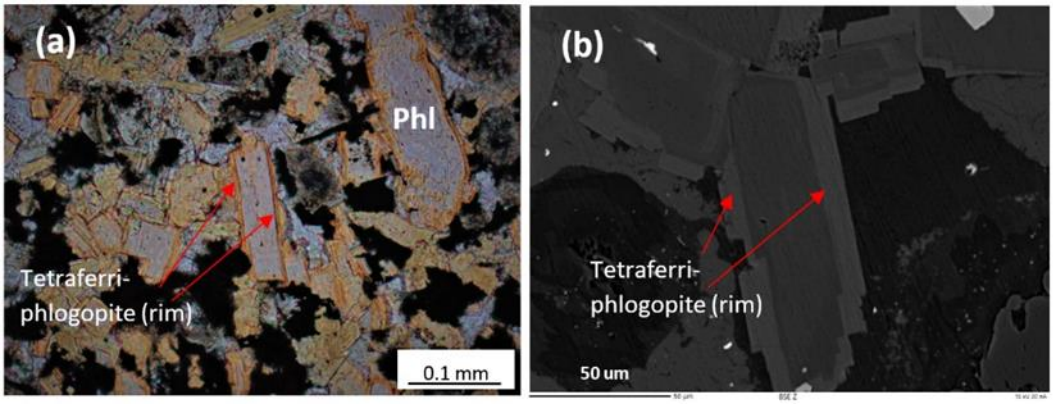

Figure 18: Groundmass phlogopite grains with tetraferriphlogopite rims. (a) A plane polarized light under a microscope. (b) A backscatter image from an electron microprobe.

Groundmass phlogopite was analysed in two representative samples (Y5770 and Y5774) from the Koidu cluster (n=26 analyses) and three representative samples (TG11-039A, TG12-176 and TG12-190) from the Tongo cluster (n=51analyses). Within the Tongo kimberlite cluster, samples TG11-039A and TG12-176 are derived from the Lando dike, while sample TG12-190 is derived from the Kundu dike. The results are displayed in Figure 19 and the full dataset is given in the supplemental online material (SOM) and Appendix C. Howarth and Giuliani (2020) collected data from Tongo dike-01 and is also displayed on Figure 19.

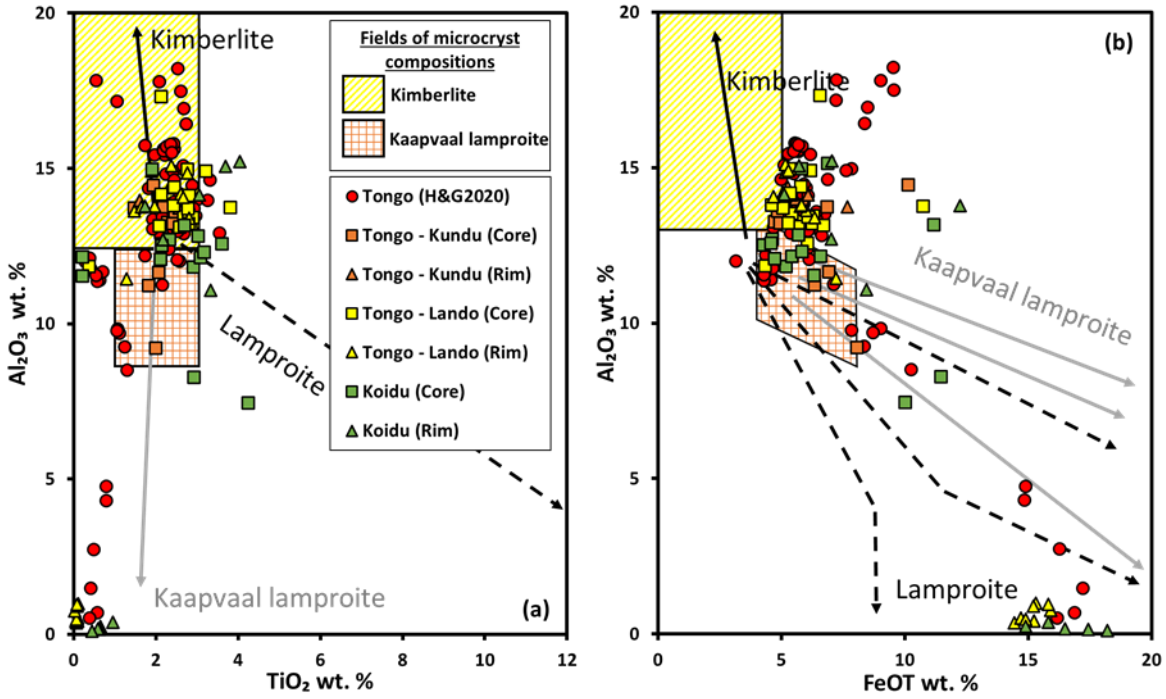

Figure 19: Phlogopite covariation plots with plotted Tongo and Koidu EPMA data and each associated field labelled. The data fields are derived from Mitchell (1995). The Tongo data is represented by groundmass phlogopite analyses done within samples from Lando (TG11-039A & TG12-176) and a sample from Kundu (TG12-190). The Koidu data is represented by groundmass phlogopite analyses done from samples Y5770 and Y5774. The axes of variation plot (a) is defined by Al_2O_3 (wt%) vs TiO_2 (wt%) and the axes of variation plot (b) is defined by Al_2O_3 (wt%) vs FeOT (wt%). H&G2020 – refers to the data from Howarth and Giuliani (2020).

a) Koidu

Two distinct compositions are observed, which represent the core and the dark brick red rims of the phlogopite grains. The core compositions for Koidu are relatively the same between analyses, while the dark brick red (tetraferriphlogopite) rim compositions are only observed in Y5770. The core composition is defined by Al_2O_3 (8-15 wt%), TiO_2 (<1-4 wt%) and FeO (4-12 wt%). The tetraferriphlogopite composition is defined by Al_2O_3 (<1 wt%), TiO_2 (<1 wt%) and FeO (15-19 wt%). The Mg# value for the cores range from 74 to 90 and has a positive correlation with both Al_2O_3 and TiO_2.

b) Tongo

The same distinct core and rim compositions observed in the Koidu phlogopites are also present in Tongo. The core composition overlaps with all three samples, while the dark brick red rim composition is only observed in TG12-176. The core composition in Tongo is defined by Al_2O_3 (9-15 wt%), TiO_2 (<1-4 wt%) and FeO (4-11 wt%). The dark brick red rim composition is defined by Al_2O_3 (<1 wt%), TiO_2 (<<1 wt%) and FeO (14-16 wt%). The Mg# for the cores range from 75 to 91 and has a positive correlation with both Al_2O_3 and TiO_2.

4.2.2. Spinel chemistry

Spinel grains from Koidu and Tongo have visually distinct core and rim zones when viewed in BSE images. As seen in Figure 20, these zones are distinct in shades of grey, which translates to the concentration of FeO present within each zone. The higher the FeO content, the lighter the shade of grey. These distinct core and rim zones are not present in all spinel grains.

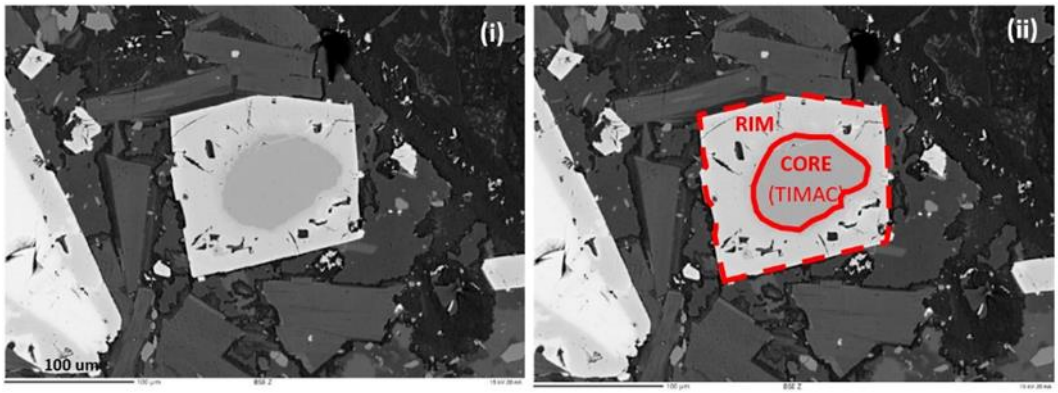

Figure 20: An electron microprobe backscatter image of a zoned spinel grain from sample TG11-048 (Tongo – Kundu). Image (i) is the unedited version and image (ii) is the edited version, highlighting the core region (TIMAC) and the rim region (MUM) of the spinel grain.

Spinels were analysed from one representative sample from Koidu (Y5770) and three representative samples from Tongo, including a representative sample from Kundu (TG11-048), Lando (TG12-189) and Pandebu (TG11-049). Spinel data from Tongo dike-01 was also added from Howarth and Giuliani (2020). The results are displayed in Figure 21 and the full dataset is given in the supplemental online material (SOM) and Appendix C.

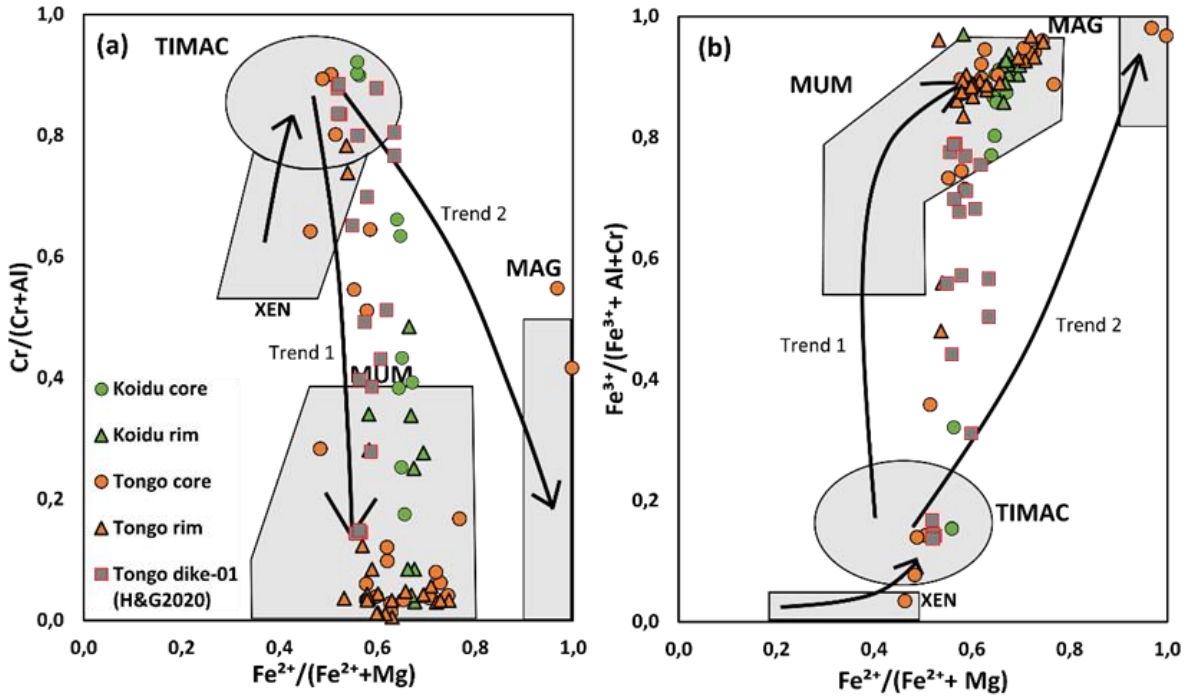

Figure 21: Spinel covariation plots with plotted Tongo and Koidu EPMA data and each associated field labelled. The Tongo data is represented by spinel analyses done within samples TG11-048, TG11-049 and TG12-189. The Koidu data is represented by spinel analyses done within sample Y5770. The axes of variation plot A is defined by Cr/(Cr+Al) vs $Fe^{2+}/(Fe^{2+}+Mg)$ and the axes of variation plot B is defined by $Fe^{3+}/(Fe^{3+}+Al+Cr)$ vs $Fe^{2+}/(Fe^{2+}+Mg)$.

a) Koidu

The core zones range in composition from 0.6 to 47.2 wt% for Cr_2O_3, 9.8 to 32.9 wt% for Fe_2O_3 and 21.3 to 33.2 wt% for FeO. The rim zones range in composition from 0.1 to 2.4 wt% for Cr_2O_3, 31.6 to 53.5 wt% for Fe_2O_3 and 20.0 to 32.4 wt% for FeO. When displaying the data on a Cr/(Cr+Al) vs $Fe^{2+}/(Fe^{2+}+Mg)$ diagram and a $Fe^{3+}/(Fe^{3+}+Al+Cr)$ vs $Fe^{2+}/(Fe^{2+}+Mg)$ diagram, a distinct trend is seen between the core and rim data (Figure 21). Three core zones plot within the titanium magnesian aluminous chromite (TIMAC) field. The remaining core analyses plot within the evolutionary field to lower Cr_2O_3 and higher Fe_2O_3 proportions relative to FeO (n=3) or plot within the magnesio- ulvöspinel-magnetite (MUM) field (n=4). The majority of the rim analyses (n=9) plot within the MUM field. The remaining rim analyses (n=1) plot within the evolutionary field to lower Cr_2O_3 and higher Fe_2O_3 proportions to FeO.

b) Tongo

The core zones range in composition from 0.1 to 48.84 wt% for Cr_2O_3, 2.8 to 63.8 wt% for Fe_2O_3 and 17.1 to 42.5 wt% for FeO. The rim zones range in composition from 0.1 to 18.9 wt% for Cr_2O_3, 23.5 to 57.0 wt% for Fe_2O_3 and 14.0 to 33.9 wt% for FeO. The data from the Tongo dikes display an overall similar composition and core-rim trend to those analysed from Koidu. Three core zones analysed plot within the TIMAC field. One grain plots in the xenocrystic (XEN) field and an additional two plot in or near the magnetite (MAG) field. The remaining core analyses plot within the evolutionary field to lower Cr_2O_3 and higher Fe_2O_3 proportions to FeO (n=3) or plot within the MUM field (n=15). The majority of the rim analyses (n=17) from Tongo plot within the MUM field. The remaining rim analyses (n=2) plot within the TIMAC field and XEN field.

4.2.3. Olivine major/ minor element chemistry

Olivine microcrysts and macrocrysts were analysed from representative samples from the various dikes (Kundu, Lando and Pandebu) within Tongo and from representative Koidu samples. In total 324 analyses were completed, 73 analyses from Koidu (two samples; Y5770 and Y5774), 79 analyses from Kundu (two samples; TG11-039A and TG11-048), 150 analyses from Lando (three samples; TG12-176, TG12-189 and TG12-190) and 22 analyses from Pandebu (one sample; TG11-049). The complete results are presented in the SOM and Appendix C.

The olivine grains from within each of these samples display distinct core and rim zones and occasionally some have more complex zoning patterns with additional internal and rind zones (Figure 22). The core zone, when present, is located in the center of the grain (Figure 22 abc), while the rim zone surrounds the core zone (Figure 22 a). When an internal zone is present, it is located between the core and rim zones (Figure 22 b). Rim zones can sometimes have additional evolved zones known as rind zones, these zones surround the original rim zone when present (Figure 22 c).

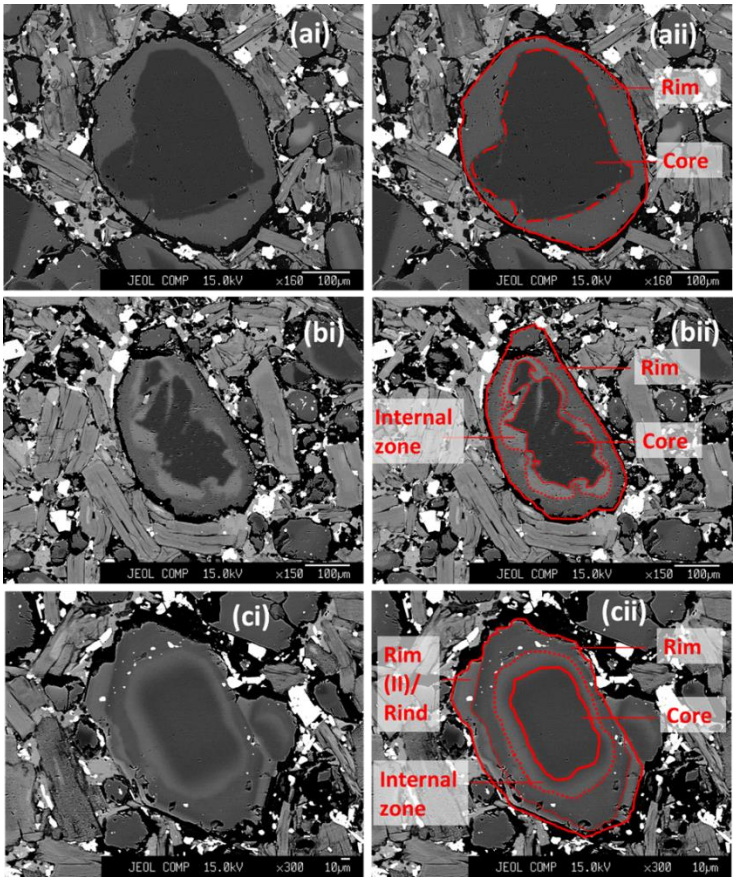

Figure 22: Backscatter imagery from sample TG12-190 (Lando) displaying the various occurrences of a zoned olivine grain. (a) A simple core and rim zoned olivine grain. (b) A more complicated zoned olivine grain with a core, internal and rim zone. (c) The most complexly zoned olivine grain in the study area, consisting of a core, internal, rim and an additional unspecified olivine zone.

a) Koidu

The composition of olivine cores are homogenous but contains inter-grain variation, i.e. there is no compositional difference within any given core zone from a single grain and differences only occur when comparing core zones between different grains. The analysed cores have Fo contents that ranges from Fo 84.7 to Fo 94.5 (n = 30; Figure 23 a). The correlation between Ni (2300 to 4200 ppm) and Fo content is positive, while the Mn (700 to 1600 ppm) to Fo content correlation is negative. No distinct correlation is observed between Ca (100 to 600 ppm) and Fo content as the Ca concentrations are consistently low.

Olivine rim zones display homogenous Fo compositions within individual samples but contain a slight difference in Fo content between the two samples analysed. Sample Y5770 has a mean Fo content of (±2sd) 87.1 ±0.6 (n = 23; Figure 23 a) and sample Y5774 has a mean Fo content of (±2sd) 88.3 ±0.5 (n = 19). Sample Y5770 displays decreasing Ni (3700 to 1800 ppm) and increasing Mn (1100 to 2100 ppm) and Ca (200 to 1500 ppm), while sample Y5774 similarly displays decreasing Ni (3100 to 1700 ppm) and increasing Mn (1100 to 1600 ppm) and Ca (300 to 600 ppm) towards the grain margin.

b) Kundu

As with the analysed Koidu olivine cores, the individual core zones are observed to have homogenous compositions, whereas the heterogeneity in composition occurs between the various grains. The analysed cores have a Fo content that ranges from Fo 83.2 to Fo 93.4 (n = 40; Figure 23 b). The correlation between Ni, Mn and Ca concentrations to Fo content is similar to the previously analysed Koidu core zones. The correlation between Ni (920 to 4300 ppm) and Fo content is positive, while the Mn (700 to 2090 ppm) to Fo content correlation is negative. No distinct correlation is observed between Ca (below detection limit to 440 ppm) and Fo content as the Ca concentrations are consistently low.

The rim zones display homogenous Fo compositions throughout all the samples analysed. Sample TG11-039A has a mean of (±2sd) 88.6 ±0.6 (n = 18) and sample TG11-048 has a mean of (±2sd) 88.8 ±0.6 (n = 8; Figure 23 b). The rim zones from Kundu display decreasing Ni (3800 to 2600 ppm) and an increasing Mn (1100 to 1800 ppm) and Ca (100 to 1000 ppm) towards the grain margin.

The internal zones display homogeneous Fo compositions with a mean of (±2sd) 86.1 ± 0.4 (n = 10; Figure 23 b). The Mn (1600 to 2000 ppm) concentrations follow a decreasing trend and the Ni (2300 to 3100 ppm) and Ca (200 to 500 ppm) concentrations follow an increasing trend towards the grain margin.

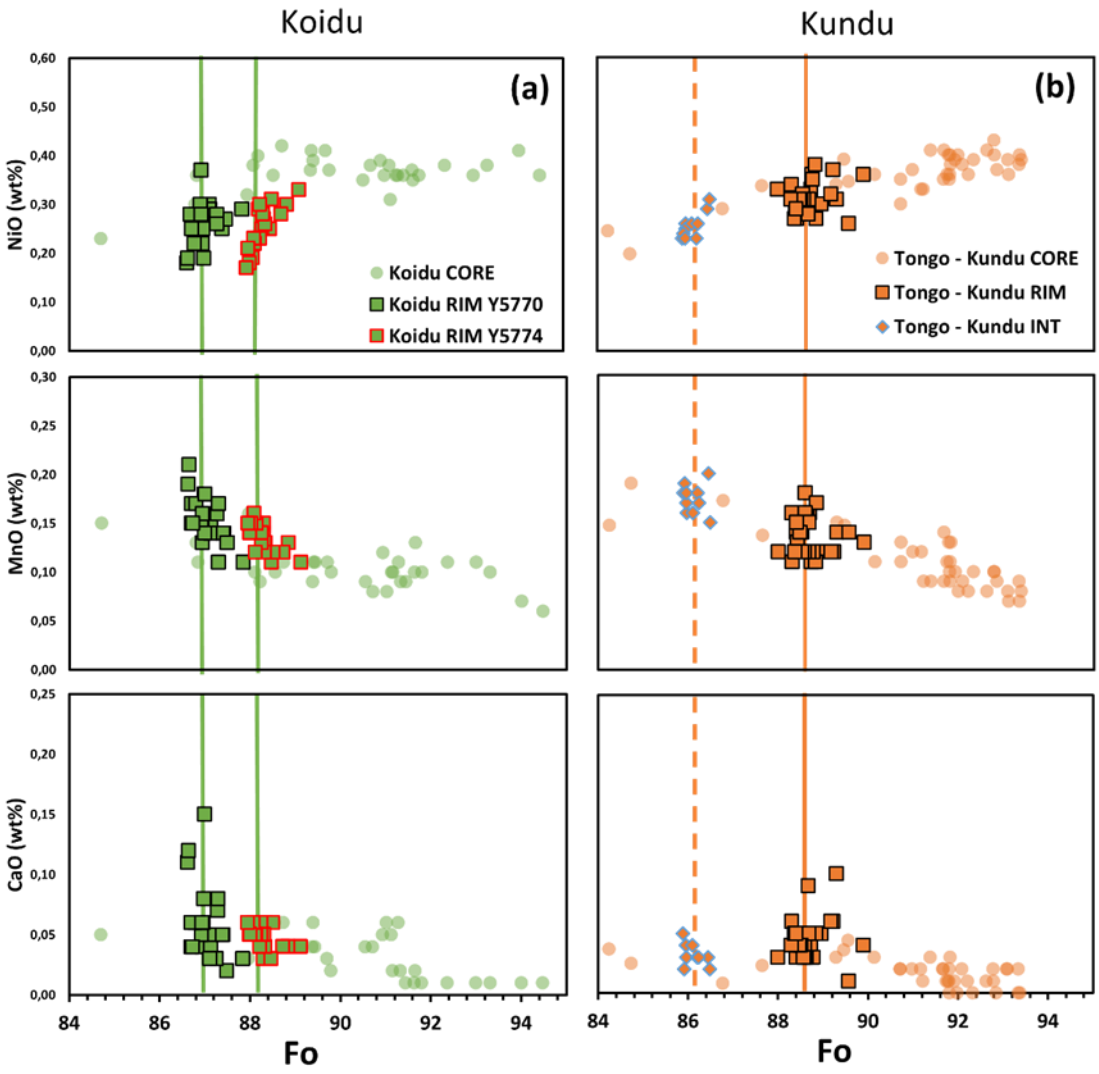

Figure 23: Fo vs NiO, MnO and CaO (wt%) covariation plots of olivine EPMA data. a) Koidu olivine core and rim analyses from samples Y5770 and Y5774. b) Tongo – Kundu olivine core and rim analyses from samples TG11-048 and TG11-039A. The solid lines are aligned on the average olivine rim Fo composition and the dashed line aligned on the average olivine internal zone Fo composition.

c) Lando

As with the previous samples, a similar observation of a homogeneous composition in individual cores and variable inter-grain compositions was observed when analysing the olivine grains from the Lando dike. The analysed cores have a Fo content that ranges from Fo 84.3 to Fo 94.0 (n = 35; Figure 24 a). This is coupled with the same trends observed in Ni, Mn and Ca concentrations to Fo content compared to the previously analysed Kundu and Koidu samples. The correlation between Ni (1500 to 4500 ppm) and Fo content is positive, while the Mn (600 to 1900 ppm) to Fo content correlation is negative. No distinct correlation is observed between Ca (below detection limit to 800 ppm) and Fo content as the Ca concentrations are consistently low.

The rim zones display homogenous Fo compositions throughout all the samples analysed. Sample TG12-176 has a mean of (±2sd) 89.4 ±0.9 (n = 29), sample TG12-189 has a mean of (±2sd) 88.8

±1.1 (n = 14) and sample TG12-190 has a mean of (±2sd) 89.0 ±0.6 (n = 53; Figure 24 a). A similar trend in Ni, Mn and Ca concentrations is observed compared to the previously analysed rim zones. This trend includes a decreasing Ni (4000 to 1300 ppm) and an increasing Mn (1000 to 2300 ppm) and Ca (100 to 1800 ppm) towards the grain margin.

Additional to the core and rim zones, sample TG12-190 from the Lando dike consists of olivine grains with internal and rind zones. Internal zones were further additionally analysed in TG12-176 from the Lando dike, with no rind zones observed.

The internal zones display homogeneous Fo compositions with a mean of (±2sd) 85.7 ±1.0 (n = 13; Figure 24 a). A similar trend in Ni, Mn and Ca concentrations is observed compared to previously analysed rim zones. The Mn (1200 to 1900 ppm) concentrations follow a decreasing trend and the Ni (1800 to 2700 ppm) and Ca (300 to 1200 ppm) concentrations follow an increasing trend.

The rind zones display homogeneous Fo compositions with a mean of (±2sd) 86.9 ±0.6 (n = 3; Figure 24 a). No distinct trend in Ni, Mn and Ca could be extrapolated due to the low number of analyses. However, the Ni (2200 to 2500 ppm) concentrations are overall lower compared to the previously analysed rim and core zones, whereas the Mn (2300 to 2600 ppm) and Ca (1500 to 2200 ppm) concentrations are overall higher compared to the previously analysed core, rim and internal zones.

d) Pandebu

The olivine cores in the Pandebu dike display the same variation in composition between the grains while having homogenous core compositions. The analysed cores have a Fo content that ranges from Fo 90.4 to Fo 94.7 (n = 15; Figure 24 b). The correlation between Ni (3300 to 4300 ppm) and Fo content is positive, while the Mn (600 to 1100 ppm) to Fo content correlation is negative. No distinct correlation is observed between Ca (100 to 700 ppm) and Fo content as the Ca concentrations are consistently low.

The rim zones display relatively homogeneous Fo compositions with a mean of (±2sd) 89.4 ±1.6 (n = 7; Figure 24 b). Although only seven analyses were done, a similar trend to the previously analysed olivine rims can be seen in the Ni, Mn and Ca concentrations. This trend includes a

decreasing Ni (3900 to 2100 ppm) and an increasing Mn (1100 to 1700 ppm) and Ca (400 to 1200 ppm) towards the grain margin.

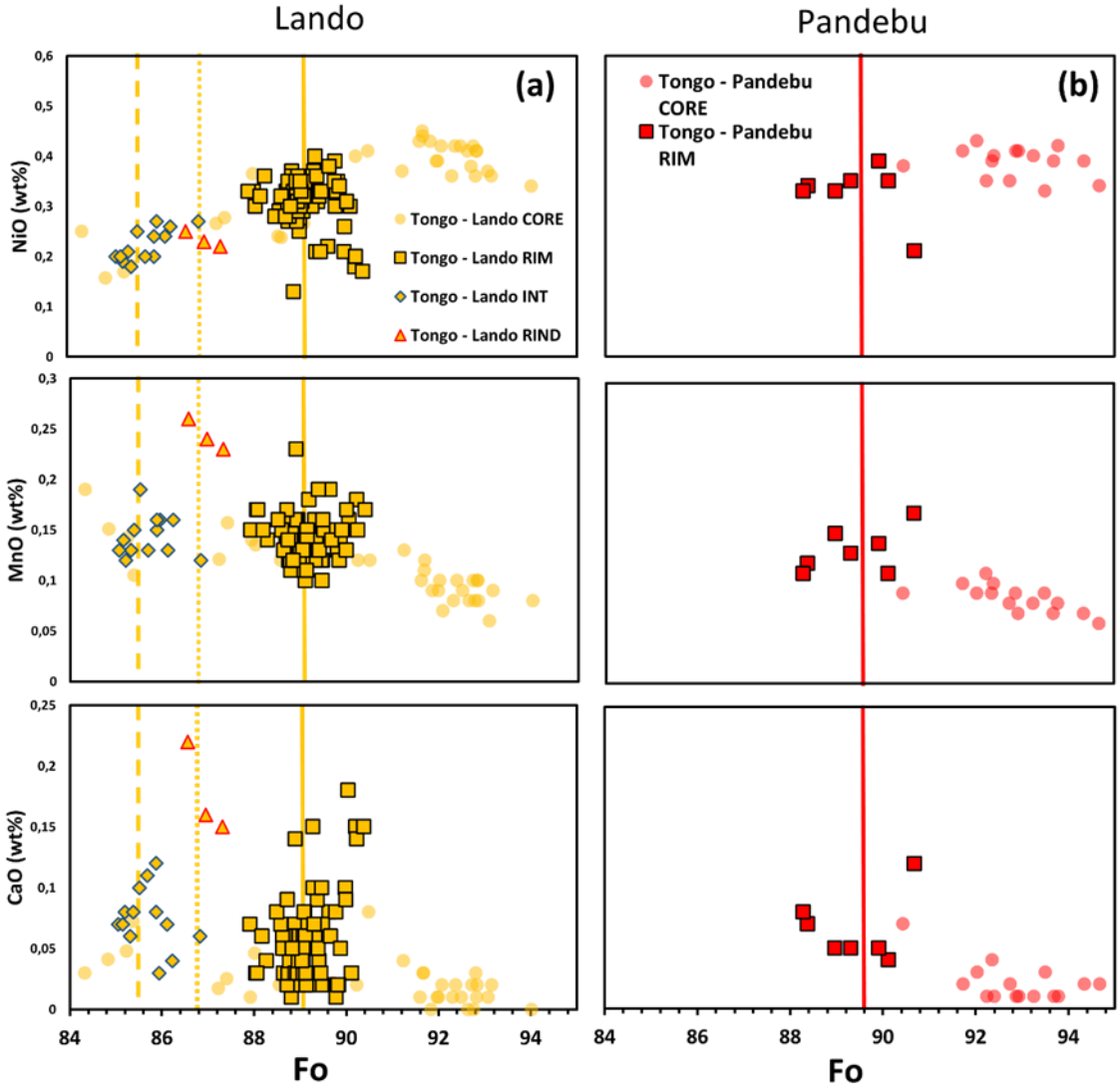

Figure 24: Fo vs NiO, MnO and CaO (wt%) covariation plots of olivine EPMA data. a) Tongo – Lando olivine core, rim, internal and rind analyses from samples TG12-176, TG12-189 and TG12-190. b) Tongo – Pandebu core and rim analyses from sample TG11-049. The solid lines are aligned on the average olivine rim Fo composition, the dashed line aligned on the average olivine internal zone Fo composition and the dotted line aligned on the average rind zone Fo composition.

Chapter 5: Discussion

5.1. Classification

Classifying rocks correctly is important for future observers to identify them easier. Further, the classification of a rock is often linked to a certain petrogenetic history and so when rocks get misclassified an incorrect interpretation of it's history is also implied.

In the next section, the mineralogy and mineral chemistry of the Koidu and Tongo rocks will be discussed and compared to archetypal kimberlites and lamproites elsewhere and a final classification will be determined. This will further be compared to bulk-rock geochemistry data derived from the Tongo area.

5.1.1. Mineralogy

The Koidu and Tongo mineral assemblage is made up of primary olivine, phlogopite, tetraferriphlogopite, spinel, perovskite, apatite and calcite. Phlogopite is abundantly present and ranges between 20-60 vol.% of the samples. The upper end of the phlogopite abundance range, however, is much higher than previously reported for any kimberlite and fall in the range observed in Kaapvaal lamproites/lamproites worldwide. This favours a K_2O-rich parent magma similar to the parent magmas of Kaapvaal lamproites/lamproites. However, these rocks do not contain any characteristic minerals observed in lamproites, but they do contain calcite, which is consistent with the absence of lamproite phases such as richterite, sanidine and leucite. Further, the mineral assemblage in Koidu and Tongo is consistent with mineral phases and phlogopite abundances seen in both phlogopite-rich kimberlites and unevolved Kaapvaal lamproites and technically could be classified as either. Thus, based on mineralogy alone the classification of these rocks is ambiguous.

The mineralogy of an archetypal kimberlite includes the presence of primary olivine, phlogopite, spinel, perovskite, monticellite, apatite and calcite (Mitchell, 1995, 1986), while lamproite are defined as having primary phlogopite, tetraferriphlogopite, K-richterite, leucite, diopside, sanidine, priderite, jeppeite, davanite, wadeite and shcherbakovite. Additional characteristics of lamproites include the absence of primary calcite and the occasional occurrence of olivine, spinel, apatite and perovskite (Mitchell and Bergman, 1991). Similarities between the two overlap with the primary mineral phases found in an unevolved Kaapvaal lamproite and includes the presence of phlogopite, olivine, spinel, apatite and perovskite. Further, unevolved Kaapvaal lamproites occasionally contain monticellite, lack diopside and contain primary calcite (Howarth et al., 2011; Mitchell, 1995). Thus, there are circumstances where an archetypal kimberlite could also be classified as an unevolved Kaapvaal lamproite and vice versa. However, differences between

archetypal kimberlites and unevolved Kaapvaal lamproites are most notable in the phlogopite abundances. Archetypal kimberlites commonly have modal abundances that range between 0 and ±10 vol.%, while Kaapvaal lamproites have modal abundances ranging from ±30 to 90 vol.% (Mitchell and Bergman, 1991). Yet, there are examples ofphlogopite-rich kimberlites that have phlogopite abundances that overlap with abundances observed in unevolved Kaapvaal lamproites. These phlogopite-rich kimberlites commonly range from ±10 to 30 vol.% in phlogopite abundance and can thus appear petrographically similar to the unevolved Kaapvaal lamproites. These micaceous kimberlites have been studied in the following locations: P-13 kimberlite, Kimberley cluster (Ramokgaba et al., 2021), Jagersfontein (South Africa; Taylor and Kingdom, 1999), the Kaalvallei cluster (South Africa; Lim et al., 2018), South Brazilia fold belt (Brazil; Lim et al., 2018), Letseng (Lesotho; Stamm et al., 2018), the Mayeng kimberlite sills (South Africa; Apter et al., 1984) Kuusamo (Finnish; Dalton et al., 2019) and the Leicester transitional kimberlite (South Africa; Becker et al., 2007).

5.1.2. Phlogopite and spinel composition

Phlogopite chemistry is useful in discriminating between kimberlites and lamproites based on Al_2O_3, TiO_2 and FeO (T) content with a greater evolution towards low Al_2O_3 and TiO_2 and elevated FeO (T) commonly observed in the latter (Figure 25). Based on Al_2O_3 and TiO_2 contents the Koidu and Tongo phlogopite core analyses mostly plot within the kimberlitic field whereas the rim analyses evolve to tetraferriphlogopite or occasionally plot within the kimberlitic field. Further, Al_2O_3 and FeO(T) contents display an unusual increase in both Al_2O_3 and FeO(T), similar to previously analysed Tongo phlogopites and some Finnish kimberlite phlogopites. Some core Al_2O_3 and FeO(T) values plot within the Kaapvaal lamproite field whereas some rim compositions evolve to tetraferriphlogopite, consistent with Kaapvaal lamproites, Finnish kimberlites and Indian lamproites (Shaikh et al., 2019). The Koidu and Tongo phlogopite compositions are overall similar to Finnish kimberlites (Dalton et al., 2020) and previously analysed Tongo samples (Howarth and Giuliani, 2020). Tetraferriphlogopite is more common in Kaapvaal lamproites but are also observed in rare cases for micaceous kimberlites (e.g., Mitchell, 1995; Taylor and Kingdom, 1999). Thus, the Koidu and Tongo phlogopite compositions contain both characteristics of kimberlite and lamproite, however, due to the majority displaying an overall increase in Al_2O_3 and TiO_2 the phlogopite compositions are more aligned with kimberlite as opposed to lamproite.

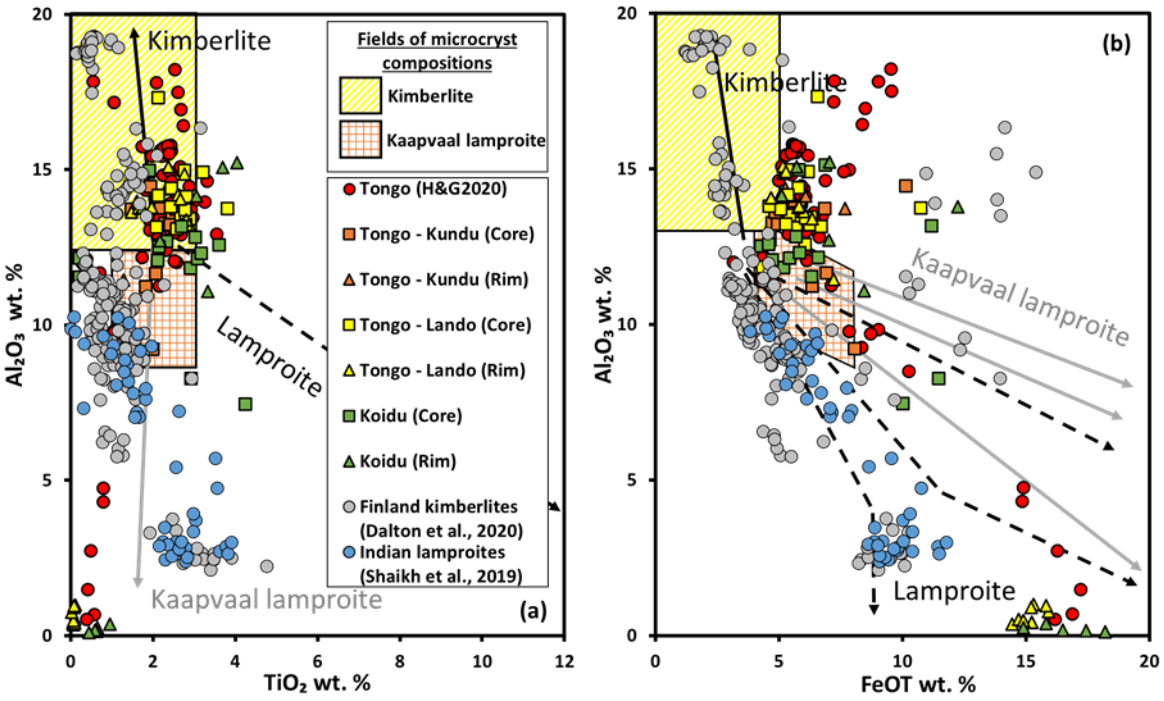

Figure 25: (a) Al_2O_3 wt % vs TiO_2 wt % for phlogopite analyses from the current study, Dalton et al. (2020) and Shaikh et al. (2019) plotted on a Al_2O_3 wt % vs TiO_2 wt % phlogopite classification diagram. (b) Al_2O_3 wt % vs FeO(t) wt % for phlogopite analyses from the current study, Dalton et al. (2020) and Shaikh et al. (2019) plotted on a Al_2O_3 wt % vs FeO(t) wt % phlogopite classification diagram. H&G2020 – refers to data from the Howarth and Giuliani (2020) study.

Kimberlitic spinels evolve from a chromium-rich spinel (TIMAC) to magnesio-ulvospinel-magnetite (MUM) (trend 1), whereas Kaapvaal lamproites and lamproitic spinels evolves from a chromium-rich spinel (TIMAC) to a magnetite (MAG) (trend 2) (Figure 26). The Koidu and Tongo core analyses display an evolution from TIMAC to MUM, whereas the rim analyses mostly plot within the MUM field. Comparing the Koidu and Tongo data to previously studied spinels in archetypal kimberlites (kimberlitic – trend 1) and previously studied lamproite spinels (lamproitic – trend 2), the alignment of the spinel evolution is closer towards trend 1 than trend 2 on the Cr/(Cr+Al) vs $Fe^{2+}/(Fe^{2+}+Mg)$ diagram (Figure 26 a). However, on the $Fe^{3+}/(Fe^{3+}+Al+Cr)$ vs $Fe^{2+}/(Fe^{2+}+Mg)$ diagram, the data trend falls between trend 1 and trend 2. This makes it appear to have spinel characteristics intermediate between kimberlite and lamproite. Roeder and Schulze (2008) similarly presented data of kimberlites and Kaapvaal lamproites with spinels that fall between trend 1 and trend 2, including data from Kirkland Lake (kimberlite), Jericho (kimberlite), Blue Hills (kimberlite), Frank Smith (kimberlite), Monastery (kimberlite), Masontown (kimberlite), New Elands (Kaapvaal lamproite) and Lace (Kaapvaal lamproite). The alignment between trend 1 and 2 was also observed in Koidu spinels from Tompkins and Haggerty (1985) and Tongo spinels from Howarth and Giuliani (2020). However, the majority of the spinels evolve to MUM compositions and ultimately indicate kimberlitic spinels.

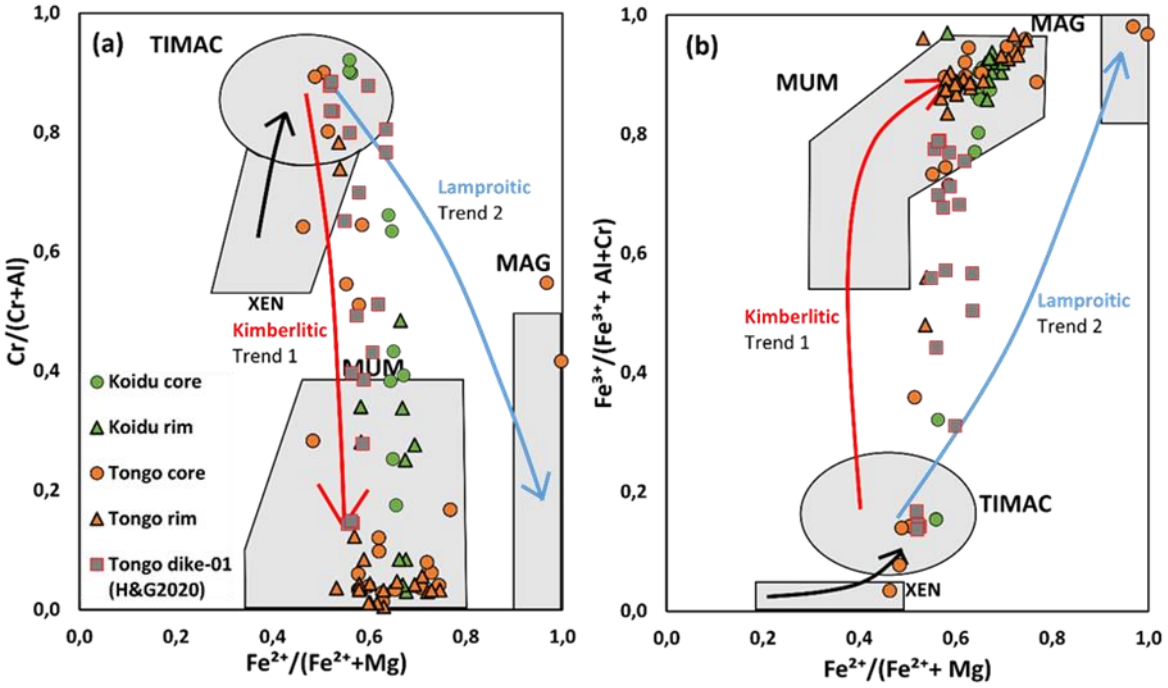

Figure 26: (a) Cr/(Cr+Al) vs $Fe^{2+}/(Fe^{2+}+Mg)$ for spinel analyses from the current study, Dalton et al. (2020) and Shaikh et al. (2019). (b) $Fe^{3+}/(Fe^{3+}+Al+Cr)$ vs $Fe^{2+}/(Fe^{2+}+Mg)$ for spinel analyses from the current study, Dalton et al. (2020) and Shaikh et al. (2019).

5.1.3. Bulk-rock geochemistry

In reviewing the work from Mathafeng (2021), It has been revealed that the phlogopite-rich nature of the Tongo (and Koidu) rocks has a considerable influence on it's major element geochemistry and is apparent when observing the TiO_2 vs K_2O values compared to archetypal kimberlites and Kaapvaal lamproites (Figure 27c). Major element geochemistry from Mathafeng (2021) reveal the Tongo rocks to be more like Kaapvaal lamproites as opposed to archetypal kimberlites. This effect of phlogopite abundance is also seen in Finnish kimberlites, where major element compositions can range from archetypal kimberlite (phlogopite-free) to Kaapvaal lamproite (phlogopite-rich) and is also reflected in their subsequent TiO_2 vs K_2O values. The Finnish kimberlites, on the other hand, have kimberlitic trace element compositions. Similarly, the Tongo rocks also have kimberlitic trace element compositions and further consists of kimberlitic Sr-Nd isotopic systematics (Figure 27 abd), indicative of a depleted mantle origin. This suggests that major element geochemistry is not robust enough to classify phlogopite-rich varieties of diamondiferous rocks and that trace element and isotopic compositions should rather be used.

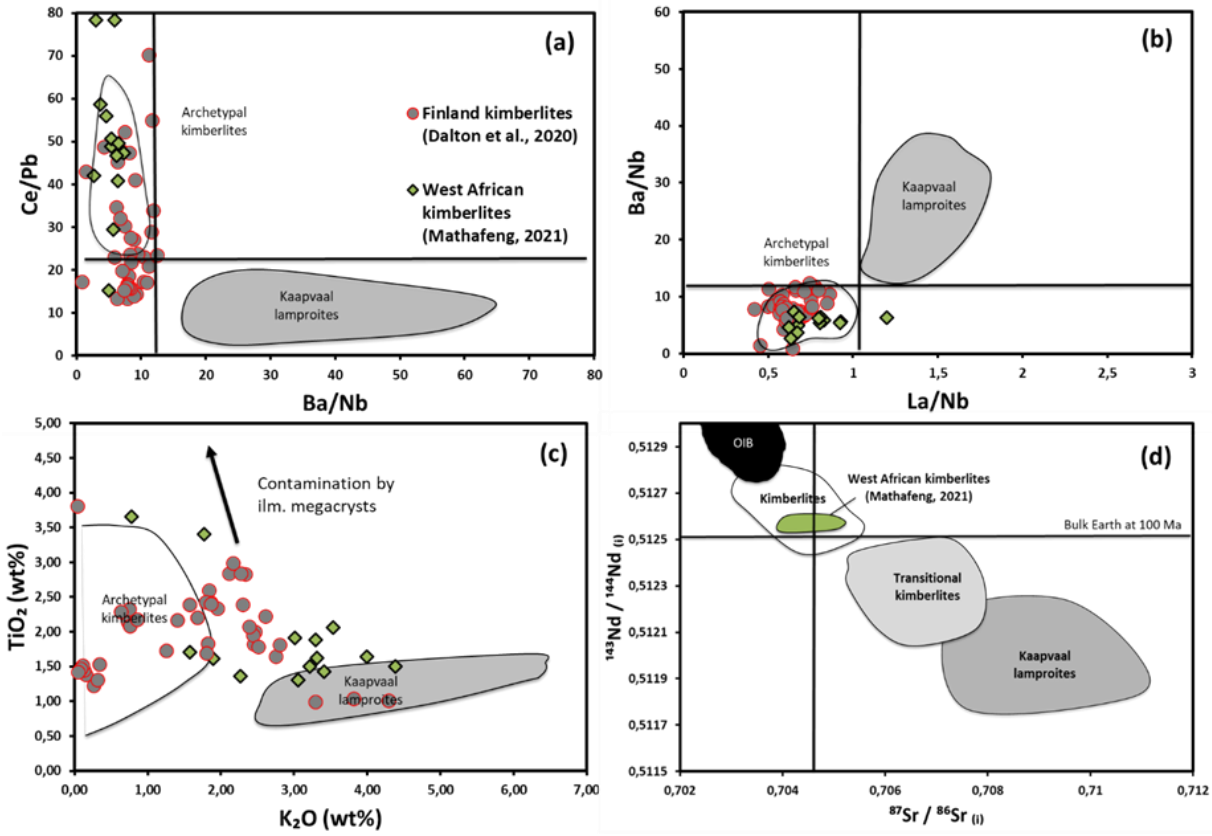

Figure 27: Variation of (a) Ce/Pb vs Ba/Nb, (b) Ba/Nb vs La/Nb from Mathafeng (2021). A distinction in kimberlite groups is provided through the dividing lines for Ba/Nb, Ce/Pb and La/Nb in (a) and (b). (c) represents the variation of TiO_2 vs K_2O in the Tongo dike-01 samples. Light shaded field represents the on-craton kimberlites (le Roex et al., 2003) and dark shaded field represents the on-craton Swartruggens and Star Kaapvaal lamproites (Coe, 2004). (d) represents the variation plot of the initial $^{143}Nd/^{144}Nd$ and $^{87}Sr/^{86}Sr$ isotope ratios in the Tongo dike-01 data. The Group II, Group I and Transitional kimberlite data fields are derived from Smith, 1983; Fraser & Hawkesworth, 1992; Tainton, 1992; Clark, 1994; Nowell et al., 1999, 2004; Coe, 2004; Becker & le Roex, 2006. The South Atlantic OIC data field was derived from O'Nions & Pankhurst, 1974; O'Nions et al., 1977; le Roex, 1985; le Roex et al., 1990.

5.1.4. Summary

Archetypal kimberlites and lamproites are often successfully classified by only using petrographic observations combined with the phlogopite and spinel chemistry. However, in this study, I show that there is an ambiguity within the petrography, major element geochemistry and mineral chemistry results, with characteristics of both kimberlite and lamproite present in all these categories. It is only when the trace element and isotopic compositions are determined that a clear and confident distinction can be made in favour of kimberlite.

5.2. Origin of olivine zoning

Olivine displays complex zoning patterns in kimberlites, and other related rock types, with distinct cores and multiple rim zones. The core zone is generally interpreted to be xenocrystic and the surrounding rim zones originated from crystallizing from the melt (Arndt et al., 2010;

Brett et al., 2009; Bussweiler et al., 2015; Cordier et al., 2015; Fedortchouk and Canil, 2004; Giuliani, 2018; Giuliani et al., 2017; Howarth and Giuliani, 2020; Howarth and Gross, 2019; Howarth and Taylor, 2016; Kamenetsky et al., 2008; Lim et al., 2018; Pilbeam et al., 2013; Shaikh et al., 2019, 2018; Sobolev et al., 2018, 2015). These complex zoning patterns have been shown to track kimberlite petrogenesis from source to emplacement (Giuliani, 2018).

In the following section, the data obtained from the various olivine zones from the Koidu and Tongo olivines will be discussed. This includes the origin of the olivine core, rim, internal and rind/ rim (II) zones. The goal of this section is to determine the origin of the ubiquitous zoned olivine grains derived from Koidu and Tongo by contrasting olivine zone compositions between the two clusters and with worldwide kimberlite and lamproite data.

5.2.1. Origin of olivine cores in the Koidu-Tongo kimberlites

The olivine cores from Koidu and Tongo contain a wide range in Fo and are visually distinct in backscatter images (Figure 28). They range in composition from Fe-rich (Fo_{83}) to Mg-rich (Fo_{94}), with Fe-rich variations appearing to be very light to light grey in colour and Mg-rich variation appearing to be more medium to dark grey in colour.

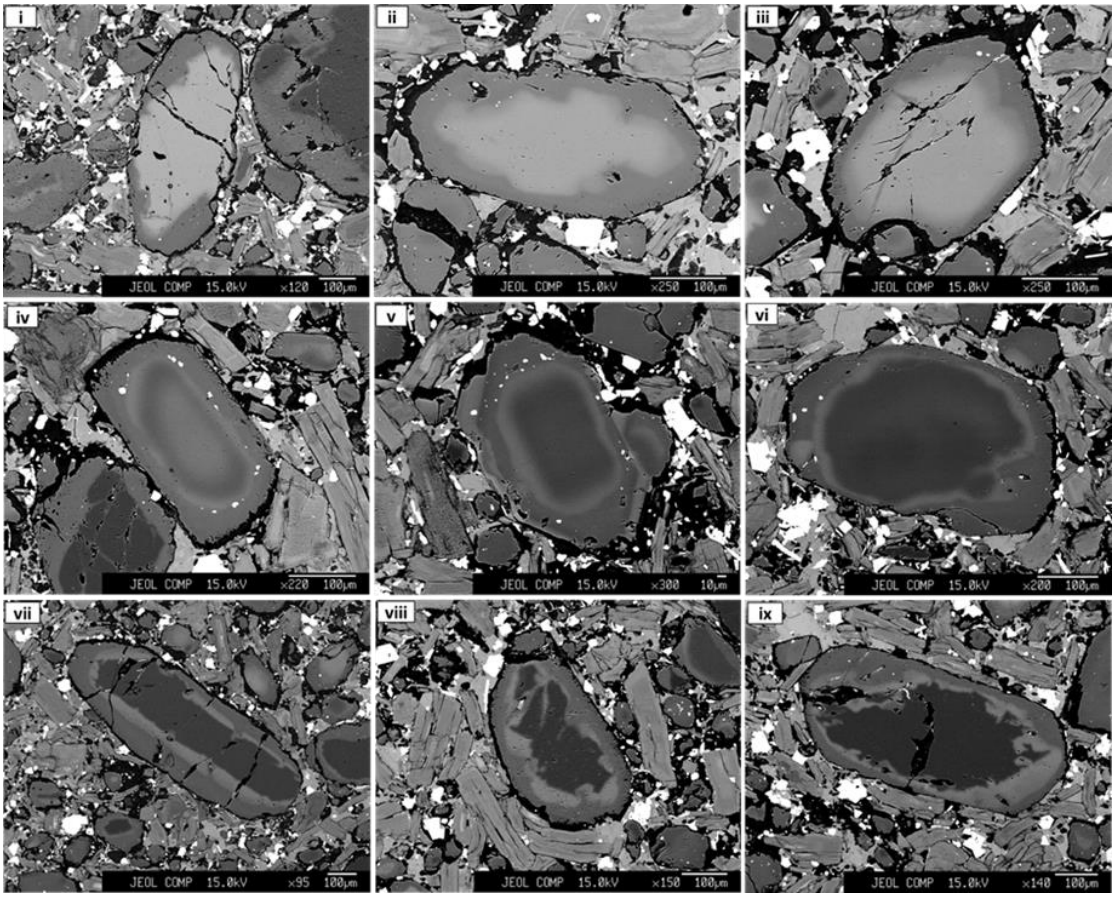

Figure 28: Backscatter imagery of the various olivine core types from sample TG12-190 (Lando). Fe-rich olivine core zones from i) to iv). Mg-rich olivine core zones from v) to ix).

a) Origin of Mg-rich cores from disaggregation of mantle xenolith lithologies

The most common variation in olivine core composition from Koidu and Tongo is the Mg-rich (Fo >89) group, consisting of 79% (99 out of 126) of the total olivine core population. Within the Koidu cluster the Mg-rich cores are made up of 74% (23 out of 31) of the total core population, while the Tongo cluster consists of 80% (76 out of 95) Mg-rich cores. Within the Tongo cluster, the Mg-rich cores make up 80% (32 out of 40) of the Kundu dike, 69% (24 out of 35) of the Lando dike and 100% (15 out of 15) for the Pandebu dike. They are found within both olivine macrocrysts and microcrysts, but more frequently occur in macrocrysts. They often have resorbed margins and can occasionally appear to have intensely resorbed margins, resulting in embayments (Figure 28vii-ix). This indicates that the cores were not in equilibrium with the host melt prior to olivine rim formation. Further, they do not contain any inclusions of groundmass minerals and undulose extinction is similarly common and occurs throughout the samples. Both these observations are considered conclusive evidence of a mantle origin. However, Moore et al (2020) demonstrated that olivine deformation in kimberlites can occur under crustal conditions, and is thus not unequivocal evidence for a mantle provenance. The composition of the Mg-rich olivine cores overlaps with those occurring in granular and sheared peridotites (Figure 29),

characterised by Fo > 89, elevated (0.25 – 0.50 wt.%) NiO and low (0.05 – 0.2 wt.%) MnO. This is further supported by the several polycrystalline grains that were observed throughout all samples from the study area, resembling a recrystallization texture and a relation to sheared peridotite xenoliths.

These textural and compositional features suggest that Mg-rich cores are xenocrystic in origin and that they originate from the disaggregation of a combination of granular and sheared peridotite mantle material.

b) Cr-poor megacrystic origin of Fe-rich olivine cores

The Fe-rich olivine compositions from Koidu and Tongo are less common than the Mg-rich compositions, consisting of 21% (27 out of 126) of the total olivine core population. Within the Koidu cluster the Fe-rich cores make up 26% (8 out of 31) of the total core population, while the Tongo cluster consists of 21% (19 out of 95) Fe-rich cores. Within the Tongo cluster, the Fe-rich cores make up 20% (8 out of 40) of the Kundu dike, 31% (11 out of 35) of the Lando dike and 0% (0 out of 15) for the Pandebu dike. The Fe-rich olivine cores are often found within olivine microcrysts but only occasionally appear within macrocrysts. They occasionally have resorbed margins but are more often found to have a semi-diffusive contact with the surrounding olivine zone (Figure 28 i-v). Like the Mg-rich population the Fe-rich cores do not contain any inclusions of groundmass minerals. The composition of the Fe-rich population overlaps with those occurring in Cr-poor megacrysts (Figure 29), characterised by an Fo < 89, very low to moderate (0.1 – 0.4 wt.%) NiO and moderate to elevated (0.1 – 0.3 wt.%) MnO. Some, but not all, of these compositions also overlap with olivine compositions of sheared peridotite, however, distinguishing between sheared peridotite and megacryst compositions remains ambiguous.

These textural and compositional features also suggest a xenocrystic origin for the Fe-rich olivine cores predominantly derived from Cr-poor olivine megacrysts and possibly also sheared peridotite.

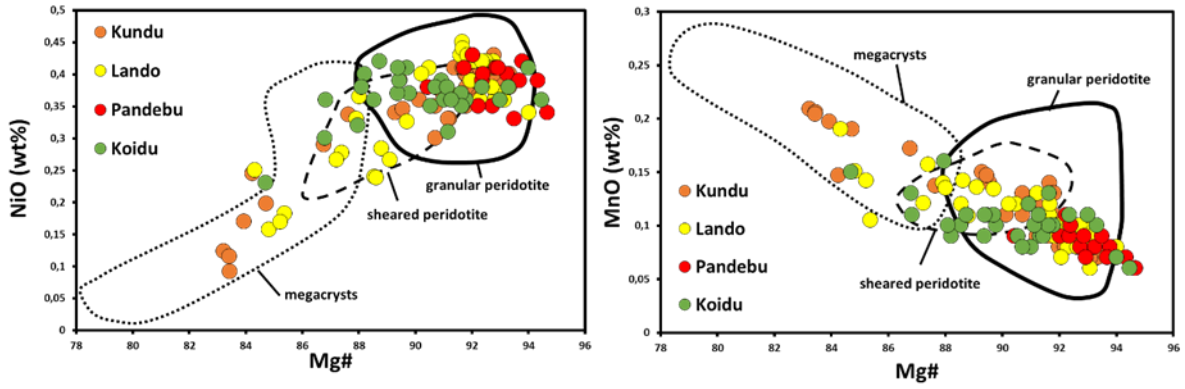

Figure 29: NiO (wt.%) vs Fo and MnO (wt.%) vs Fo diagrams with olivine core from Koidu and Tongo. Granular peridotite, sheared peridotite and megacryst data fields added from Giuliani (2018).

5.2.2. Origin of olivine internal zones in the Koidu-Tongo kimberlites

Zoned olivine grains can occasionally have an additional zone between the core and rim known as the internal zone. The Kundu and Lando dikes (i.e. Tongo cluster) are the only two locations where this zone is observed in the olivines from the study area. As seen on Figure 28, the shape often takes the form of the core and occurs as a narrow zone between the core and rim. The composition of Kundu and Lando internal zones range between Fo 85.0 and 86.5. They do not contain any groundmass mineral inclusions and surround both the Mg-rich and Fe-rich cores. The greater the difference in composition between the internal zone and the core the higher the degree of resorption observed in the cores. This is clearly seen in Figure 28, where the Fe-rich core surrounded by the Fe-rich internal zone only displays partial resorption, whereas the Mg-rich core surrounded by the Fe-rich internal zone displays a highly resorbed texture.

As discussed in section 5.2.1 the Fe-rich olivine cores are derived from the disaggregation of Cr-poor megacrysts. The Fe-rich internal zones have NiO (0.15 to 0.30 wt.%) and MnO (0.11 to 0.20 wt.%) compositions that similarly correspond to the composition of Cr-poor megacrysts and could represent a genetic link with a proto-kimberlite melt development in the source (Figure 30). This would also explain the higher degrees of resorption seen in the Mg-rich cores. If the initial proto-kimberlite melt was Fe-rich, the disaggregation of the surrounding Mg-rich mantle material would not be in equilibrium with the surrounding Fe-rich melt and would form excessive resorption textures. This agrees with the findings from Howarth and Taylor (2016) who suggested that internal zones in kimberlitic olivine crystallize before kimberlite ascent and after assimilation of orthopyroxene in the upper lithospheric mantle. Lim et al. (2018) also suggested a similar origin, where the internal zone crystallized at mantle depths from an early pulse of evolved kimberlite melt before entrainment in the ascending kimberlite magma.

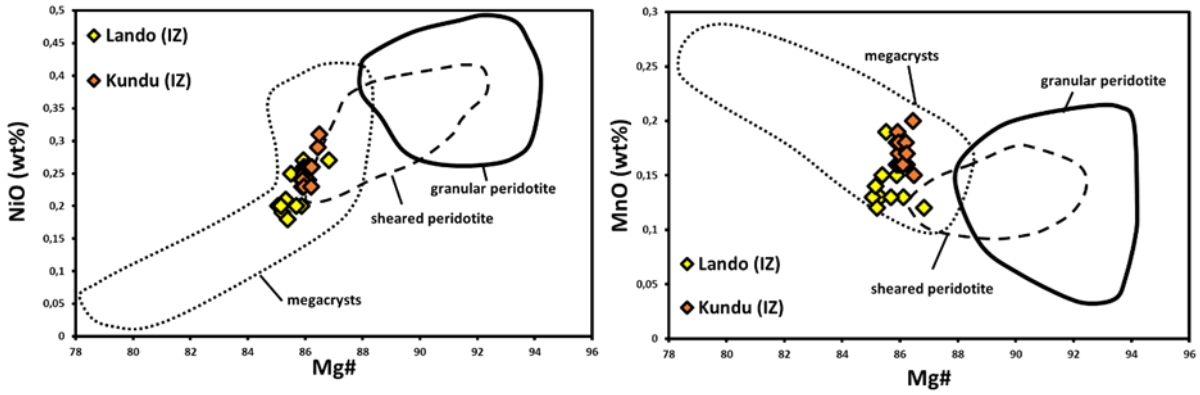

Figure 30: NiO (wt.%) vs Fo and MnO (wt.%) vs Fo diagrams with olivine internal zone data from Lando and Kundu. Granular peridotite, sheared peridotite and megacryst data fields added from Giuliani (2018).

5.2.3. Origin of olivine rim zones in the Koidu-Tongo kimberlites

Olivine rim zones are present in all analysed olivines from within the current study. Backscatter images reveal that they are visually distinct from the core zones in that they are either slightly lighter or darker in colour. They often contain anhedral and euhedral oxides, resembling groundmass spinel grains, indicating growth from a kimberlitic magma (Figure 28).

The composition of the olivine rims from Koidu and Tongo are distinct compared to the olivine core compositions and often consists of a narrow range in Fo. The NiO (0.4 to 0.1 wt.%) content decreases from the inner rim zone towards the outer rim zone, while the MnO (0.1 to 0.23 wt.%) and CaO (0.01 to 0.18 wt.%) increase from the inner rim zone towards the outer rim zone. This indicates olivine fractionation and evolution of the kimberlite magma. Fo composition of the rim can thus be used as a proxy for parent melt Mg# compositions (Figure 31). This has been observed in numerous previous studies (e.g., Brett et al., 2009; Bussweiler et al., 2015; Dalton et al., 2020; Giuliani, 2018; Howarth and Giuliani, 2020; Lim et al., 2018; Pilbeam et al., 2013; Soltys et al., 2020; Tovey et al., 2020).

The rim compositions at Koidu appear to have a statistically distinct difference between the two rim populations analysed from sample Y5770 and Y5774 (Figure 31). The Fo composition at Y5770 ranges from 86.6 to 87.8, with a mean of (±2sd) 87.1 ±0.6, while the Fo composition at Y5774 ranges from 88.0 to 89.1, with a mean of (±2sd) 88.3 ±0.5. This indicates the two rim populations originated from slightly differentiated parental melts. The rim compositions at Tongo all overlap in error between the various dikes. The Fo composition at Kundu ranges from 88.0 to 89.9, with a mean of (±2sd) 88.71 ±0.8. The Fo composition at Lando ranges from 87.9 to 90.4, with a mean of (±2sd) 89.09 ±0.9. The Fo composition at Pandebu ranges from 88.3 to 90.7, with a mean of (±2sd) 89.37 ±1.6. Although there is a slight difference in mean Fo between the dikes, the difference is not of statistical significance, and it can be interpreted that each dike at Tongo

and the rim analyses from Y5774 from Koidu are derived from a parental magma of similar composition.

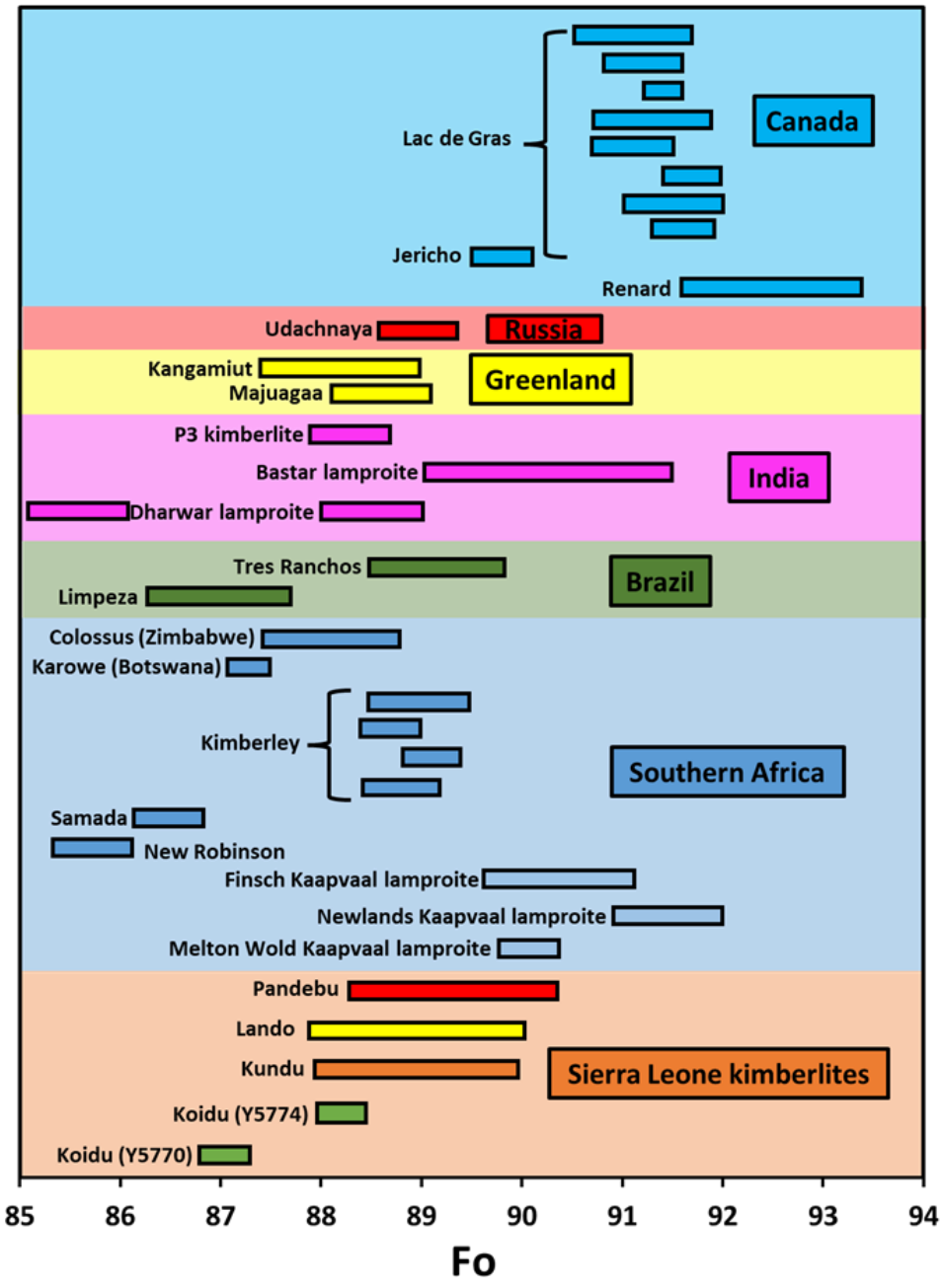

Figure 31: Fo content compilation of magmatic olivine rims from worldwide archetypal and phlogopite-rich kimberlites, Kaapvaal lamproites and Indian lamproites adapted from Howarth and Giuliani (2020). Data are compiled from the following sources: Koidu and Tongo cluster (current study); Newlands Kaapvaal lamproite from Moore (1988), Finsch Kaapvaal lamproite from Howarth (2018) and Melton Wold Kaapvaal lamproite from Howarth and Nembambula (2021); Karowe data from Arndt et al. (2010); Colossus data from Moore and Costin (2016); Kimberley area data from Arndt et al. (2010), Howarth and Taylor (2016) and Giuliani et al. (2017); Samada and New Robinson (Kaalvallei, South Africa), and Brazilian kimberlites data from Lim et al (2018); Indian P3 kimberlite from Shaikh et al. (2018); and Bastar and Dharwar craton lamproites from Shaikh et al. (2019); Greenland kimberlites from Nielson and Sand (2008), Arndt et al. (2010), Cordier et al. (2015), and Pilbeam et al. (2013); Udachnaya kimberlite from Kamenetsky et al. (2008) and Sobolev et al. (2015); Canadian kimberlites from Fedortchouk and Canil (2004), Brett et al. (2009), Patterson et al. (2009), Hilchie et al. (2014), Bussweiler et al. (2015).

An additional evolved olivine zone surrounding the rim was observed in two grains from one Lando sample (TG12-190; Figure 28 v). Similar to olivine rims, the zone also consists of inclusions of highly reflective groundmass spinel grains. The zone is Fe-rich with a Fo ranging from 86.6 to 87.3 and a mean Fo of (±2sd) 86.9 ±0.6. Further, the zone displays an overall higher MnO and CaO and lower NiO wt.% compared to the olivine rim compositions, representing the last stage of melt development. Comparing the mean olivine rim Fo composition at Lando (89.09) with the evolved rim Fo composition (86.9) suggests the kimberlite melt became more Fe-rich during the final stages of its evolution. This can be due to the crystallization of relatively Mg-rich (Fo 88.3 – 89.3) olivine rim zones during the kimberlite ascent, which enriched the melt in Fe. This corresponds to the late-stage crystallization of other Fe-rich phases such as MUM spinels and tetraferriphlogopite.

5.3. Petrogenesis

The proportion of Mg- to Fe-rich cores varies substantially in kimberlites worldwide. For example, kimberlites from Lac de Gras (Canada) have the highest proportion of Mg-rich cores (>88%) and high Fo rim compositions (>Fo_{90}) (Bussweiler et al., 2015; Giuliani et al., 2020; Lim et al., 2018; Tovey et al., 2020), whereas kimberlites from the phlogopite-rich Kaalvallei kimberlites (South Africa) have low proportion of Mg-rich cores (±25%) and low Fo rim compositions (±Fo_{84}) (e.g., Lim et al., 2018). This implies that Lac de Gras kimberlites sampled a relatively depleted SCLM and Kaalvallei sampled a more fertile (i.e., Fe-rich) metasomatised SCLM. Giuliani et al. (2020) showed that all other kimberlites fall along a trend between these two end members displaying a positive correlation between core and rim chemistry (Figure 32). They further suggested that the proportion of cores (i.e., the average core composition) reflects the degree to which the kimberlite has sampled a metasomatised mantle. The rim compositions correlate with this and thus kimberlites sampling more metasomatised mantle become more Fe-rich.

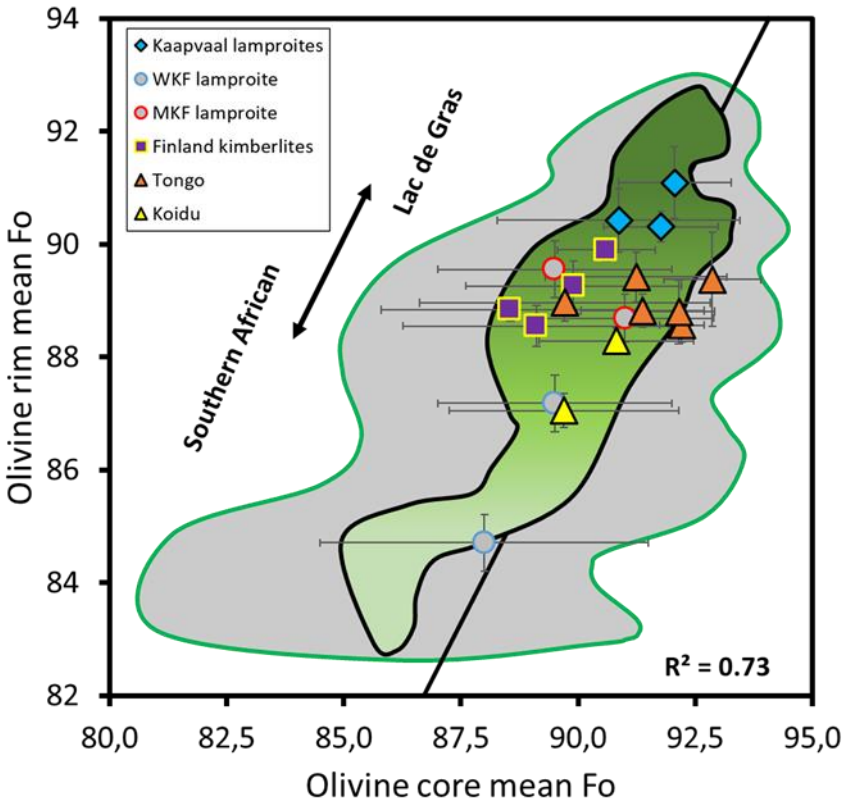

Figure 32: Average olivine rim Fo vs average core Fo from Koidu and Tongo and associated error bars (2sdv). Data fields and the linear regression line derived from Giuliani et al. (2020). Original data points from Giuliani et al. (2020) have been merged and is represented as a green gradient figure with a grey envelope representing the error bars associated with the original data points.

The Koidu and Tongo kimberlites have a core population dominated by 74 to 80% Mg-rich olivine cores (Figure 29) and have olivine rim compositions between Fo 86.6 and 90.4 (Figure 31). This range is more similar to that of the Kimberley kimberlites in South Africa as well as the Tres Ranchos kimberlite in Brazil that have sampled ±80% Mg-rich olivine cores and have olivine rim compositions between Fo 87.0 and 88.5 (Giuliani et al., 2020; Soltys et al., 2020). According to the Giuliani et al. (2020) model, the Tongo and Koidu kimberlites should therefore be sampling a mantle column more similar to that of the Kimberley kimberlites and on the more depleted end of the spectrum and indicative of the assimilation of a relatively refractory to partially metasomatised SCLM.

Kimberlite olivine rim compositions display a negative correlation with groundmass phlogopite + oxide abundances (Lim et al., 2018). These groundmass phases, expecially phlogopite, have been inferred to reflect magma derivation from a K-rich metasomatised source. This model is similar to that proposed by Giuliani et al (2020), and also suggests that the sampling of a fertile metasomatised mantle source will result in a lower Fo melt and subsequently lower Fo olivine rim compositions. This is then further associated with the phlogopite and oxide abundances, where the assimilation of a metasomatised SCLM source will result in a higher proportion of

phlogopite and oxide abundances. Thus, olivine rim compositions with a lower Fo generally have high groundmass phlogopite + oxide abundances and olivine rim compositions with a higher Fo have a lower groundmass phlogopite + oxide abundance (Figure 33). For example, The Samada and Newrobinson kimberlites from the Kaalvallei cluster is phlogopite-rich and has Fe-rich rims and indicates a kimberlite that has sampled a metasomatised SCLM. However, the phlogopite abundances in the Koidu and Tongo samples are even higher than Kaalvallei and suggests the sampling of a highly metasomatised phlogopite-rich source. Moreover, the Koidu-Tongo kimberlites have olivine rim compositions and phlogopite abundances more similar to Kaapvaal lamproites rather than kimberlites. The olivine compositions and phlogopite abundances from Koidu, Tongo and those from Kaapvaal lamproites put into question the models suggested by Giuliani et al. (2020) and Lim et al. (2018) and how robust it is.

The Kaalvallei and Lac de Gras kimberlites represent the two endmembers of both the Giuliani et al. (2020) and the Lim et al. (2018) models. The high proportion of Fe-rich olivine cores, low-Fo rims and the high abundance of groundmass phlogopite in the Kaalvallei kimberlites is reflective of the interaction and assimilation of a highly metasomatised SCLM. In contrast, the Lac de Gras kimberlites are dominated by Mg-rich cores, high-Fo rims and low abundance of groundmass phlogopite which is reflective of the interaction and assimilation of a refractory SCLM (Bussweiler et al., 2015; Tovey et al., 2020). The Koidu and Tongo (Sierra Leone) kimberlites from the current study have similar core-rim compositions to the Kimberley (South Africa) and Tres Ranchos (Brazil) kimberlites (Figure 31 & Figure 33). The Kimberley and Tres Ranchos kimberlites indicate the assimilation of a refractory to partially metasomatised SCLM based on the olivine core – rim trend and phlogopite + oxide abundances. The olivine core-rim trends in the Koidu and Tongo kimberlites also suggest the assimilation of a relatively refractory to partially metasomatised SCLM, however, the phlogopite + oxide abundances indicate the assimilation of a highly metasomatised SCLM (Figure 33). Kimberley kimberlites contain relatively low proportions of phlogopite whereas Koidu and Tongo have high proportions of phlogopite and so it may be better to compare Koidu and Tongo with other highly micaceous rocks.

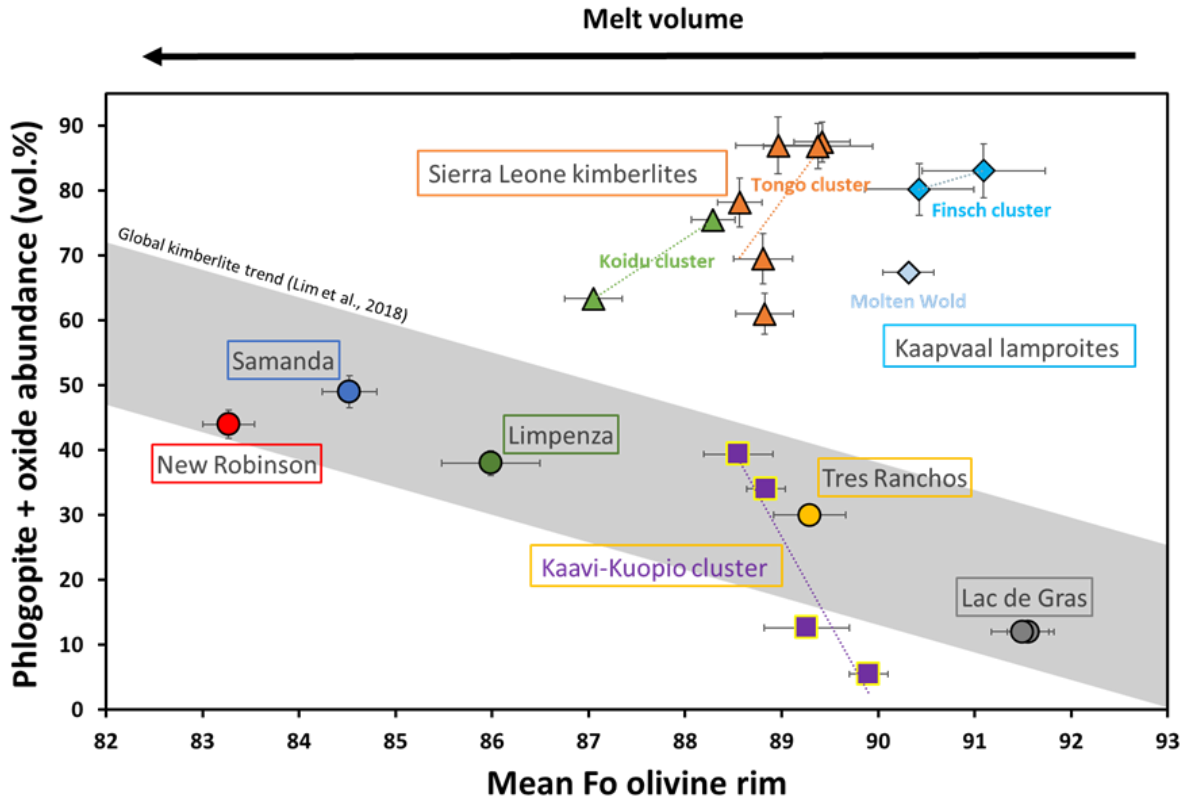

Figure 33: Phlogopite + oxides abundances (vol.%) vs mean Fo olivine rim for Koidu and Tongo with Lim et al. (2018), Shaikh et al. (2019), Dalton et al. (2020) and Howarth and Nembambula (2021) data added. Both datasets contain their respective error bars (2std).

Kaapvaal lamproites are highly micaceous and more similar in terms of petrography to the Koidu-Tongo kimberlites relative to typical monticellite kimberlites (i.e., Lac de gras). Additionally, Kaapvaal lamproites have ±10% higher proportions of Mg-rich cores and subsequently higher Mg-olivine rim compositions (>Fo_{90}) compared to the Koidu and Tongo kimberlites (Figure 33). The olivine core-rim trend in the Kaapvaal lamproites is indicative of interaction with a refractory SCLM, similar to Lac de Gras. The main difference between the Kaapvaal lamproites and Lac de Gras kimberlites is in the source region, where the Kaapvaal lamproites have been interpreted as originating from a garnet peridotite with cross-cutting phlogopite-rich (±clinopyroxene) metasomatic veins and the Lac de Gras kimberlites originated purely from a refractory SCLM (Becker and Le Roex, 2006; Coe et al., 2008; Howarth and Nembambula, 2021). The SCLM source of the Kaapvaal lamproites then underwent low volume melt generation within the phlogopite-rich (±clinopyroxene) cross cutting vein and the melt equilibrated with the surrounding refractory Mg-rich mantle source. This subsequently produced a parent magma that is enriched in incompatible elements (i.e., K) as well as being refractory, Mg-rich and Ni-rich (e.g. Becker and Le Roex, 2006). This magma then gave rise to Kaapvaal lamproites.

As seen on Figure 33, the phlogopite + oxide abundances from the Kaapvaal lamproites are similar to those from the Koidu-Tongo kimberlites and differ slightly in olivine rim composition, i.e. parental melt composition. This difference in parental melt composition reflects the source region, where the melt produced from the Koidu-Tongo kimberlites would have interacted with a refractory SCLM to partially metasomatised SCLM due to the slightly lower proportion of Mg-rich olivine cores and lower Fo rims compared to the Kaapvaal lamproites. This SCLM would also consist of cross-cutting phlogopite-rich (±clinopyroxene) veins, however, they would have been formed from pre-existing melts derived from the asthenosphere to produce kimberlitic trace element and isotopic signatures. Low to medium melt generation would need to occur within these cross-cutting veins and partially equilibrate with the surrounding SCLM. This subsequently produced a parent magma that is enriched in incompatible elements (i.e., K) as well as being partially refractory, Mg-rich and Ni-rich. This would then give rise to the phlogopite-rich kimberlites with the Mg-rich olivine material seen at Koidu and Tongo.

5.4. Implications for the use of olivine chemistry to constrain melt-SCLM interactions

The broad kimberlite trend seen in Giuliani et al. (2020) and Lim et al. (2018) are models that uses olivine chemistry in diamondiferous rocks to constrain their origin and evolution. The Koidu and Tongo kimberlite clusters display olivine core-rim compositions and phlogopite abundances that do not align with this broader trend of worldwide kimberlites. They are highly micaceous and contain Mg-rich olivine core-rim compositions that correspond more with Kaapvaal lamproites. This is the first example where multiple kimberlite clusters do not align with the broader kimberlite trend and puts into question whether olivine chemistry can effectively be used to constrain melt-SCLM interactions. The model thus needs to be adjusted for other factors and needs to be applicable to phlogopite-rich diamondiferous rocks with Mg-rich olivine core-rim compositions.

The current study has provided further insight in understanding melt-SCLM interactions in diamondiferous rock types. The SCLM is a region of the lithosphere that is extremely heterogeneous in composition and melts that interact with this region generate magmas that reflect this heterogeneity. Further, factors such as melt volume also fundamentally contribute to the variability observed in the emplaced diamondiferous deposit and need to be accounted for when generating predictive models.

Chapter 6: Conclusion

The Koidu-Tongo rocks represent unusual kimberlites that are highly micaceous where the mineralogy is ambiguous between an archetypal kimberlite and unevolved Kaapvaal lamproite. The phlogopite compositions evolve toward either decreasing Al_2O_3 and increasing Fe_2O_3 (tetraferriphlogopite) or have unusual concurrent increases in Al_2O_3 and FeO. Spinel Cr/(Cr+Al) and $Fe^{2+}/(Fe^{2+}+Mg)$ compositions are mostly aligned with archetypal kimberlite, whereas the $Fe^{3+}/(Fe^{3+}+Al+Cr)$ compositions can either be attributed to a lamproite or an archetypal kimberlite. Major element geochemistry (elevated K2O, reflected by high modal phlogopite) resembles that of a Kaapvaal lamproite, while trace element and isotopic compositions indicate an archetypal kimberlite. Both the Koidu and Tongo clusters have thus been classified as highly micaceous kimberlites.

As with the classification, the olivine compositions and zonation in the Koidu-Tongo kimberlites are similar. Both contain a range of xenocrystic core compositions from Fe-rich (Fo <89) similar to typical Cr-poor megacryst suits to Mg-rich (Fo >89) similar to refractory granular peridotites. The majority of the total core population in both clusters consist of Mg-rich cores, making up 74% of the Koidu core population and 80% of the Tongo core population. The Koidu-Tongo olivine rim compositions mostly overlap in composition and are relatively Fo-rich (~Fo 89). However, one Koidu sample contains olivine rims with a statistically lower composition indicating an origin from a slightly differentiated parental magma.

The high proportion of Mg-rich cores and Fo-rich rims in the Koidu-Tongo kimberlites resemble olivines from the Kimberley kimberlites. However, unlike the Kimberley kimberlites, the Koidu-Tongo kimberlites have much higher modal abundances of phlogopite and do not align with global kimberlite trends for phlogopite abundances and olivine rim compositions. In terms of high phlogopite abundance and Fo-rich rims, the Koidu-Tongo kimberlites align more with Kaapvaal lamproites and have likely undergone a similar melt equilibration process. The interpretation for the petrogenetic histroy follows the same approach taken by Howarth and Nembambula (2021) whereby the melt generated from partial melting originated from cross-cutting metasomatic veins within a refractory SCLM to account for the high phlogopite abundances. The relatively high proportion of Mg-rich cores and Fo-rich rims were the result of the melt further partially equilibrating with the refractory lithologies and were subsequently incorporated into the kimberlite during its development.

References

Andrews-Jones, D.A., 1968. Petrogenesis and geochemistry of the rocks of the Kenema district, Sierra Leone (PhD thesis abs.). Leeds University, England.

Apter, D.B., Harper, F.J., Wyatt, B.A., Scott Smith, B.H., 1984. The geology of the Mayeng kimberlite sill complex, South Africa. In Kornprobst 1, 43–57.

Arndt, N.T., Guitreau, M., Boullier, A.M., Le Roex, A., Tommasi, A., Cordier, P., Sobolev, A., 2010. Olivine, and the origin of kimberlite. J. Petrol. 51, 573–602.

Becker, M., Le Roex, A., Class, C., 2007. Geochemistry and petrogenesis of South African transitional kimberlites located on and off the Kaapvaal Craton. South African Journal of Geology. South African J. Geol. 110, 631–646.

Becker, M., Le Roex, A.P., 2006. Geochemistry of South African On- and Off-craton, Group I and Group II: Petrogenesis and Source Region Evolution. J. Petrol. 47, 673–703.

Brett, R.C., Russell, J.K., Moss, S., 2009. Origin of olivine in kimberlite: Phenocryst or imposter? Lithos 112, 201–212.

Bussweiler, Y., Foley, S.F., Prelević, D., Jacob, D.E., 2015. The olivine macrocryst problem: new insights from minor and trace element compositions of olivine from Lac de Gras kimberlites, Canada. Lithos 220, 238–252.

Clement, C.R., Skinner, E.M.W., Scott Smith, B.H., 1984. Kimberlite redefined. J. Geol 92, 223–228.

Coe, N., Roex, A., Gurney, J., Pearson, G.D., Nowell, G., 2008. Petrogenesis of the Swartruggens and Star Group II kimberlite dyke swarms, South Africa: Constraints from whole rock geochemistry. Contrib. to Mineral. Petrol. 156, 627–652.

Compton-Jones, C., Hughes, H., McDonald, I., Bybee, G., Kinnaird, J., Andersen, J., 2021. Bulk rock geochemistry of a swarm of orangeite dykes intersecting the Western Limb of the Bushveld Complex. In: Complex, EGU General Assembly.

Cordier, C., Sauzeat, L., Arndt, N.T., Boullier, A.M., Batanova, V., Barou, F., 2015. Metasomatism of the lithospheric mantle immediately precedes kimberlite eruption: new evidence from olivine composition and microstructures. J. Petrol. 56, 1775–1796.

Dalton, H., Giuliani, A., Brien, H.O., Phillips, D., Hergt, J., 2020. Lithos The role of lithospheric heterogeneity on the composition of kimberlite magmas from a single fi eld : The case of Kaavi-Kuopio , Finland. LITHOS 354–355, 105333.

Dalton, H., Giuliani, A., O'Brien, H., Phillips, D., Hergt, J., Roland, M., 2019. Petrogenesis of a Hybrid Cluster of Evolved Kimberlites and Ultramafic Lamprophyres in the Kuusamo Area, Finland. J. Petrol. 60, 2025–2050.

Dawson, J.B., 1987. The Kimberlite clan: relationship to olivine and leucite lamproites and inferences for upper-mantle metasomatism in J. G. Fitton and B. G. J. Upton, eds. Alkaline Igneous Rocks, Spec. publ. Geol. Soc. London 30, 95–101.

DePaolo, D.J., Wasserburg, G.J., 1976. Nd isotopic variations and petrogenetic models. Geophys. Res 3, 249–252.

Downes, P.J., Ferguson, D., Griffin, B.J., 2007. Volcanology of the Aries micaceous kimberlite, central Kimberley Basin, Western Australia. Volcanol Geotherm Res 159, 85–107.

Edwards, D., Rock, N.M.S., Taylor, W.R., Griffin, B.K., Ramsay, R.R., 1992. Mineralogy and Petrology of the Aries Diamondiferous Kimberlite Pipe, Central Kimberley Block, Western

Australia. J. Petrol. 33, 1157–1191.

Fedortchouk, Y., Canil, D., 2004. Intensive variables in kimberlite magmas, Lac de Gras, Canada and implications for diamond survival. J. Petrol. 45, 1725–1745.

Fraser, K., 1987. Petrogenesis ofkimberlites from South Africa and lamproites from Western Australia and North America. The Open University, Milton Keynes, UK.

Fraser, K., Hawkesworth, C., Erlank, A.J., Mitchell, R.H., Scott Smith, B.H., 1985. Sr, Nd, and Pb isotope and minor element geochemistry of lamproites and kimberlites. Earth Planet. Sc. Lett. 76, 57–70.

Fraser, K.J., Hawkesworth, C.J., 1992. The petrogenesis of group 2 ultrapotassic kimberlite from Finsch mine, South Africa. Lithos 28, 327–345.

Giuliani, A., 2018. Insights into kimberlite petrogenesis and mantle metasomatism from a review of the compositional zoning of olivine in kimberlites worldwide. Lithos 312–313, 322–342.

Giuliani, A., Foley, S., 2016. The Geochemical Complexity of Kimberlite Rocks and their Olivine Populations: a Comment on Cordier et al. J. Petrol. 56, 1775–1796.

Giuliani, A., Graham Pearson, D., Soltys, A., Dalton, H., Phillips, D., Foley, S.F., Lim, E., Goemann, K., Griffin, W.L., Mitchell, R.H., 2020. Kimberlite genesis from a common carbonate-rich primary melt modified by lithospheric mantle assimilation. Sci. Adv. 6.

Giuliani, A., Phillips, D., Woodhead, J.D., Kamenetsky, V.S., Fiorentini, M.L., Maas, R., Soltys, A., Armstrong, R.A., 2015. Did diamond-bearing orangeites originate from MARID-veined peridotites in the lithospheric mantle? Nat. Commun. 6.

Giuliani, A., Soltys, A., Phillips, D., Kamenetsky, V.S., Maas, R., Goemann, K., Griffin, W.L., 2017. The final stages of kimberlite petrogenesis: petrography, mineral chemistry, melt inclusions and Sr-CO isotope geochemistry of the Bultfontein kimberlite (Kimberley, South Africa). Chem. Geol. 455, 342–356.

Giuliani, M., Pianosi, F., Castelletti, A., 2015. Making the most of data: an information selection and assessment framework to improve water systems operations. Water Resour. Res. 51, 9073–9093.

Haggerty, S.E., 1982. Kimberlites in Western Liberia: an overview of the geological setting in a plate tectonic framework. J. Geophys. Res. 87, 10811 –10826.

Haggerty, S.E., 2017. Kimberlite discoveries in NW Liberia: Tropical exploration and preliminary results. J. Geochemical Explor. 173, 99–109.

Howarth, G., Giuliani, A., 2020. Contrasting types of micaceous kimberlite-lamproite magmatism from the Man Craton (West Africa): New insights from petrography and mineral chemistry. Lithos 362–363.

Howarth, G., Skinner, E., Skinner, W., Prevec, S., 2011. Petrology of the hypabyssal kimberlite of the Kroonstad group II kimberlite (orangeite) cluster, South Africa: Evolution of the magma within the cluster. Lithos 125, 795–808.

Howarth, G.H., Gross, J., 2019. Diffusion-controlled and concentric growth zoning revealed by phosphorous in olivine from rapidly ascending kimberlite magma, Benfontein, South Africa. Geochim. Cosmochim. Acta.

Howarth, G.H., Nembambula, I., 2021. Petrogenesis of Kaapvaal lamproites (aka orangeites) constrained by olivine composition and similarities with kimberlites and other diamondiferous lamproites. Lithos.

Howarth, G.H., Taylor, L.A., 2016. Multi-stage kimberlite evolution tracked in zoned olivine from the Benfontein sill, South Africa. Lithos 262, 384–397.

Kamenetsky, V.S., Kamenetsky, M.B., Sobolev, A.V., Golovin, A.V., Demouchy, S., Faure, K., Sharygin, V.V., Kuzmin, D.V., 2008. Olivine in the Udachnaya-East Kimberlite (Yakutia, Russia): types, compositions and origins. J. Pet. 49, 823–839.

Kamenetsky, V.S., Kamenetsky, M.B., Sobolev, A.V., Golovin, A.V., Sharygin, V.V., Pokhilenko, N.P., Sobolev, N.V., 2009. Can pyroxenes be liquidus minerals in the kimberlite magma? Lithos 112, 213–222.

Kornilova, V.P., Nikishov, K.N., Kovalskii, V. V., 1983. Atlas of the Textures and Structures of Kimberlitic Rocks. Atlas Textures Struct. Kimberlitic Rocks. lzdat. Nauk. Moscow (Russian).

Lenzen, G., 1980. South Africa and the birth of a great industry. In J. Legrand (ed.), Diamonds: Myth, Magic and Reality. Crown, New York.

Lewis, H.C., 1888. The matrix of diamond. Geol. Mag. 5, 129–131.

Lewis, H.C., n.d. On diamantiferous peridotite and the genesis of the diamond. Geol. Mag. 4, 22–24.

Lim, E., Giuliani, A., Phillips, D., Goemann, K., 2018. Origin of complex zoning in olivine from diverse, diamondiferous kimberlites and tectonic settings: Ekati (Canada), Alto Paranaiba (Brazil) and Kaalvallei (South Africa). Miner. Pet. 112, 539–554.

Mathafeng, K., 2021. Classification and petrogenesis of the Tongo dike-01 from the Tongo-Tongoma cluster, Sierra Leone: constraints from bulk-rock geochemistry (MSc thesis). University of Cape Town., South Africa.

Mitchell, R., 1986. Kimberlites; Mineralogy, Geochemistry. Petrology.

Mitchell, R., 1991. What's in a Name? Suggestions for Revisions to the Terminology of Kimberlites and Lamprophyres from a Genetic Viewpoint. In: International Kimberlite Conference: Extended Abstracts. pp. 295–297.

Mitchell, R., 1994. The lamprophyre facies. Mineralogy and Petrology. Mineral. Petrol. 51.

Mitchell, R., 1995. Kimberlites, Orangeites, and Related Rocks.

Mitchell, R., 2008. Petrology of hypabyssal kimberlites: Relevance to primary magma compositions. J. Volcanol. Geotherm. Res. 174, 1–8.

Mitchell, R., Bergman, S., 1991. Petrology of Lamproites.

Mitchell, R., Giuliani, A., O'Brien, H., 2019. What is a Kimberlite? Petrology and Mineralogy of Hypabyssal Kimberlites. Elements 15, 381–386.

Mitchell, R.H., Meyer, H.O.A., 1989. Mineralogy of micaceous kimberlites from the New Elands and Star Mines. Orange Free State. South Africa. Ross al. q.v. 1, 83–96.

Moore, A., Costin, G., 2016. Kimberlitic olivines derived from the Cr-poor and Cr-rich megacryst suites. Lithos 258.

Moss, S., Webb, K., Hetman, C., Manyumbu, A., Muchechetere, C., 2012. Geology for K1 and K2 kimberlite pipes at Murowa, Zimbabwe. In: Extended Abstract, 10th International Kimberlite Conference, Bangalore, India.

Newfield resources limited, 2019. June 2019 quarterly activities report.

Nkere, J., Janney, P.E., Tinguely, C., 2021. Cr-poor and Cr-rich clinopyroxene and garnet

megacrysts from southern African Group 1 and Group 2 kimberlites: Clues to megacryst origins and their relationship to kimberlites.

Nowell, G., Pearson, G., Bell, D., Carlson, R., Smith, C., Kempton, P., Noble, S., 2004. Hf Isotope Systematics of Kimberlites and their Megacrysts: New Constraints on their Source Regions. J. Petrol. 45.

Nowell, G., Pearson, G., Kempton, P., 1999. Hafnium-Isotopic Systematics of Kimberlites, Lamproites and Megacrysts: Implications for Mantle Reservoirs and the Composition of Bulk Silicate Earth (BSE).

Octea limited, 2014. Mining investment opportunity March 2014.

Pearson, G., Woodhead, J., Janney, P., 2019. Kimberlites as Geochemical Probes of Earth's Mantle. Elements 15, 387–392.

Pilbeam, L., Nielsen, T., Waight, T., 2013. Digestion Fractional Crystallization (DFC): an Important Process in the Genesis of Kimberlites. Evidence from Olivine in the Majuagaa Kimberlite, Southern West Greenland. J. Petrol. 54.

Ramokgaba, L., Le Roex, A.P., Robey, J., 2021. Phlogopite-rich and phlogopite-poor kimberlite intrusions within the Du Toitspan kimberlite pipe, South Africa: Petrogenetic relationships and localised source heterogeneity. Lithos 390–391.

Roberts, B., 1976. Kimberley: Turbulent City. David Philip, Cape Town, South Africa.

Roeder, P., Schulze, D., 2008. Crystallization of Groundmass Spinel in Kimberlite. J. Petrol. 49.

Scott Smith, B., Nowicki, T., Russell, J., Webb, K., Mitchell, R., Hetman, C., Harder, M., Skinner, E., Robey, J., 2013. Kimberlite Terminology and Classification 2, 1–17.

Scott Smith, B.H., Nowicki, T.E., Russell, J.K., Webb, K.J., Mitchell, R.H., Hetman, C.M., Robey, J. vA., 2018. A Glossary of Kimberlite and Related Terms.

Shaikh, A., Patel, S., Bussweiler, Y., Kumar, S., Tappe, S., Ravi, S., Mainkar, D., 2018. Olivine trace element compositions in diamondiferous lamproites from India: Proxies for magma origins and the nature of the lithospheric mantle beneath the Bastar and Dharwar cratons. Lithos.

Shaikh, A., Patel, S., Bussweiler, Y., Tappe, S., 2019. Trace elements in olivine from diamondiferous lamproites: Proxies for magma origin and cratonic mantle lithosphere evolution.

Shaikh, A.M., Patel, S.C., Ravi, S., Behera, D., Pruseth, K.L., 2016. Mineralogy of the TK1 and TK4 'kimberlites' in the Timmasamudram cluster, Wajrakarur Kimberlite Field, India: Implications for lamproite magmatism in a field of kimberlites and ultramafic lamprophyres. Chem. Geol. 455, 208–230.

Skinner, E., Apter, D., Morelli, C., Smithson, N., 2004. Kimberlites of the Man craton, West Africa. Lithos 76, 233–259.

Skinner, E.M.W., 1986. Contrasting Group 1 and 2 kimberlite petrology: Towards a genetic model for kimberlites. In: Fourth Int. Kimberlite Conr., Perth, Australia. Extended Abstracts. pp. 202–204.

Skinner, E.M.W., 1989. Contrasting group I and II kimberlite petrology: Towards a genetic model for kimberlites. Ross al. q.v. 1, 528–544.

Skinner, E.M.W., Viljoen, K.S., Clark, T.C., Smith, C.B., 1994. The petrography, tectonic setting and emplacement ages ofkimberlites in the south western border region of the Kaapvaal craton, Prieska area. In Meyer and Leonardos 1, 80–97.

Smith, C.B., 1983. Pb, Sr, and Nd isotopic evidence for sources of African Cretaceous kimberlites. Nature 304, 51–54.

Smith, C.B., Gurney, J.J., Skinner, E.M. w., Clement, C.R., Ebrahim, N., 1985. Geochemical character of southern African kimberlites: a new approach based on isotopic constraints. Trans. Geol. Soc. S. Afr. 88, 267–280.

Sobolev, N.V., Sobolev, A., Tomilenko, A., Kuz'min, D.V., Grakhanov, S.A., Batanova, V., Logvinova, A., Bul'bak, T.A., Kostrovitskii, S.I., Yakovlev, D.A., Fedorova, E.N., Anastasenko, G.F., Nikolenko, E., Tolstov, A., Reutsky, V., 2018. Prospects of search for diamondiferous kimberlites in the northeastern Siberian Platform. Russ. Geol. Geophys. 59, 1365–1379.

Sobolev, N.V., Sobolev, A., Tomolenko, A.A., Batanova, V., Tolstov, Alexandr Logonova, A., Kuzmin, D., 2015. Unique Compositional Peculiarities of Olivine Phenocrysts from the Post Flood Basalt Diamondiferous Malokuonapskaya Kimberlite Pipe, Yakutia. Dokl. Earth Sci. 463, 828–832.

Soltys, A., Giuliani, A., Phillips, D., 2018. A new approach to reconstructing the composition and evolution of kimberlite melts: a case study of the archetypal Bultfontein kimberlite (Kimberley, South Africa). Lithos 304–307, 1–15.

Soltys, A., Giuliani, A., Phillips, D., Kamenetsky, V., 2020. Kimberlite Metasomatism of the Lithosphere and the Evolution of Olivine in Carbonate-rich Melts — Evidence from the Kimberley Kimberlites (South Africa). J. Petrol. 61.

Stamm, N., Schmidt, M.W., Szymanowski, D., von Quadt, A., Mohapi, T., Fourie, A., 2018. Primary petrology, mineralogy and age of the Letšeng-la-Terae kimberlite (Lesotho, Southern Africa) and parental magmas of Group-I kimberlites. Contrib. Miner. Pet. 173, 76.

Tainton, K.M.., Browning, P., 1991. The group-2 kimberlite-Iarnproite connection: Some constraints from the Barkly West District, northern Cape Province. In: Fifth Int. Kimberlite Conf ., Araxa, Brazi!. Extended Abstracts. pp. 405–407.

Tainton, K.M.., McKenzie, D., 1994. The generation of kimberlites, lamproites and their source rocks. J. Pet. 35, 787–817.

Tainton, K.M., 1992. The petrogenesis of group-2 kimberlites and lamproites from the northern Cape Province. South Africa. University of Cambridge, UK.

Taylor, W.R., Kingdom, L., 1999. Mineralogy of the Jagersfontein kimberliteçan unusual Group I micaceous kimberlite and a comment on the robustness of the mineralogical definition of 'orangeite'. In: Gurney, J. J., Gurney, J. L., Pascoe, M. D. & Richardson, S. H. (eds). In: Proceedings of the 7th International Kimberlite Conference. pp. 861–866.

Taylor, W.R., Tompkins, L.A., Haggerty, S.E., 1994. Comparative geochemistry of West African kimberlites: evidence for a micaceous end member of sublithospheric origin. Geochim. Cosmochim. 58, 4011 – 4037.

Tompkins, L.A.., Haggerty, S.E., 1984. The Koidu kimberlite complex. Sierra Leone: Geological setting. Petrol. Miner. Chem. 1, 81–105.

Tovey, M., Giuliani, A., Phillips, D., Moss, S., 2020. Controls on the explosive emplacement of diamondiferous kimberlites: New insights from hypabyssal and pyroclastic units in the Diavik mine, Canada. Lithos 360–361.

Wagner, P.A., 1914. The Diamond Fields of South Africa. Transvaal Leader. Johannesburg. South Africa.

Wagner, P.A., 1928. The evidence of the kimberlite pipes on the constitution of the outer part of

the Earth. S. Afr. J. Sci. 25, 127–148.

Wilson, A.N., 1982. Diamondsfrom Birth to Eternity. Gemol. Inst. Am. St. Monica, CA.

Wilson, M., 1989. Igneous Petrogenesis. A Global Tectonic Approach. Unwin Hyman, London 325–416.

Woodhead, J., Hergt, J., Giuliani, A., Maas, R., Phillips, D., Pearson, D.G., Nowell, G., 2019. Kimberlites reveal 2.5-billion-year evolution of a deep, isolated mantle reservoir. Nature 573, 578–581.

Woodhead, J., Hergt, J., Phillips, D., Paton, C., 2009. African kimberlites revisited: In situ Srisotope analysis of groundmass perovskite. Lithos 112, 311–317.

Appendix A

Sample list

Sample Number	Location	Prospect
TP0101	Tongo-Tonguma	Dike-01
TP0202	Tongo-Tonguma	Dike-01
TP0203	Tongo-Tonguma	Dike-01
TP0204	Tongo-Tonguma	Dike-01
TP0305	Tongo-Tonguma	Dike-01
TP0306	Tongo-Tonguma	Dike-01
TP0307	Tongo-Tonguma	Dike-01
TP0408	Tongo-Tonguma	Dike-01
TP0509	Tongo-Tonguma	Dike-01
TP0510	Tongo-Tonguma	Dike-01
TP0811	Tongo-Tonguma	Dike-01
TP0812	Tongo-Tonguma	Dike-01
TP1013	Tongo-Tonguma	Dike-01
TP1014	Tongo-Tonguma	Dike-01
TP1115	Tongo-Tonguma	Dike-01
TG11-039A	Tongo-Tonguma	Kundu
TG11-048	Tongo-Tonguma	Kundu
TG11-042	Tongo-Tonguma	Kundu
TG11-039B	Tongo-Tonguma	Kundu
TG12-189	Tongo-Tonguma	Lando
TG12-065	Tongo-Tonguma	Lando
TG11-020A	Tongo-Tonguma	Lando
TG11-020B	Tongo-Tonguma	Lando
TG12-176	Tongo-Tonguma	Lando
TG11-005	Tongo-Tonguma	Lando
TG12-190	Tongo-Tonguma	Lando
TG11-004	Tongo-Tonguma	Lando
TG11-049	Tongo-Tonguma	Pandebu
S0125	Koidu	Unknown
S0124	Koidu	Unknown
Y5770	Koidu	Unknown
Y5774	Koidu	Unknown
Y5776	Koidu	Unknown
Y5772	Koidu	Unknown

Appendix B

Tongo – Tonguma dike-01 full petrography descriptions

The Tongo dike-01 samples are comprised of several separate sub-phases which are petrographically distinct from one another and are described below.

a) Aphanitic variation 1

The Aphanitic variation 1 is only made up of one diagnostic sample (TP0101). The sample is very fresh and contains olivines which are all unaltered. Olivine macrocrysts make up 5 vol.% (i.e., aphanitic). One 1.5mm in length phlogopite macrocryst lath was observed. The olivine macrocrysts ranges in size from 0.5-4mm, well sorted, and sub-rounded. They are also aligned slightly in a preferred orientation. The phlogopite macrocryst is light brown and is 2mm in length and is prismatic with rounded edges.

The groundmass consists of olivine microcrysts, phlogopite, calcite, serpentine, spinel, and perovskite. The olivine microcrysts occur as slightly aligned rounded to sub-rounded grains and make up 33 vol.% of the modal abundance. Phlogopite occurs as pale orange-brown lath-shaped grains and makes up 18 vol.% and ranges in length from 0.05-0.5mm. These phlogopite laths often have a dark brick red tetraferriphlogopite rims which are 0.005-0.05 mm in width. Spinel and perovskite can occasionally be found as inclusions within phlogopite laths but are found more frequently surrounding phlogopite laths or as inclusions in the interstitial calcite. Calcite occurs as interstitial material and makes up 3 vol.% of the modal abundance. The calcite contains inclusions of phlogopite, spinel and perovskite. Spinel is abundant – most abundant sample of the study – making up 26 vol.% of the modal abundance. They occur as euhedral opaque grains located throughout the sample and are between 0.01-0.05mm in size. Serpentine is up to 13 vol.% in modal abundance surrounding other groundmass minerals as interstitial material. Perovskite occurs as ~0.05mm sized semi-opaque, high relief, dark brown grains and makes up 2 vol.% of the sample.

The rock is classified as an aphanitic micaceous coherent kimberlite containing abundant fresh olivine microcrysts. Petrographically it is of moderate to low interest, due to the very low abundance of olivine macrocrysts (5 vol.%) but still having sufficiently small spinel grains (<0.07 mm).

b) Aphanitic to macrocrystic variation 1

The Aphanitic to macrocrystic variation 1 consists out of three samples (TP0202, TP0812 and TP1014). These samples are relatively fresh, containing fresh unaltered olivine, except for sample

TP1014, which has altered (serpentinized) olivine. Olivine macrocrysts make up 6-18 vol.% of the modal abundance. Phlogopite macrocrysts are present and more abundant (3 vol.% modal abundance) in TP0812 than the other two samples (trace amounts). The olivine macrocrysts range in size from 0.5-8mm, well sorted, and sub-rounded. The phlogopite macrocrysts range in size from 0.5-3mm, moderately sorted, elongated, and occasionally rounded. One garnet macrocryst (2mm in size) with a kelyphite rim was also observed.

The groundmass consists of olivine microcrysts, calcite, phlogopite, serpentine, spinel, atoll-textured spinel, and perovskite. The olivine microcrysts are variable and range from 18-31 vol.% in modal abundance. Most are sub-rounded to rounded and unaltered, except for sample TP1014 containing serpentinized olivine microcrysts. Calcite occurs as interstitial material and makes up 17-24 vol.%. The calcite contains inclusions of phlogopite, spinel and perovskite. Phlogopite occurs as pale orange-brown lath-shaped grains varying in abundance from 21-37 vol.% and ranges in length from 0.05-0.5mm. Spinel and perovskite can occasionally be found as inclusions within phlogopite laths. These phlogopite laths often have a dark brick red tetraferriphlogopite rim which is 0.005-0.05 mm in width. Serpentine is present in low abundances (2-6 vol.%) as interstitial material. Spinel occurs as euhedral opaque phases distributed in varying abundances (6-15 vol.%) throughout the samples and range in size from 0.01-0.05mm. Spinel is also very abundant in a region of sample TP1014 where possible density layering has taken place (figure 5E). Atoll-textured spinel is also present in sample TP1014 in low abundances. Perovskite occurs as ~0.05mm sized semi-opaque to high relief dark brown grains, however, it is a rarely observed mineral and makes up trace amounts of the sample's modal abundance.

The rocks are classified as aphanitic to macrocrystic micaceous coherent kimberlites. Petrographically it is rated as moderate interest due to the lack of sufficient abundance of olivine macrocrysts (6-18 vol.%) but still having sufficiently small spinel grains (<0.07 mm). Sample TP0202, consisting of >15 vol.% olivine macrocrysts, might be of moderate to high interest.

c) Aphanitic to macrocrystic variation 2

The Aphanitic to macrocrystic variation 2 consists out of three samples (TP0203, TP0204, TP0509). These samples are all altered, with ~20 vol.% fresh olivines present. Olivine macrocrysts are present in two out of the three samples, with sample TP0203 not containing any olivine macrocrysts. The olivine macrocryst content for the two remaining samples are both 8 vol.% in modal abundance. The olivine macrocrysts present in the two samples range in size from 0.5-8mm, moderately to well sorted, and sub-rounded. No phlogopite macrocrysts were observed.

The groundmass consists of olivine microcrysts, phlogopite, calcite, apatite, serpentine, spinel, and perovskite. The olivine microcrysts make up 8-17 vol.% of the modal abundance, are almost all altered (serpentinized) and are rounded to sub-rounded. Phlogopite occurs as pale orange-brown lath-shaped grains varying in abundance from 39-43 vol.% and ranges in length from 0.05-0.5mm. Spinel and perovskite can occasionally be found as inclusions within phlogopite laths but are found more frequently surrounding phlogopite laths. These phlogopite laths often have a dark brick red tetraferriphlogopite rims which are 0.005-0.05 mm in width. Due to alteration, some phlogopite grains have been partially altered to chlorite. Calcite occurs as interstitial material and makes up 11-28 vol.% of the modal abundance. The calcite contains inclusions of phlogopite, spinel and perovskite. Apatite is relatively abundant (compared to the other samples), ranging from 2-10 vol.% in modal abundance. They occur as elongated laths or as radial textured grains and are ~0.1-0.2 mm in length (figure 5F). Serpentine is present in variable abundances (1-11 vol.%) surrounding other groundmass minerals as interstitial material. Spinel occurs as euhedral opaque phases distributed in varying abundances (9-15 vol.%) throughout the samples and range in size from 0.02-0.15mm (<0.07 mm avg). Perovskite occurs as ~0.05mm sized semi-opaque, high relief, dark brown grains, however, it is a rarely observed mineral and makes up trace amounts of the sample's modal abundance.

The rock is classified as aphanitic to macrocrystic apatite-rich micaceous coherent kimberlite. Petrographically it is of moderate to low interest, due to the very low abundance of olivine macrocrysts (0-8 vol.%) but still having sufficiently small spinel grains (<0.07 mm).

d) Aphanitic variation 2

The Aphanitic variation 2 consists out of two altered samples (TP0305, TP1115), consisting of no fresh olivines. Both samples do not contain macrocrystic material and is referred to as an aphanitic variation.

The groundmass consists of phlogopite, calcite, olivine microcrysts, spinel, oxide laths and serpentine. Phlogopite occurs as pale orange-brown lath-shaped grains varying in abundance from 50-54 vol.% and ranges in length from 0.05-0.5mm. These phlogopite laths often have a dark brick red tetraferriphlogopite rims which are 0.005-0.05 mm in width. Spinel and perovskite can occasionally be found as inclusions within phlogopite laths but are found more frequently surrounding phlogopite laths. Calcite occurs as interstitial material and makes up 30 vol.% of the modal abundance and is anhedral. The calcite contains inclusions of phlogopite, spinel, perovskite and the oxide laths. Olivine microcrysts are not as abundant as the other samples in this study and only makes up 5-9 vol.% of the modal abundance. They occur as well sorted, rounded and altered (serpentinized) grains. Spinel occurs as euhedral opaque phases ranging from 1-5 vol.%

and are located throughout the samples and range in size from 0.02-0.05mm. Unidentified opaque laths make up roughly 4 vol.% of the modal abundance, distributed throughout the samples, and range in length from 0.05-0.2mm. Serpentine is present in low abundances (1-6 vol.%) surrounding other groundmass minerals as interstitial material.

The rock is classified as an aphanitic micaceous coherent kimberlite. Petrographically it is of very low interest, due to the not containing any olivine macrocrysts.

e) Aphanitic variation 3

The Aphanitic variation 3 consists of three samples (TP0306, TP0307, TP0408, TP0510). All the samples are altered with roughly all olivines serpentinized. Olivine macrocrysts make up 5-12 vol.% of the modal abundance. Phlogopite macrocrysts are present in one sample (TP0510) and make up roughly 5 vol.% of that sample. The olivine macrocrysts range in size from 0.5-8mm, well sorted and sub-rounded. The phlogopite macrocrysts range in size from 0.5-7mm, moderately sorted, prismatic, and occasionally rounded.

The groundmass consists of phlogopite, olivine microcrysts, calcite, serpentine, spinel, atoll-textured spinel, and occasional minor perovskite. Phlogopite occurs as pale orange-brown lath-shaped grains varying in abundance from 39-46 vol.% and ranges in size from 0.05-0.5mm in length. These phlogopite laths often have a dark brick red tetraferriphlogopite rims which are 0.005-0.05 mm in width. Spinel and perovskite can occasionally be found as inclusions within phlogopite laths but are found more frequently surrounding phlogopite laths. Calcite occurs as interstitial material and makes up 12-31 vol.% of the modal abundance. The calcite contains inclusions of phlogopite, spinel and perovskite. The olivine microcrysts are variable in abundance and range from <1-14 vol.%, are rounded, well sorted and completely altered to serpentine. Serpentine is present in variable abundances (5-30 vol.%) as interstitial material. Spinel occurs as euhedral opaque phases distributed in low abundances (4-7 vol.%) throughout the samples and range in size from 0.01-0.07 mm. Atoll-textured spinel is often found with spinel in these samples, however, TP0307 does not contain atoll spinel. Perovskite occurs as ~0.05mm sized semi-opaque, high relief, dark brown grains, however, it is a rarely observed mineral and makes up ~1 vol.% of the sample.

The rock is classified as an aphanitic micaceous coherent kimberlite. Petrographically it is rated as moderate to low interest due to the lack of abundance of olivine macrocrysts (5-12 vol.%) but still having sufficiently small spinel grains (<0.07mm).

f) Macrocrystic variation

The Macrocrystic variation is only made up of one diagnostic sample (TP1013). The sample is altered and contains olivines which have been altered to serpentine. Olivine macrocrysts make up 20 vol.% of the sample. The olivine macrocrysts range in size from 0.5-16mm, is moderately sorted and sub-rounded to sub-angular.

The groundmass consists of phlogopite, calcite, olivine microcrysts, serpentine, spinel, and atoll-textured spinel. Phlogopite occurs as pale orange-brown lath-shaped grains, makes up 18 vol.% and ranges from 0.05-0.5mm in length. These phlogopite laths often have a dark brick red tetraferriphlogopite rims which are 0.005-0.05 mm in width. Spinel can occasionally be found as inclusions within phlogopite laths but are found more frequently surrounding phlogopite laths. Calcite occurs as interstitial material and makes up 23 vol.% of the modal abundance and is anhedral. The calcite contains inclusions of spinel and atoll-textured spinel. The olivine microcrysts occur as slightly aligned rounded to sub-rounded grains and make up only 5 vol.% of the modal abundance. Spinel occurs as euhedral opaque grains located throughout the sample and makes up 8 vol.% of the modal abundance and are 0.01-0.03mm in size. Atoll-textured spinel is relatively abundant and occurs near the spinel grains. Serpentine is present up to 8 vol.% surrounding other groundmass minerals as interstitial material.

The rock is classified as a macrocrystic micaceous coherent kimberlite. Petrographically it is rated as moderate to high interest due to the relatively abundant olivine macrocryst content (20 vol.%), the sufficiently small size of groundmass spinels (<0.07mm) and the proven diamond grades from the kimberlites in Tongo.

Appendix C

Olivine, Phlogopite and Spinel EPMA data

a) Olivine EPMA data

SOM Table. Koidu olivine core EPMA analyses

				Oxide wt%												Cations																
Sample_ID	Location	Grain	Type	Analysis#	SiO2	TiO2	Al2O3	Cr2O3	FeO	MnO	MgO	CaO	NiO	Na2O	K2O	Total	Si	Ti	Al	Cr	Fe	Mn	Mg	Ca	Ni	Na	K	Total	Mg#
Y5770	Koidu	Ol	Core	1	41,14	0,03	0,00	0,05	8,36	0,09	49,35	0,02	0,36	0,03	0,01	99,44	1,01	0,00	0,00	0,00	0,17	0,00	1,80	0,00	0,01	0,00	0,00	2,99	91,3175
Y5770	Koidu	Ol	Core	2	40,51	0,03	0,04	0,02	10,94	0,11	47,01	0,06	0,36	0,04	0,01	99,01	1,01	0,00	0,00	0,00	0,23	0,00	1,74	0,00	0,01	0,00	0,00	2,99	88,54624
Y5770	Koidu	Ol	Core	3	40,15	0,03	0,03	0,04	11,16	0,09	46,84	0,06	0,44	0,04	0	99,13	1,01	0,00	0,00	0,00	0,23	0,00	1,74	0,00	0,01	0,00	0,00	2,99	88,24241
Y5770	Koidu	Ol	Core	4	39,42	0,02	0,03	0,02	14,75	0,11	47,51	0,06	0,42	0,04	0,01	99,69	1,01	0,00	0,00	0,00	0,31	0,00	1,75	0,00	0,01	0,00	0,00	2,99	86,79171
Y5770	Koidu	Ol	Core	5	39,94	0,04	0,01	0	14,35	0,15	46,58	0,05	0,23	0,04	0,01	99,4	1,01	0,00	0,00	0,00	0,30	0,00	1,67	0,00	0,01	0,00	0,00	2,99	84,7647
Y5770	Koidu	Ol	Core	6	41,1	0	0,04	7,33	0,11	49,71	0,01	0,38	0,01	0	0	98,71	1,01	0,00	0,00	0,00	0,15	0,00	1,82	0,00	0,01	0,00	0,00	2,99	92,36017
Y5770	Koidu	Ol	Core	7	40,33	0,02	0,02	12,48	0,13	46,65	0,06	0,3	0,03	0	0	99,42	1,01	0,00	0,00	0,00	0,26	0,00	1,73	0,00	0,01	0,00	0,00	2,99	86,80344
Y5770	Koidu	Ol	Core	8	40,45	0,03	0,02	0,03	11,21	0,1	46,57	0,06	0,38	0,05	0	98,9	1,01	0,00	0,00	0,00	0,23	0,00	1,73	0,00	0,01	0,00	0,00	2,99	88,10321
Y5770	Koidu	Ol	Core	9	40,83	0,02	0	0,01	8,35	0,1	49,44	0,02	0,31	0,02	0	99,29	1,00	0,00	0,00	0,00	0,18	0,00	1,81	0,00	0,01	0,00	0,00	3,00	91,15669
Y5770	Koidu	Ol	Core	10	41,64	0,01	0,01	0,05	5,94	0,07	51,41	0,01	0,41	0,02	0	99,27	1,01	0,00	0,00	0,00	0,12	0,00	1,85	0,00	0,01	0,00	0,00	2,99	94,00934
Y5770	Koidu	Ol	Core	11	41,11	0,03	0	0,03	8,24	0,09	49,38	0,01	0,36	0,03	0	99,28	1,01	0,00	0,00	0,00	0,17	0,00	1,80	0,00	0,01	0,00	0,00	2,99	91,44041
Y5770	Koidu	Ol	Core	12	41,21	0,02	0,01	0,03	7,93	0,1	49,76	0,01	0,36	0,01	0	99,44	1,01	0,00	0,00	0,00	0,16	0,00	1,81	0,00	0,01	0,00	0,00	2,99	91,79875
Y5770	Koidu	Ol	Core	13	40,74	0,04	0,01	0,03	9,78	0,1	48,23	0,02	0,37	0,02	0,01	99,36	1,01	0,00	0,00	0,00	0,20	0,00	1,77	0,00	0,01	0,00	0,00	2,99	89,78657
Y5770	Koidu	Ol	Core	14	41,1	0,04	0	0,04	8,08	0,1	49,64	0,01	0,37	0,02	0	99,42	1,01	0,00	0,00	0,00	0,17	0,00	1,81	0,00	0,01	0,00	0,00	2,99	91,63299
Y5770	Koidu	Ol	Core	15	41,55	0,1	0,04	0,05	12,37	0,11	45,79	0,06	0,36	0,02	0,01	100,45	1,02	0,00	0,00	0,00	0,25	0,00	1,68	0,00	0,01	0,00	0,00	2,97	86,83996
Y5774	Koidu	Ol	Core	1	40,99	0,01	0,01	0,03	5,33	0,06	51,15	0,01	0,36	0,01	0,01	97,97	1,01	0,00	0,00	0,00	0,11	0,00	1,87	0,00	0,01	0,00	0,00	2,99	94,47734
Y5774	Koidu	Ol	Core	2	40,06	0,05	0,02	10,03	0,09	47,22	0,04	0,37	0,04	0,01	0,01	98,08	1,00	0,00	0,00	0,00	0,21	0,00	1,77	0,00	0,01	0,00	0,00	3,00	89,37211
Y5774	Koidu	Ol	Core	3	40,26	0,04	0,03	0,08	8,96	0,08	48,66	0,06	0,36	0,03	0,01	98,18	1,00	0,00	0,00	0,00	0,18	0,00	1,80	0,00	0,01	0,00	0,00	3,00	91,0181
Y5774	Koidu	Ol	Core	4	40,12	0,02	0,01	0,05	8,96	0,09	48,13	0,04	0,35	0,02	0,01	97,8	1,00	0,00	0,00	0,00	0,19	0,00	1,79	0,00	0,01	0,00	0,00	3,00	90,54433
Y5774	Koidu	Ol	Core	5	40,25	0,05	0,04	0,03	10	0,11	47,49	0,04	0,39	0,03	0	98,44	1,00	0,00	0,00	0,00	0,21	0,00	1,77	0,00	0,01	0,00	0,00	2,99	89,43555
Y5774	Koidu	Ol	Core	6	40,16	0,01	0,02	0,04	9,76	0,11	47,7	0,03	0,41	0,05	0,01	98,5	1,01	0,00	0,00	0,00	0,20	0,00	1,77	0,00	0,01	0,00	0,00	3,00	89,70371
Y5774	Koidu	Ol	Core	7	40,18	0,03	0,04	0,03	9,97	0,11	47,15	0,06	0,41	0,03	0,01	98,01	1,01	0,00	0,00	0,00	0,21	0,00	1,76	0,00	0,01	0,00	0,00	2,99	89,39599
Y5774	Koidu	Ol	Core	8	40,59	0,03	0,03	0,04	8,64	0,12	48,62	0,05	0,39	0,06	0	98,55	1,01	0,00	0,00	0,00	0,18	0,00	1,79	0,00	0,01	0,00	0,00	3,00	90,59499
Y5774	Koidu	Ol	Core	9	40,3	0,04	0,02	0,03	8,85	0,08	48,47	0,04	0,38	0,02	0,02	98,27	1,00	0,00	0,00	0,00	0,18	0,00	1,80	0,00	0,01	0,00	0,00	3,00	90,70906
Y5774	Koidu	Ol	Core	10	40,91	0,03	0,04	0,08	8,49	0,1	48,92	0,05	0,38	0,04	0	99,04	1,01	0,00	0,00	0,00	0,17	0,00	1,79	0,00	0,01	0,00	0,00	2,99	91,12818
Y5774	Koidu	Ol	Core	11	40,54	0,01	0,02	0,01	7,98	0,13	49,14	0,02	0,35	0,01	0,02	98,22	1,00	0,00	0,00	0,00	0,17	0,00	1,81	0,00	0,01	0,00	0,00	3,00	91,65084
Y5774	Koidu	Ol	Core	12	40,52	0,02	0,04	0,11	8,27	0,11	48,57	0,06	0,36	0,03	0,01	98,1	1,01	0,00	0,00	0,00	0,17	0,00	1,80	0,00	0,01	0,00	0,00	3,00	91,28119
Y5774	Koidu	Ol	Core	13	40,72	0,06	0,02	0,03	6,41	0,1	50,15	0,01	0,38	0,01	0,01	97,91	1,00	0,00	0,00	0,00	0,13	0,00	1,84	0,00	0,01	0,00	0,00	2,99	93,3096
Y5774	Koidu	Ol	Core	14	39,82	0	0	0	11,24	0,16	46,1	0,03	0,32	0,02	0,02	97,7	1,01	0,00	0,00	0,00	0,24	0,00	1,74	0,00	0,01	0,00	0,00	2,99	87,98822
Y5774	Koidu	Ol	Core	15	40,98	0,01	0	0	6,78	0,11	50,54	0,01	0,36	0,01	0	98,82	1,00	0,00	0,00	0,00	0,14	0,00	1,84	0,00	0,01	0,00	0,00	3,00	93,00123

SOM Table. Koidu olivine rim EPMA analyses

				Oxide wt%												Cations																
Sample_ID	Location	Grain	Type	Analysis#	SiO2	TiO2	Al2O3	Cr2O3	FeO	MnO	MgO	CaO	NiO	Na2O	K2O	Total	Si	Ti	Al	Cr	Fe	Mn	Mg	Ca	Ni	Na	K	Total	Mg#
Y5770	Koidu	Ol	Rim	1 (Line) Pt 1	40,06	0,08	0,01	0,07	12,34	0,13	46,08	0,04	0,37	0,03	0	99,21	1,00	0,00	0,00	0,00	0,26	0,00	1,72	0,00	0,01	0,00	0,00	3,00	86,93953
Y5770	Koidu	Ol	Rim	1 (Line) Pt 2	40,26	0,04	0	0,02	12,17	0,14	46,23	0,04	0,29	0,02	0,01	99,21	1,01	0,00	0,00	0,00	0,25	0,00	1,72	0,00	0,01	0,00	0,00	2,99	87,13272
Y5770	Koidu	Ol	Rim	1 (Line) Pt 3	40,14	0,04	0,01	0,05	12,14	0,15	46,08	0,05	0,3	0,01	0	98,97	1,01	0,00	0,00	0,00	0,25	0,00	1,72	0,00	0,01	0,00	0,00	2,99	87,12395
Y5770	Koidu	Ol	Rim	1 (Line) Pt 4	39,85	0,03	0	0,07	12,44	0,18	46,58	0,06	0,22	0,02	0	99,44	1,00	0,00	0,00	0,00	0,26	0,00	1,74	0,00	0,00	0,00	0,00	3,00	86,9704
Y5770	Koidu	Ol	Rim	2 (Line) Pt 2	40,34	0,02	0,01	0,03	11,52	0,11	46,7	0,03	0,29	0,03	0	99,08	1,01	0,00	0,00	0,00	0,24	0,00	1,74	0,00	0,01	0,00	0,00	2,99	87,8441
Y5770	Koidu	Ol	Rim	2 (Line) Pt 3	40,21	0,03	0,01	0,04	11,93	0,14	46,44	0,05	0,25	0,01	0	99,11	1,00	0,00	0,00	0,00	0,25	0,00	1,73	0,00	0,01	0,00	0,00	2,99	87,40436
Y5770	Koidu	Ol	Rim	2 (Line) Pt 4	40,25	0,05	0	0,06	11,98	0,14	46,57	0,05	0,27	0,03	0	99,41	1,00	0,00	0,00	0,00	0,25	0,00	1,73	0,00	0,01	0,00	0,00	3,00	87,38909
Y5770	Koidu	Ol	Rim	3 (Line) Pt 1	40,37	0,04	0,01	0,04	11,86	0,13	46,51	0,02	0,27	0	0,01	99,26	1,01	0,00	0,00	0,00	0,25	0,00	1,73	0,00	0,01	0,00	0,00	2,99	87,48551
Y5770	Koidu	Ol	Rim	3 (Line) Pt 2	40,21	0,04	0,01	0,05	12,05	0,16	46,3	0,03	0,28	0,02	0	99,15	1,00	0,00	0,00	0,00	0,25	0,00	1,72	0,00	0,01	0,00	0,00	2,99	87,26024
Y5770	Koidu	Ol	Rim	3 (Line) Pt 3	40,21	0,05	0,01	0,04	12,11	0,14	45,92	0,03	0,29	0,01	0,01	98,82	1,01	0,00	0,00	0,00	0,25	0,00	1,72	0,00	0,01	0,00	0,00	2,99	87,11269
Y5770	Koidu	Ol	Rim	3 (Line) Pt 4	40,24	0,04	0,01	0,06	12,26	0,15	45,74	0,05	0,3	0,02	0	98,87	1,01	0,00	0,00	0,00	0,26	0,00	1,71	0,00	0,01	0,00	0,00	2,99	86,92929
Y5774	Koidu	Ol	Rim	1 (Line) Pt 1	40,24	0,05	0,03	0,04	10,45	0,11	48,01	0,04	0,33	0,03	0,02	99,34	1,00	0,00	0,00	0,00	0,22	0,00	1,77	0,00	0,01	0,00	0,00	3,00	89,11845
Y5774	Koidu	Ol	Rim	1 (Line) Pt 2	40,44	0,05	0	0,04	10,7	0,13	47,81	0,04	0,3	0,02	0	99,54	1,00	0,00	0,00	0,00	0,22	0,00	1,76	0,00	0,01	0,00	0,00	3,00	88,84575
Y5774	Koidu	Ol	Rim	1 (Line) Pt 3	40,37	0,06	0,04	0,03	10,78	0,12	47,59	0,04	0,28	0,02	0,01	99,35	1,00	0,00	0,00	0,00	0,22	0,00	1,76	0,00	0,01	0,00	0,00	3,00	88,72566
Y5774	Koidu	Ol	Rim	1 (Line) Pt 4	40,28	0,05	0,01	0,05	11,2	0,14	47,4	0,03	0,25	0,02	0,01	99,42	1,00	0,00	0,00	0,00	0,23	0,00	1,75	0,00	0,01	0,00	0,00	3,00	88,29635
Y5774	Koidu	Ol	Rim	1 (Line) Pt 5	40,38	0,02	0,04	0,03	10,97	0,11	47,22	0,03	0,25	0,03	0,03	99,12	1,00	0,00	0,00	0,00	0,23	0,00	1,75	0,00	0,01	0,00	0,00	3,00	88,47033
Y5774	Koidu	Ol	Rim	1 (Line) Pt 6	40,01	0,03	0,03	0,03	11,1	0,13	47,14	0,04	0,27	0,03	0,02	98,81	1,00	0,00	0,00	0,00	0,23	0,00	1,76	0,00	0,01	0,00	0,00	3,00	88,33215
Y5774	Koidu	Ol	Rim	1 (Line) Pt 7	40,25	0,01	0,02	0,02	11,15	0,13	47,26	0,06	0,28	0,02	0	99,21	1,00	0,00	0,00	0,00	0,23	0,00	1,75	0,00	0,01	0,00	0,00	3,00	88,31201
Y5774	Koidu	Ol	Rim	1 (Line) Pt 8	39,98	0,06	0,03	0,03	11,09	0,15	46,93	0,06	0,25	0,05	0,08	98,7	1,00	0,00	0,00	0,00	0,23	0,00	1,75	0,00	0,01	0,00	0,00	3,00	88,29537
Y5774	Koidu	Ol	Rim	1 (Line) Pt 9	40,21	0,04	0,04	0,04	11,07	0,12	47,18	0,06	0,26	0,04	0,01	99,05	1,00	0,00	0,00	0,00	0,23	0,00	1,75	0,00	0,01	0,00	0,00	3,00	88,36873
Y5774	Koidu	Ol	Rim	1 (Line) Pt 10	39,97	0,05	0,04	0,04	10,82	0,12	46,74	0,06	0,31	0,03	0,01	98,17	1,00	0,00	0,00	0,00	0,23	0,00	1,75	0,00	0,01	0,00	0,00	3,00	88,5065
Y5774	Koidu	Ol	Rim	2 (Line) Pt 1	40,08	0,04	0,01	0,05	11,11	0,12	46,67	0,04	0,29	0,02	0,01	98,45	1,00	0,00	0,00	0,00	0,23	0,00	1,74	0,00	0,01	0,00	0,00	2,99	88,21492
Y5774	Koidu	Ol	Rim	2 (Line) Pt 2	40,06	0,03	0,02	0,05	11	0,12	46,65	0,05	0,28	0,04	0,01	98,32	1,01	0,00	0,00	0,00	0,23	0,00	1,74	0,00	0,01	0,00	0,00	2,99	88,31772
Y5774	Koidu	Ol	Rim	2 (Line) Pt 3	40,02	0,05	0,02	0,08	11,02	0,13	46,41	0,06	0,3	0,04	0,01	98,14	1,01	0,00	0,00	0,00	0,23	0,00	1,74	0,00	0,01	0,00	0,00	2,99	88,24557
Y5774	Koidu	Ol	Rim	2 (Line) Pt 4	39,73	0,03	0,03	0,11	11,12	0,14	46,84	0,05	0,23	0,03	0,01	98,32	1,00	0,00	0,00	0,00	0,23	0,00	1,75	0,00	0,01	0,00	0,00	3,00	88,24753
Y5774	Koidu	Ol	Rim	2 (Line) Pt 5	39,8	0,03	0,02	0,07	11,18	0,15	46,59	0,05	0,22	0,04	0,01	98,17	1,00	0,00	0,00	0,00	0,24	0,00	1,75	0,00	0,01	0,00	0,00	3,00	88,13576
Y5774	Koidu	Ol	Rim	2 (Line) Pt 6	40,44	0,02	0,02	0,08	11,18	0,12	46,48	0,05	0,23	0,03	0,01	98,64	1,01	0,00	0,00	0,00	0,23	0,00	1,73	0,00	0,01	0,00	0,00	2,99	88,11102
Y5774	Koidu	Ol	Rim	2 (Line) Pt 7	39,87	0,04	0	0,11	11,22	0,16	46,51	0,06	0,19	0,04	0,01	98,2	1,00	0,00	0,00	0,00	0,24	0,00	1,73	0,00	0,00	0,00	0,00	3,00	88,08033
Y5774	Koidu	Ol	Rim	2 (Line) Pt 8	40,3	0,04	0,01	0,11	11,24	0,14	46,2	0,05	0,21	0,03	0,01	98,34	1,01	0,00	0,00	0,00	0,24	0,00	1,73	0,00	0,00	0,00	0,00	2,99	87,99113
Y5774	Koidu	Ol	Rim	2 (Line) Pt 9	40,3	0,03	0,01	0,07	11,25	0,15	46,34	0,05	0,18	0,04	0,02	98,44	1,01	0,00	0,00	0,00	0,24	0,00	1,73	0,00	0,00	0,00	0,00	2,99	88,01369
Y5774	Koidu	Ol	Rim	2 (Line) Pt 10	40,29	0,06	0,02	0,11	11,25	0,15	46,08	0,06	0,17	0,04	0,01	98,25	1,01	0,00	0,00	0,00	0,24	0,00	1,72	0,00	0,00	0,00	0,00	2,99	87,95421
Y5770	Koidu	Ol	Rim	4pt1	40,3	0,05	0	0,05	12,08	0,11	46,53	0,07	0,28	0,02	0,01	99,5	1,00	0,00	0,00	0,00	0,25	0,00	1,73	0,00	0,01	0,00	0,00	3,00	87,28766
Y5770	Koidu	Ol	Rim	4pt2	39,15	0,05	0,01	0,04	12,53	0,17	48,28	0,08	0,26	0,03	0,01	100,61	0,97	0,00	0,00	0,00	0,26	0,00	1,78	0,00	0,01	0,00	0,00	3,03	87,2915
Y5770	Koidu	Ol	Rim	5pt1	40,7	0,04	0,01	0,05	12,61	0,17	46,09	0,04	0,28	0,02	0,01	100,03	1,01	0,00	0,00	0,00	0,26	0,00	1,70	0,00	0,01	0,00	0,00	2,99	86,6943
Y5770	Koidu	Ol	Rim	5pt2	41,01	0,04	0,01	0,02	12,53	0,19	45,3	0,11	0,18	0,02	0,01	99,6	1,02	0,00	0,00	0,00	0,26	0,00	1,69	0,00	0,00	0,00	0,00	2,98	86,61892
Y5770	Koidu	Ol	Rim	6pt1	40,09	0,03	0	0,03	12,29	0,15	45,82	0,06	0,3	0,01	0	98,79	1,01	0,00	0,00	0,00	0,26	0,00	1,72	0,00	0,00	0,00	0,00	2,99	86,92137
Y5770	Koidu	Ol	Rim	6pt2	39,79	0,05	0,01	0,05	12,47	0,17	45,95	0,06	0,22	0,02	0,01	98,81	1,00	0,00	0,00	0,00	0,26	0,00	1,72	0,00	0,00	0,00	0,00	3,00	86,78777
Y5770	Koidu	Ol	Rim	7pt1	40,24	0,03	0	0,02	12,54	0,15	45,86	0,06	0,28	0	0	99,18	1,01	0,00	0,00	0,00	0,26	0,00	1,71	0,00	0,01	0,00	0,00	2,99	86,70081
Y5770	Koidu	Ol	Rim	7pt2	40,54	0,04	0,01	0,03	12,16	0,18	45,63	0,15	0,19	0	0,01	98,94	1,01	0,00	0,00	0,00	0,25	0,00	1,70	0,00	0,01	0,00	0,00	2,98	86,99485
Y5770	Koidu	Ol	Rim	8pt1	39,96	0,05	0,01	0,06	12,29	0,16	45,89	0,06	0,28	0,02	0	98,79	1,00	0,00	0,00	0,00	0,26	0,00	1,72	0,00	0,01	0,00	0,00	2,99	86,93872
Y5770	Koidu	Ol	Rim	8pt2	39,85	0,05	0,01	0,08	12,34	0,14	46,25	0,08	0,25	0	0,01	99,06	1,00	0,00	0,00	0,00	0,26	0,00	1,73	0,00	0,01	0,00	0,00	3,00	86,98129
Y5770	Koidu	Ol	Rim	9pt1	40,51	0,02	0	0,05	12,5	0,15	45,81	0,04	0,25	0,02	0,01	99,35	1,01	0,00	0,00	0,00	0,26	0,00	1,70	0,00	0,01	0,00	0,00	2,99	86,72505
Y5770	Koidu	Ol	Rim	9pt2	40,29	0,04	0,01	0,03	12,48	0,21	45,41	0,12	0,19	0,01	0,02	98,8	1,01	0,00	0,00	0,00	0,26	0,00	1,70	0,00	0,00	0,00	0,00	2,99	86,6423

SOM Table. Kundu olivine core EPMA analyses

					Oxide wt%											Cations													
Sample_ID	Location	Grain	Type	Analysis#	SiO2	TiO2	Al2O3	Cr2O3	FeO	MnO	MgO	CaO	NiO	Na2O	K2O	Total	Si	Ti	Al	Cr	Fe	Mn	Mg	Ca	Ni	Na	K	Total	Mg#
TG11-048	Tongo - Kundu	Ol	Core	1	41,24	0,01	0	0,04	7,93	0,1	49,75	0,01	0,35	0,04	0,03	99,51	1,01	0,00	0,00	0,00	0,16	0,00	1,81	0,00	0,01	0,00	0,00	2,99	91,79224
TG11-048	Tongo - Kundu	Ol	Core	2	40,94	0,03	0	0,01	8,65	0,12	48,94	0,02	0,37	0,02	0,01	99,11	1,01	0,00	0,00	0,00	0,18	0,00	1,80	0,00	0,01	0,00	0,00	2,99	90,97943
TG11-048	Tongo - Kundu	Ol	Core	3	41,7	0	0,01	0,03	6,36	0,08	50,34	0	0,39	0,02	0,01	98,94	1,02	0,00	0,00	0,00	0,13	0,00	1,83	0,00	0,01	0,00	0,00	2,98	93,38173
TG11-048	Tongo - Kundu	Ol	Core	4	41,21	0,02	0,01	0,02	7,63	0,09	49,78	0,02	0,38	0,03	0	99,19	1,01	0,00	0,00	0,00	0,16	0,00	1,82	0,00	0,01	0,00	0,00	2,99	92,08254
TG11-048	Tongo - Kundu	Ol	Core	5	41,29	0,03	0,01	0,02	6,67	0,08	50,35	0,02	0,39	0,03	0	98,9	1,01	0,00	0,00	0,00	0,14	0,00	1,83	0,00	0,01	0,00	0,00	2,99	93,08274
TG11-048	Tongo - Kundu	Ol	Core	6	40,52	0,04	0	0,01	9,32	0,11	47,8	0,03	0,36	0,03	0,01	98,21	1,01	0,00	0,00	0,00	0,19	0,00	1,77	0,00	0,01	0,00	0,00	2,99	90,14067
TG11-048	Tongo - Kundu	Ol	Core	7	40,84	0,02	0	0,01	8,82	0,13	48,33	0,02	0,35	0,02	0,01	98,55	1,01	0,00	0,00	0,00	0,18	0,00	1,78	0,00	0,01	0,00	0,00	2,99	90,7133
TG11-048	Tongo - Kundu	Ol	Core	8	40,91	0,01	0	0,02	8,03	0,14	49,54	0,02	0,35	0,02	0,01	99,06	1,00	0,00	0,00	0,00	0,16	0,00	1,81	0,00	0,01	0,00	0,00	3,00	91,66507
TG11-048	Tongo - Kundu	Ol	Core	9	41,07	0,03	0,02	0,04	8,27	0,09	49,17	0,03	0,41	0,02	0	99,16	1,01	0,00	0,00	0,00	0,17	0,00	1,80	0,00	0,01	0,00	0,00	2,99	91,37841
TG11-048	Tongo - Kundu	Ol	Core	10	41,62	0,03	0,01	0,01	6,45	0,09	50,7	0,02	0,38	0,02	0,02	99,33	1,01	0,00	0,00	0,00	0,13	0,00	1,84	0,00	0,01	0,00	0,00	2,99	93,3388
TG11-048	Tongo - Kundu	Ol	Core	11	40,66	0,03	0,02	0,04	10,1	0,15	47,24	0,03	0,34	0,02	0,01	98,65	1,01	0,00	0,00	0,00	0,21	0,00	1,75	0,00	0,01	0,00	0,00	2,99	89,2908
TG11-048	Tongo - Kundu	Ol	Core	12	41,3	0	0	0,02	6,45	0,07	50,74	0	0,4	0,02	0	99,01	1,01	0,00	0,00	0,00	0,13	0,00	1,84	0,00	0,01	0,00	0,00	2,99	93,34377
TG11-048	Tongo - Kundu	Ol	Core	13	41,22	0,03	0	0,01	8,39	0,09	48,88	0,01	0,33	0,01	0,01	99	1,01	0,00	0,00	0,00	0,17	0,00	1,79	0,00	0,01	0,00	0,00	2,99	91,21696
TG11-048	Tongo - Kundu	Ol	Core	14	40,98	0,02	0	0,03	8,42	0,12	48,77	0,02	0,33	0,02	0,01	98,73	1,01	0,00	0,00	0,00	0,17	0,00	1,79	0,00	0,01	0,00	0,00	2,99	91,1702
TG11-048	Tongo - Kundu	Ol	Core	15	40,99	0,04	0	0,02	8,84	0,11	48,45	0,02	0,3	0,02	0,01	98,8	1,01	0,00	0,00	0,00	0,18	0,00	1,78	0,00	0,01	0,00	0,00	2,99	90,71511
TG11-039A	Tongo - Kundu	Ol	Core	1	41,22	0	0	0,02	7,03	0,1	50,73	0,01	0,4	0,03	0,01	99,55	1,00	0,00	0,00	0,00	0,14	0,00	1,84	0,00	0,01	0,00	0,00	3,00	92,78699
TG11-039A	Tongo - Kundu	Ol	Core	2	41,13	0	0	0	7,06	0,1	50,87	0,02	0,43	0,02	0,01	99,64	1,00	0,00	0,00	0,00	0,14	0,00	1,84	0,00	0,01	0,00	0,00	3,00	92,77693
TG11-039A	Tongo - Kundu	Ol	Core	3	41,24	0	0	0,03	7,81	0,1	49,84	0,01	0,39	0,02	0,01	99,45	1,01	0,00	0,00	0,00	0,16	0,00	1,81	0,00	0,01	0,00	0,00	2,99	91,91982
TG11-039A	Tongo - Kundu	Ol	Core	4	41,13	0,03	0,01	0,01	7,77	0,08	50,01	0	0,4	0,03	0,01	99,5	1,00	0,00	0,00	0,00	0,16	0,00	1,82	0,00	0,01	0,00	0,00	3,00	91,98302
TG11-039A	Tongo - Kundu	Ol	Core	5	40,87	0	0	0,01	7,96	0,13	49,81	0,01	0,4	0,01	0	99,21	1,00	0,00	0,00	0,00	0,16	0,00	1,82	0,00	0,01	0,00	0,00	3,00	91,77285
TG11-039A	Tongo - Kundu	Ol	Core	6	41,04	0,03	0,01	0,02	7,93	0,13	49,95	0,03	0,38	0,03	0,01	99,54	1,00	0,00	0,00	0,00	0,16	0,00	1,82	0,00	0,01	0,00	0,00	3,00	91,82241
TG11-039A	Tongo - Kundu	Ol	Core	7	40,86	0,02	0,01	0,02	7,43	0,1	50,15	0	0,39	0,01	0,01	99,01	1,00	0,00	0,00	0,00	0,15	0,00	1,83	0,00	0,01	0,00	0,00	3,00	92,32667
TG11-039A	Tongo - Kundu	Ol	Core	8	41,07	0,01	0	0,01	7,18	0,08	50,58	0,01	0,41	0,02	0,02	99,4	1,00	0,00	0,00	0,00	0,15	0,00	1,84	0,00	0,01	0,00	0,00	3,00	92,62421
TG11-039A	Tongo - Kundu	Ol	Core	9	40,85	0	0	0,01	6,68	0,07	50,57	0,02	0,36	0,02	0,02	98,6	1,00	0,00	0,00	0,00	0,14	0,00	1,85	0,00	0,01	0,00	0,00	3,00	93,10114
TG11-039A	Tongo - Kundu	Ol	Core	10	41,08	0	0	0,02	8	0,11	49,85	0,01	0,36	0,02	0	99,44	1,00	0,00	0,00	0,00	0,16	0,00	1,82	0,00	0,01	0,00	0,00	3,00	91,74101
TG11-039A	Tongo - Kundu	Ol	Core	11	40,89	0	0,01	0,01	7,94	0,09	49,91	0,02	0,4	0,02	0,01	99,31	1,00	0,00	0,00	0,00	0,16	0,00	1,82	0,00	0,01	0,00	0,00	3,00	91,80692
TG11-039A	Tongo - Kundu	Ol	Core	12	41,31	0,01	0	0,01	7,94	0,11	49,88	0	0,36	0,01	0	99,63	1,01	0,00	0,00	0,00	0,16	0,00	1,81	0,00	0,01	0,00	0,00	2,99	91,80240
TG11-039A	Tongo - Kundu	Ol	Core	13	41,17	0	0,02	0,01	7,5	0,08	49,82	0,01	0,36	0,04	0,01	99,03	1,01	0,00	0,00	0,00	0,15	0,00	1,82	0,00	0,01	0,00	0,00	2,99	92,21270
TG11-039A	Tongo - Kundu	Ol	Core	14	40,94	0	0	0,01	8,05	0,09	49,72	0,02	0,41	0,03	0,02	99,29	1,00	0,00	0,00	0,00	0,16	0,00	1,82	0,00	0,01	0,00	0,00	3,00	91,67377
TG11-039A	Tongo - Kundu	Ol	Core	15	41,04	0,04	0,01	0,04	6,94	0,09	50,54	0	0,37	0,02	0,02	99,12	1,00	0,00	0,00	0,00	0,14	0,00	1,84	0,00	0,01	0,00	0,00	3,00	92,84788
TG11-039A-Ol_Fe_1	Tongo - Kundu	Ol	Core	1	40,05	0,03	0,01	0,02	14,45	0,19	44,97	0,03	0,20	0,02	0,01	99,97	1,00	0,00	0,00	0,00	0,30	0,00	1,68	0,00	0,00	0,00	0,00	3,00	84,73233
TG11-039A-Ol_Fe_2	Tongo - Kundu	Ol	Core	2	39,75	0,04	0,01	0,01	15,86	0,21	44,15	0,03	0,12	0,02	0,01	100,21	1,00	0,00	0,00	0,00	0,33	0,00	1,66	0,00	0,00	0,00	0,00	3,00	83,22965
TG11-039A-Ol_Fe_3	Tongo - Kundu	Ol	Core	3	39,66	0,02	0,00	0,02	15,60	0,21	44,12	0,02	0,09	0,03	0,01	99,78	1,00	0,00	0,00	0,00	0,33	0,00	1,66	0,00	0,00	0,00	0,00	3,00	83,44827
TG11-039A-Ol_Fe_4	Tongo - Kundu	Ol	Core	4	39,78	0,01	0,01	0,00	15,56	0,20	43,96	0,02	0,12	0,06	0,02	99,71	1,00	0,00	0,00	0,00	0,33	0,00	1,65	0,00	0,00	0,00	0,00	3,00	83,42988
TG11-039A-Ol_Fe_5	Tongo - Kundu	Ol	Core	5	39,72	0,01	0,00	0,00	15,13	0,20	44,37	0,03	0,17	0,04	0,01	99,67	1,00	0,00	0,00	0,00	0,32	0,00	1,67	0,00	0,00	0,00	0,00	3,00	83,94066
TG11-039A-Ol_Fe_6	Tongo - Kundu	Ol	Core	6	40,71	0,01	0,02	0,02	10,02	0,14	48,25	0,04	0,35	0,02	0,02	99,59	1,00	0,00	0,00	0,00	0,21	0,00	1,77	0,00	0,01	0,00	0,00	3,00	89,56146
TG11-039A-Ol_Fe_7	Tongo - Kundu	Ol	Core	7	40,83	0,03	0,01	0,00	10,15	0,15	48,35	0,04	0,39	0,03	0,01	99,98	1,00	0,00	0,00	0,00	0,21	0,00	1,77	0,00	0,01	0,00	0,00	3,00	89,46217
TG11-039A-Ol_Fe_8	Tongo - Kundu	Ol	Core	8	40,30	0,00	0,01	0,02	12,63	0,17	46,47	0,01	0,29	0,03	0,03	99,97	1,00	0,00	0,00	0,00	0,26	0,00	1,72	0,00	0,01	0,00	0,00	3,00	86,77063
TG11-039A-Ol_Fe_9	Tongo - Kundu	Ol	Core	9	39,90	0,00	0,01	0,02	14,80	0,15	44,39	0,04	0,25	0,05	0,01	99,61	1,00	0,00	0,00	0,00	0,31	0,00	1,67	0,00	0,00	0,00	0,00	3,00	84,24405
TG11-039A-Ol_Fe_10	Tongo - Kundu	Ol	Core	10	40,39	0,00	0,01	0,01	11,77	0,14	46,83	0,02	0,34	0,03	0,02	99,55	1,00	0,00	0,00	0,00	0,24	0,00	1,74	0,00	0,01	0,00	0,00	3,00	87,6445

SOM Table. Kundu olivine rim EPMA analyses

					Oxide wt%											Cations													
Sample_ID	Location	Grain	Type	Analysis#	SiO2	TiO2	Al2O3	Cr2O3	FeO	MnO	MgO	CaO	NiO	Na2O	K2O	Total	Si	Ti	Al	Cr	Fe	Mn	Mg	Ca	Ni	Na	K	Total	Mg#
TG11-048	Tongo - Kundu	Ol	Rim	1 (Line) Pt 1	40,64	0,04	0,01	0,05	9,64	0,13	48,11	0,04	0,36	0,02	0	99,04	1,01	0,00	0,00	0,00	0,20	0,00	1,77	0,00	0,01	0,00	0,00	2,99	89,89543
TG11-048	Tongo - Kundu	Ol	Rim	1 (Line) Pt 2	40,34	0,04	0	0,06	10,22	0,12	47,45	0,06	0,37	0,04	0,01	98,71	1,00	0,00	0,00	0,00	0,21	0,00	1,76	0,00	0,01	0,00	0,00	3,00	89,22007
TG11-048	Tongo - Kundu	Ol	Rim	1 (Line) Pt 3	40,18	0,05	0	0,07	10,46	0,12	47,28	0,05	0,3	0,03	0,01	98,55	1,00	0,00	0,00	0,00	0,22	0,00	1,76	0,00	0,01	0,00	0,00	3,00	88,95958
TG11-048	Tongo - Kundu	Ol	Rim	1 (Line) Pt 4	40,5	0,02	0	0,05	10,18	0,14	47,64	0,1	0,31	0,02	0	98,97	1,01	0,00	0,00	0,00	0,21	0,00	1,76	0,00	0,01	0,00	0,00	2,99	89,29599
TG11-048	Tongo - Kundu	Ol	Rim	2 (Line) Pt 1	40,36	0,03	0,03	0,02	10,26	0,12	47,39	0,06	0,32	0,02	0,01	98,61	1,01	0,00	0,00	0,00	0,21	0,00	1,76	0,00	0,01	0,00	0,00	2,99	89,17023
TG11-048	Tongo - Kundu	Ol	Rim	2 (Line) Pt 2	40,16	0,08	0,01	0,03	11,02	0,11	46,66	0,06	0,34	0,02	0,01	98,49	1,01	0,00	0,00	0,00	0,23	0,00	1,74	0,00	0,01	0,00	0,00	2,99	88,30118
TG11-048	Tongo - Kundu	Ol	Rim	2 (Line) Pt 3	40,33	0,03	0,01	0,02	10,64	0,11	47,11	0,03	0,36	0,03	0,02	98,69	1,01	0,00	0,00	0,00	0,22	0,00	1,75	0,00	0,01	0,00	0,00	2,99	88,75499
TG11-048	Tongo - Kundu	Ol	Rim	2 (Line) Pt 4	40,1	0,03	0	0,04	10,63	0,11	46,93	0,04	0,33	0,03	0,01	98,24	1,01	0,00	0,00	0,00	0,22	0,00	1,75	0,00	0,01	0,00	0,00	2,99	88,72613
TG11-048	Tongo - Kundu	Ol	Rim	3 (Line) Pt 2	40,52	0,04	0,02	0,04	10,47	0,11	46,68	0,05	0,38	0,04	0,02	98,39	1,01	0,00	0,00	0,00	0,22	0,00	1,74	0,00	0,01	0,00	0,00	2,99	88,82403
TG11-048	Tongo - Kundu	Ol	Rim	3 (Line) Pt 3	40,7	0,04	0,01	0,04	10,46	0,12	46,4	0,03	0,35	0,04	0	98,18	1,02	0,00	0,00	0,00	0,22	0,00	1,73	0,00	0,01	0,00	0,00	2,98	88,7737
TG11-048	Tongo - Kundu	Ol	Rim	3 (Line) Pt 4	40,56	0,07	0	0,06	10,59	0,12	45,95	0,04	0,32	0,02	0,01	97,74	1,02	0,00	0,00	0,00	0,22	0,00	1,72	0,00	0,01	0,00	0,00	2,98	88,55158
TG11-039A	Tongo - Kundu	Ol	Rim	rim1 (Line) Pt 1	40,53	0,04	0	0	10,01	0,14	48,2	0,01	0,26	0	0,01	99,19	1,00	0,00	0,00	0,00	0,21	0,00	1,78	0,00	0,01	0,00	0,00	3,00	89,56561
TG11-039A	Tongo - Kundu	Ol	Rim	rim1 (Line) Pt 4	40,12	0,03	0,02	0,03	11,12	0,14	47,53	0,03	0,29	0,01	0	99,33	1,00	0,00	0,00	0,00	0,23	0,00	1,76	0,00	0,01	0,00	0,00	3,00	88,39835
TG11-039A	Tongo - Kundu	Ol	Rim	rim1 (Line) Pt 5	40,4	0,03	0	0,06	10,98	0,14	47,52	0,04	0,29	0,02	0,01	99,52	1,00	0,00	0,00	0,00	0,23	0,00	1,76	0,00	0,01	0,00	0,00	3,00	88,52552
TG11-039A	Tongo - Kundu	Ol	Rim	rim1 (Line) Pt 6	40,34	0,04	0	0,1	11,07	0,13	47,39	0,04	0,27	0,01	0,02	99,41	1,00	0,00	0,00	0,00	0,23	0,00	1,75	0,00	0,01	0,00	0,00	3,00	88,4143
TG11-039A	Tongo - Kundu	Ol	Rim	rim1 (Line) Pt 7	40,44	0,02	0,01	0,06	10,89	0,18	47,43	0,04	0,29	0,03	0,01	99,4	1,00	0,00	0,00	0,00	0,23	0,00	1,75	0,00	0,01	0,00	0,00	3,00	88,58971
TG11-039A	Tongo - Kundu	Ol	Rim	rim1 (Line) Pt 8	40,43	0,05	0,01	0,09	10,81	0,16	47,53	0,05	0,3	0,02	0,01	99,44	1,00	0,00	0,00	0,00	0,22	0,00	1,76	0,00	0,01	0,00	0,00	3,00	88,68518
TG11-039A	Tongo - Kundu	Ol	Rim	rim1 (Line) Pt 9	40,22	0,03	0,01	0,09	10,89	0,16	47,65	0,03	0,31	0,01	0,01	99,41	1,00	0,00	0,00	0,00	0,23	0,00	1,76	0,00	0,01	0,00	0,00	3,00	88,6364
TG11-039A	Tongo - Kundu	Ol	Rim	rim1 (Line) Pt 10	40,31	0,05	0	0,08	10,64	0,17	47,52	0,05	0,27	0,01	0,01	99,11	1,00	0,00	0,00	0,00	0,22	0,00	1,76	0,00	0,01	0,00	0,00	3,00	88,84118
TG11-039A	Tongo - Kundu	Ol	Rim	rim3 (Line) Pt 1	40,42	0,05	0	0,03	11,37	0,12	46,75	0,03	0,33	0,02	0,01	99,13	1,01	0,00	0,00	0,00	0,24	0,00	1,74	0,00	0,01	0,00	0,00	2,99	87,99467
TG11-039A	Tongo - Kundu	Ol	Rim	rim3 (Line) Pt 2	40,21	0,06	0	0,04	10,84	0,16	47,19	0,03	0,3	0,02	0,01	98,85	1,00	0,00	0,00	0,00	0,23	0,00	1,75	0,00	0,01	0,00	0,00	3,00	88,58495
TG11-039A	Tongo - Kundu	Ol	Rim	rim3 (Line) Pt 3	39,98	0,05	0,01	0,02	10,73	0,12	47,11	0,09	0,28	0,04	0,01	98,43	1,00	0,00	0,00	0,00	0,22	0,00	1,76	0,00	0,01	0,00	0,00	3,00	88,67064
TG11-039A	Tongo - Kundu	Ol	Rim	rim3 (Line) Pt 4	40,22	0,03	0	0,04	10,74	0,15	47,2	0,05	0,31	0,03	0,01	98,78	1,00	0,00	0,00	0,00	0,22	0,00	1,76	0,00	0,01	0,00	0,00	3,00	88,68046
TG11-039A	Tongo - Kundu	Ol	Rim	rim3 (Line) Pt 5	39,96	0,04	0	0,05	10,83	0,12	47,07	0,03	0,31	0,02	0	98,43	1,00	0,00	0,00	0,00	0,23	0,00	1,76	0,00	0,01	0,00	0,00	3,00	88,56852
TG11-039A	Tongo - Kundu	Ol	Rim	rim3 (Line) Pt 6	40,36	0,06	0,01	0,04	10,89	0,12	47,05	0,04	0,31	0,02	0	98,9	1,01	0,00	0,00	0,00	0,23	0,00	1,75	0,00	0,01	0,00	0,00	2,99	88,50814
TG11-039A	Tongo - Kundu	Ol	Rim	rim3 (Line) Pt 7	40,16	0,03	0	0,04	10,91	0,14	46,98	0,04	0,31	0,02	0,01	98,65	1,00	0,00	0,00	0,00	0,23	0,00	1,75	0,00	0,01	0,00	0,00	3,00	88,47429
TG11-039A	Tongo - Kundu	Ol	Rim	rim3 (Line) Pt 8	39,15	0,06	0	0,04	11,08	0,16	46,87	0,04	0,31	0,01	0,01	97,72	0,99	0,00	0,00	0,00	0,23	0,00	1,77	0,00	0,01	0,00	0,00	3,01	88,29147
TG11-039A	Tongo - Kundu	Ol	Rim	rim3 (Line) Pt 9	39,39	0,03	0	0,05	10,96	0,12	46,68	0,05	0,27	0,02	0	97,57	1,00	0,00	0,00	0,00	0,23	0,00	1,76	0,00	0,01	0,00	0,00	3,00	88,36187
TG11-039A	Tongo - Kundu	Ol	Rim	rim3 (Line) Pt 10	40,73	0,03	0	0,06	10,82	0,15	46,26	0,05	0,29	0,02	0	98,42	1,02	0,00	0,00	0,00	0,23	0,00	1,72	0,00	0,01	0,00	0,00	2,98	88,40107

SOM Table. Kundu olivine internal zone EPMA analyses

						Oxide wt%											Cations													Mg#
Sample_ID	Location	Grain	Type	Grain#	Analysis#	SiO2	TiO2	Al2O3	Cr2O3	FeO	MnO	MgO	CaO	NiO	Na2O	K2O	Total	Si	Ti	Al	Cr	Fe	Mn	Mg	Ca	Ni	Na	K	Total	Mg#
TG11-039A	Tongo - Kundu	Ol	Internal	1	Pt 2	40,21	0,03	0	0,01	12,8	0,2	45,77	0,03	0,29	0,02	0	99,36	1,01	0,00	0,00	0,00	0,27	0,00	1,71	0,00	0,01	0,00	0,00	2,99	86,48
TG11-039A	Tongo - Kundu	Ol	Internal	1	Pt 3	39,9	0,02	0	0,03	12,78	0,15	45,87	0,02	0,31	0,01	0,01	99,09	1,00	0,00	0,00	0,00	0,27	0,00	1,72	0,00	0,01	0,00	0,00	3,00	85,88
TG11-039A	Tongo - Kundu	Ol	Internal	2	Pt 3	40,19	0,02	0,01	0,01	13,19	0,18	45,01	0,05	0,23	0,04	0,01	98,94	1,01	0,00	0,00	0,00	0,28	0,00	1,69	0,00	0,00	0,00	0,00	2,99	85,96
TG11-039A	Tongo - Kundu	Ol	Internal	2	Pt 4	40,02	0,02	0,02	0,03	13,1	0,16	45	0,03	0,26	0,04	0	98,67	1,01	0,00	0,00	0,00	0,28	0,00	1,69	0,00	0,01	0,00	0,00	2,99	85,95
TG11-039A	Tongo - Kundu	Ol	Internal	2	Pt 5	39,56	0,04	0	0,02	13,23	0,17	45,42	0,04	0,25	0,05	0,03	98,8	1,00	0,00	0,00	0,00	0,28	0,00	1,71	0,00	0,01	0,00	0,00	3,00	85,91
TG11-039A	Tongo - Kundu	Ol	Internal	2	Pt 6	38,58	0,04	0,02	0,03	13,36	0,19	45,71	0,02	0,24	0,04	0,02	98,23	0,98	0,00	0,00	0,00	0,28	0,00	1,74	0,00	0,00	0,00	0,00	3,02	85,95
TG11-039A	Tongo - Kundu	Ol	Internal	2	Pt 7	39,02	0,02	0	0,04	13,41	0,18	46,03	0,04	0,23	0,04	0,01	99,02	0,99	0,00	0,00	0,00	0,28	0,00	1,73	0,00	0,00	0,00	0,00	3,01	86,09
TG11-039A	Tongo - Kundu	Ol	Internal	2	Pt 8	38,92	0,02	0	0	13,21	0,16	45,88	0,04	0,26	0,05	0,01	98,55	0,99	0,00	0,00	0,00	0,28	0,00	1,73	0,00	0,01	0,00	0,00	3,01	86,20
TG11-039A	Tongo - Kundu	Ol	Internal	2	Pt 9	38,7	0,02	0,01	0	13,21	0,18	46,29	0,03	0,23	0,05	0,01	98,72	0,98	0,00	0,00	0,00	0,28	0,00	1,75	0,00	0,00	0,00	0,00	3,02	86,23
TG11-039A	Tongo - Kundu	Ol	Internal	2	Pt 10	38,92	0,02	0,01	0	13,11	0,17	46,05	0,03	0,26	0,05	0	98,62	0,99	0,00	0,00	0,00	0,28	0,00	1,74	0,00	0,01	0,00	0,00	3,01	

SOM Table. Lando olivine core EPMA analyses

					Oxide wt%											Cations												
Sample_ID	Location	Grain	Type	Analysis#	SiO2	TiO2	Al2O3	Cr2O3	FeO	MnO	MgO	CaO	NiO	Na2O	K2O	Total	Si	Ti	Al	Cr	Fe	Mn	Mg	Ca	Ni	Na	K	Total	Mg#
TG12-189	Tongo - Lando	Ol	Core	1	41,33	0,02	0,03	0,02	6,74	0,06	50,85	0,01	0,37	0,01	0,01	99,45	1,00	0,00	0,00	0,00	0,14	0,00	1,84	0,00	0,01	0,00	0,00	2,99	93,07914
TG12-189	Tongo - Lando	Ol	Core	2	41,27	0	0	0,03	8,09	0,1	49,51	0,01	0,43	0,02	0,01	99,47	1,01	0,00	0,00	0,00	0,17	0,00	1,80	0,00	0,01	0,00	0,00	2,99	91,60336
TG12-189	Tongo - Lando	Ol	Core	3	41,65	0,02	0,01	0,03	6,96	0,1	50,44	0,03	0,36	0,02	0,01	99,64	1,01	0,00	0,00	0,00	0,14	0,00	1,82	0,00	0,01	0,00	0,00	2,99	92,81555
TG12-189	Tongo - Lando	Ol	Core	4	41,54	0	0,02	0,03	7,75	0,1	50,02	0,01	0,39	0,02	0,01	99,89	1,01	0,00	0,00	0,00	0,16	0,00	1,81	0,00	0,01	0,00	0,00	2,99	92,00348
TG12-189	Tongo - Lando	Ol	Core	5	41,31	0	0,01	0	7	0,08	50,35	0	0,42	0,01	0,01	99,19	1,01	0,00	0,00	0,00	0,14	0,00	1,83	0,00	0,01	0,00	0,00	2,99	92,76526
TG12-189	Tongo - Lando	Ol	Core	6	41,47	0	0,01	0,05	7,77	0,09	49,93	0,01	0,39	0	0	99,73	1,01	0,00	0,00	0,00	0,16	0,00	1,81	0,00	0,01	0,00	0,00	2,99	91,97121
TG12-189	Tongo - Lando	Ol	Core	7	41,23	0	0,02	0,04	8,37	0,13	48,87	0,04	0,37	0,02	0,01	99,09	1,01	0,00	0,00	0,00	0,17	0,00	1,79	0,00	0,01	0,00	0,00	2,99	91,23442
TG12-189	Tongo - Lando	Ol	Core	8	41,38	0,01	0,01	0,03	6,59	0,09	50,31	0,02	0,36	0,03	0,01	98,83	1,01	0,00	0,00	0,00	0,13	0,00	1,83	0,00	0,01	0,00	0,00	2,99	93,15496
TG12-189	Tongo - Lando	Ol	Core	9	40,97	0	0,01	0	7,96	0,11	49,12	0,03	0,45	0,03	0,01	98,71	1,01	0,00	0,00	0,00	0,16	0,00	1,80	0,00	0,01	0,00	0,00	2,99	91,66691
TG12-189	Tongo - Lando	Ol	Core	10	41,19	0	0	0,03	7,35	0,08	49,44	0,01	0,36	0,03	0,01	98,5	1,01	0,00	0,00	0,00	0,15	0,00	1,81	0,00	0,01	0,00	0,00	2,99	92,30231
TG12-189	Tongo - Lando	Ol	Core	11	41,29	0	0	0	6,89	0,1	50,08	0,01	0,41	0,02	0,01	98,82	1,01	0,00	0,00	0,00	0,14	0,00	1,83	0,00	0,01	0,00	0,00	2,99	92,83517
TG12-189	Tongo - Lando	Ol	Core	12	41,2	0,02	0,01	0,05	7,98	0,12	49,32	0,03	0,44	0,03	0	99,2	1,01	0,00	0,00	0,00	0,16	0,00	1,80	0,00	0,01	0,00	0,00	2,99	91,67877
TG12-189	Tongo - Lando	Ol	Core	13	41,32	0	0,01	0,01	7,64	0,07	49,78	0,02	0,42	0,02	0,01	99,3	1,01	0,00	0,00	0,00	0,16	0,00	1,81	0,00	0,01	0,00	0,00	2,99	92,07299
TG12-189	Tongo - Lando	Ol	Core	14	41,9	0,01	0,01	0,01	7,39	0,09	51,1	0,01	0,42	0,02	0,01	100,97	1,01	0,00	0,00	0,00	0,15	0,00	1,83	0,00	0,01	0,00	0,00	2,99	92,49612
TG12-189	Tongo - Lando	Ol	Core	15	41,19	0	0,02	0	7,21	0,08	50,91	0	0,41	0,01	0,01	99,85	1,00	0,00	0,00	0,00	0,15	0,00	1,84	0,00	0,01	0,00	0,00	3,00	92,64013
TG12-190	Tongo - Lando	Ol	Core	1	41,25	0,01	0,02	0,03	6,92	0,08	50,36	0,02	0,41	0,03	0	99,12	1,01	0,00	0,00	0,00	0,14	0,00	1,83	0,00	0,01	0,00	0,00	2,99	92,84335
TG12-190	Tongo - Lando	Ol	Core	2	40,35	0,02	0,01	0,01	10,93	0,12	47,44	0,02	0,24	0,03	0,01	99,17	1,00	0,00	0,00	0,00	0,23	0,00	1,76	0,00	0,00	0,00	0,00	3,00	88,55473
TG12-190	Tongo - Lando	Ol	Core	3	39,77	0,04	0,02	0,01	14,79	0,19	44,63	0,03	0,25	0,02	0,01	99,76	1,00	0,00	0,00	0,00	0,31	0,00	1,67	0,00	0,01	0,00	0,00	3,00	84,32412
TG12-190	Tongo - Lando	Ol	Core	4	40,96	0,02	0,04	0,05	9,09	0,12	48,52	0,08	0,41	0,03	0	99,32	1,01	0,00	0,00	0,00	0,19	0,00	1,78	0,00	0,01	0,00	0,00	2,99	90,48996
TG12-190	Tongo - Lando	Ol	Core	5	41,14	0	0,01	0,01	7,4	0,1	50,27	0,02	0,42	0,02	0,01	99,39	1,00	0,00	0,00	0,00	0,15	0,00	1,83	0,00	0,01	0,00	0,00	3,00	92,37214
TG12-176	Tongo - Lando	Ol	Core	1	40,66	0,04	0,01	0,01	11,46	0,14	46,81	0,01	0,33	0,02	0,01	99,49	1,01	0,00	0,00	0,00	0,24	0,00	1,73	0,00	0,01	0,00	0,00	2,99	87,92476
TG12-176	Tongo - Lando	Ol	Core	2	41,6	0	0,02	0,05	5,8	0,08	51,14	0	0,34	0,04	0,02	99,09	1,01	0,00	0,00	0,00	0,12	0,00	1,85	0,00	0,01	0,00	0,00	2,99	94,01838
TG12-176	Tongo - Lando	Ol	Core	3	40,86	0,06	0,01	0,03	9,35	0,12	48,45	0,02	0,4	0,03	0,01	99,33	1,01	0,00	0,00	0,00	0,19	0,00	1,78	0,00	0,01	0,00	0,00	2,99	90,23177
TG12-176	Tongo - Lando	Ol	Core	4	41,5	0,01	0	0,01	7,03	0,1	50,26	0,02	0,38	0,04	0,01	99,35	1,01	0,00	0,00	0,00	0,14	0,00	1,82	0,00	0,01	0,00	0,00	2,99	92,72445
TG12-176	Tongo - Lando	Ol	Core	5	41,14	0,03	0	0,02	7,91	0,09	49,95	0	0,43	0,05	0,02	99,66	1,00	0,00	0,00	0,00	0,16	0,00	1,82	0,00	0,01	0,00	0,00	3,00	91,84136
TG12-190A-Ol_Fe_1	Tongo - Lando	Ol	Core	1	40,56	0,04	0,02	0,02	10,70	0,11	47,59	0,02	0,28	0,03	0,01	99,38	1,00	0,00	0,00	0,00	0,22	0,00	1,76	0,00	0,01	0,00	0,00	2,99	88,80089
TG12-190A-Ol_Fe_2	Tongo - Lando	Ol	Core	2	40,50	0,04	0,01	0,07	11,38	0,14	46,87	0,05	0,37	0,04	0,01	99,46	1,01	0,00	0,00	0,00	0,24	0,00	1,74	0,00	0,01	0,00	0,00	2,99	88,01319
TG12-190A-Ol_Fe_3	Tongo - Lando	Ol	Core	3	40,76	0,05	0,00	0,01	10,96	0,14	47,90	0,03	0,24	0,03	0,00	100,11	1,00	0,00	0,00	0,00	0,23	0,00	1,76	0,00	0,00	0,00	0,00	3,00	88,62662
TG12-190A-Ol_Fe_4	Tongo - Lando	Ol	Core	4	40,35	0,05	0,01	0,01	11,96	0,16	46,57	0,03	0,28	0,02	0,00	99,43	1,00	0,00	0,00	0,00	0,25	0,00	1,73	0,00	0,01	0,00	0,00	2,99	87,40405
TG12-190A-Ol_Fe_5	Tongo - Lando	Ol	Core	5	40,13	0,04	0,02	0,00	14,29	0,15	44,85	0,04	0,16	0,04	0,02	99,73	1,01	0,00	0,00	0,00	0,30	0,00	1,68	0,00	0,00	0,00	0,00	2,99	84,83429
TG12-190A-Ol_Fe_6	Tongo - Lando	Ol	Core	6	40,83	0,03	0,00	0,01	9,91	0,13	48,40	0,02	0,33	0,02	0,01	99,70	1,00	0,00	0,00	0,00	0,20	0,00	1,78	0,00	0,01	0,00	0,00	3,00	89,70094
TG12-190A-Ol_Fe_7	Tongo - Lando	Ol	Core	7	40,36	0,04	0,01	0,01	12,11	0,12	46,38	0,02	0,27	0,01	0,01	99,32	1,01	0,00	0,00	0,00	0,25	0,00	1,72	0,00	0,01	0,00	0,00	2,99	87,22645
TG12-190A-Ol_Fe_8	Tongo - Lando	Ol	Core	8	40,00	0,04	0,03	0,00	13,72	0,11	44,93	0,07	0,18	0,05	0,01	99,14	1,01	0,00	0,00	0,00	0,29	0,00	1,69	0,00	0,00	0,00	0,00	2,99	85,38008
TG12-190A-Ol_Fe_9	Tongo - Lando	Ol	Core	9	40,49	0,01	0,01	0,01	10,60	0,14	48,66	0,02	0,27	0,01	0,00	100,22	0,99	0,00	0,00	0,00	0,22	0,00	1,78	0,00	0,01	0,00	0,00	3,00	89,10599
TG12-190A-Ol_Fe_10	Tongo - Lando	Ol	Core	10	40,12	0,07	0,01	0,00	13,92	0,14	45,07	0,05	0,17	0,03	0,02	99,60	1,01	0,00	0,00	0,00	0,29	0,00	1,68	0,00	0,00	0,00	0,00	2,99	85,23018

SOM Table. Lando olivine internal and rind zones EPMA analyses

						Oxide wt%											Cations												
Sample_ID	Location	Grain	Type	Grain#	Analysis#	SiO2	TiO2	Al2O3	Cr2O3	FeO	MnO	MgO	CaO	NiO	Na2O	K2O	Total	Si	Ti	Al	Cr	Fe	Mn	Mg	Ca	Ni	Na	K	Total	Mg#
TG12-190	Tongo - Lando	Ol	Internal	6	Pt 1	40,23	0,02	0	0,02	13,63	0,19	45,13	0,1	0,25	0,02	0,01	99,59	1,01	0,00	0,00	0,00	0,29	0,00	1,69	0,00	0,01	0,00	0,00	2,99	85,51
TG12-190	Tongo - Lando	Ol	Internal	6	Pt 2	39,95	0,04	0	0,04	13,25	0,16	45,42	0,03	0,27	0,01	0	99,17	1,00	0,00	0,00	0,00	0,28	0,00	1,70	0,00	0,01	0,00	0,00	3,00	85,94
TG12-190	Tongo - Lando	Ol	Internal	6	Pt 3	39,83	0,02	0,01	0,03	12,97	0,16	45,55	0,04	0,26	0,03	0,01	98,91	1,00	0,00	0,00	0,00	0,27	0,00	1,71	0,00	0,01	0,00	0,00	3,00	86,23
TG12-176	Tongo - Lando	Ol	Internal	3	Pt 1	40,01	0,05	0,03	0,03	12,52	0,12	46,3	0,06	0,27	0,05	0,02	99,47	1,00	0,00	0,00	0,00	0,26	0,00	1,72	0,00	0,01	0,00	0,00	3,00	86,83
TG12-176	Tongo - Lando	Ol	Internal	3	Pt 2	40,4	0,07	0,02	0,01	13,07	0,13	45,46	0,07	0,24	0,05	0	99,52	1,01	0,00	0,00	0,00	0,27	0,00	1,69	0,00	0,00	0,00	0,00	2,99	86,11
TG12-176	Tongo - Lando	Ol	Internal	3	Pt 3	40,12	0,05	0,03	0	13,26	0,15	45,22	0,08	0,2	0,05	0,01	99,17	1,01	0,00	0,00	0,00	0,28	0,00	1,69	0,00	0,00	0,00	0,00	2,99	85,87
TG12-176	Tongo - Lando	Ol	Internal	3	Pt 4	39,87	0,07	0,01	0,02	13,83	0,13	45,07	0,06	0,21	0,05	0,01	99,31	1,00	0,00	0,00	0,00	0,29	0,00	1,69	0,00	0,00	0,00	0,00	3,00	85,31
TG12-176	Tongo - Lando	Ol	Internal	3	Pt 5	39,93	0,07	0	0	14,11	0,13	45,05	0,07	0,2	0,05	0,02	99,62	1,00	0,00	0,00	0,00	0,30	0,00	1,69	0,00	0,00	0,00	0,00	3,00	85,06
TG12-176	Tongo - Lando	Ol	Internal	3	Pt 6	39,63	0,05	0,02	0,02	13,95	0,12	45,05	0,08	0,19	0,04	0,01	99,16	1,00	0,00	0,00	0,00	0,29	0,00	1,69	0,00	0,00	0,00	0,00	3,00	85,20
TG12-176	Tongo - Lando	Ol	Internal	3	Pt 7	39,54	0,03	0,02	0	14	0,14	45,04	0,07	0,2	0,05	0,02	99,09	1,00	0,00	0,00	0,00	0,30	0,00	1,70	0,00	0,00	0,00	0,00	3,00	85,15
TG12-176	Tongo - Lando	Ol	Internal	3	Pt 8	39,63	0,05	0,03	0,02	13,83	0,15	45,31	0,08	0,18	0,07	0,02	99,38	1,00	0,00	0,00	0,00	0,29	0,00	1,70	0,00	0,00	0,00	0,00	3,00	85,38
TG12-176	Tongo - Lando	Ol	Internal	3	Pt 9	39,47	0,07	0,03	0,01	13,51	0,13	45,36	0,11	0,2	0,06	0,02	98,98	1,00	0,00	0,00	0,00	0,29	0,00	1,71	0,00	0,00	0,00	0,00	3,00	85,68
TG12-176	Tongo - Lando	Ol	Internal	3	Pt 10	39,94	0,08	0,04	0,01	13,36	0,16	45,56	0,12	0,24	0,04	0,02	99,56	1,00	0,00	0,00	0,00	0,28	0,00	1,70	0,00	0,00	0,00	0,00	3,00	85,87
TG12-190	Tongo - Lando	Ol	Rind	6	Pt 8	40,19	0,05	0,01	0,01	12,03	0,23	46,43	0,15	0,22	0,01	0	99,33	1,00	0,00	0,00	0,00	0,25	0,00	1,73	0,00	0,00	0,00	0,00	3,00	87,31
TG12-190	Tongo - Lando	Ol	Rind	6	Pt 9	40,06	0,03	0,01	0,01	12,33	0,24	46,1	0,16	0,23	0,02	0	99,2	1,00	0,00	0,00	0,00	0,26	0,01	1,72	0,00	0,00	0,00	0,00	3,00	86,95
TG12-190	Tongo - Lando	Ol	Rind	6	Pt 10	39,96	0	0,02	0,02	12,74	0,26	46,01	0,22	0,25	0,01	0	99,48	1,00	0,00	0,00	0,00	0,27	0,01	1,72	0,01	0,01	0,00	0,00	3,00	86,56

SOM Table. Lando olivine rim EPMA analyses

					Oxide wt%												Cations														
Sample_ID	Location	Grain	Type	Analysis#	SiO2	TiO2	Al2O3	Cr2O3	FeO	MnO	MgO	CaO	NiO	Na2O	K2O	Total	Si	Ti	Al	Cr	Fe	Mn	Mg	Ca	Ni	Na	K	Total	Mg#
TG12-189	Tongo - Lando	Ol	Rim	1 (Line) Pt 1	40,64	0,05	0,01	0,01	11,18	0,14	47,18	0,04	0,36	0,04	0,02	99,66	1,01	0,00	0,00	0,00	0,23	0,00	1,74	0,00	0,01	0,00	0,00	2,99	88,26672
TG12-189	Tongo - Lando	Ol	Rim	1 (Line) Pt 2	40,59	0,05	0,01	0	11,47	0,17	47,33	0,03	0,33	0,01	0,02	100	1,00	0,00	0,00	0,00	0,24	0,00	1,74	0,00	0,01	0,00	0,00	3,00	88,03237
TG12-189	Tongo - Lando	Ol	Rim	1 (Line) Pt 3	40,55	0,03	0	0	11,45	0,17	47,38	0,03	0,3	0,02	0	99,92	1,00	0,00	0,00	0,00	0,24	0,00	1,75	0,00	0,01	0,00	0,00	3,00	88,06185
TG12-189	Tongo - Lando	Ol	Rim	1 (Line) Pt 4	39,94	0,06	0,01	0,01	11,62	0,15	47,4	0,07	0,33	0,03	0,02	99,64	0,99	0,00	0,00	0,00	0,24	0,00	1,76	0,00	0,01	0,00	0,00	3,01	87,91053
TG12-189	Tongo - Lando	Ol	Rim	2 (Line) Pt 1	40,89	0,02	0,02	0,01	10,69	0,14	47,57	0,01	0,28	0,02	0	99,65	1,01	0,00	0,00	0,00	0,22	0,00	1,75	0,00	0,01	0,00	0,00	2,99	88,80508
TG12-189	Tongo - Lando	Ol	Rim	2 (Line) Pt 2	40,96	0,04	0	0,02	9,84	0,13	48,56	0,02	0,3	0,02	0,01	99,91	1,00	0,00	0,00	0,00	0,20	0,00	1,78	0,00	0,01	0,00	0,00	2,99	89,79301
TG12-189	Tongo - Lando	Ol	Rim	2 (Line) Pt 3	40,81	0,03	0	0,04	10,16	0,12	48,39	0,02	0,33	0,03	0,01	99,93	1,00	0,00	0,00	0,00	0,21	0,00	1,77	0,00	0,01	0,00	0,00	3,00	89,46293
TG12-189	Tongo - Lando	Ol	Rim	2 (Line) Pt 4	40,18	0,07	0,01	0,02	10,4	0,15	48,58	0,15	0,31	0,03	0,03	99,93	0,99	0,00	0,00	0,00	0,21	0,00	1,79	0,00	0,01	0,00	0,00	3,01	89,27837
TG12-189	Tongo - Lando	Ol	Rim	3 (Line) Pt 1	40,89	0,04	0	0,01	9,43	0,15	48,23	0,03	0,3	0,04	0,02	99,14	1,01	0,00	0,00	0,00	0,19	0,00	1,77	0,00	0,01	0,00	0,00	2,99	90,11595
TG12-189	Tongo - Lando	Ol	Rim	3 (Line) Pt 2	40,53	0,03	0,01	0,04	10,5	0,14	47,79	0,05	0,27	0,02	0,01	99,39	1,00	0,00	0,00	0,00	0,22	0,00	1,76	0,00	0,01	0,00	0,00	3,00	89,02728
TG12-189	Tongo - Lando	Ol	Rim	3 (Line) Pt 3	40,2	0,03	0,01	0,03	10,47	0,15	47,57	0,06	0,25	0,03	0,01	98,81	1,00	0,00	0,00	0,00	0,22	0,00	1,77	0,00	0,01	0,00	0,00	3,00	89,01015
TG12-190	Tongo - Lando	Ol	Rim	1 (Line) Pt 1	40,39	0,04	0	0,02	10,41	0,12	47,8	0,02	0,3	0,03	0	99,13	1,00	0,00	0,00	0,00	0,22	0,00	1,77	0,00	0,01	0,00	0,00	3,00	89,11313
TG12-190	Tongo - Lando	Ol	Rim	1 (Line) Pt 2	40,64	0,05	0,01	0,04	10,35	0,14	47,88	0,02	0,31	0,02	0,01	99,48	1,00	0,00	0,00	0,00	0,21	0,00	1,76	0,00	0,01	0,00	0,00	2,99	89,18522
TG12-190	Tongo - Lando	Ol	Rim	1 (Line) Pt 3	40,52	0,05	0,01	0,06	10,7	0,13	47,74	0,07	0,31	0,01	0,02	99,62	1,00	0,00	0,00	0,00	0,22	0,00	1,76	0,00	0,01	0,00	0,00	3,00	88,83122
TG12-190	Tongo - Lando	Ol	Rim	1 (Line) Pt 4	40,36	0,03	0	0,03	10,75	0,11	47,7	0,03	0,27	0,03	0	99,32	1,00	0,00	0,00	0,00	0,22	0,00	1,76	0,00	0,01	0,00	0,00	3,00	88,77651
TG12-190	Tongo - Lando	Ol	Rim	1 (Line) Pt 5	40,33	0,06	0,01	0,04	10,81	0,14	47,93	0,03	0,29	0,02	0	99,66	1,00	0,00	0,00	0,00	0,22	0,00	1,77	0,00	0,01	0,00	0,00	3,00	88,769
TG12-190	Tongo - Lando	Ol	Rim	1 (Line) Pt 6	40,44	0,05	0,01	0,02	10,66	0,16	47,82	0,05	0,32	0,02	0	99,55	1,00	0,00	0,00	0,00	0,22	0,00	1,76	0,00	0,01	0,00	0,00	3,00	88,88488
TG12-190	Tongo - Lando	Ol	Rim	1 (Line) Pt 7	40,52	0,04	0	0,03	10,69	0,12	47,9	0,04	0,29	0,03	0,01	99,68	1,00	0,00	0,00	0,00	0,22	0,00	1,76	0,00	0,01	0,00	0,00	3,00	88,87362
TG12-190	Tongo - Lando	Ol	Rim	1 (Line) Pt 9	40,37	0,03	0	0,03	10,51	0,18	48,53	0,05	0,33	0,01	0,01	100,04	0,99	0,00	0,00	0,00	0,22	0,00	1,78	0,00	0,01	0,00	0,00	3,01	89,1673
TG12-190	Tongo - Lando	Ol	Rim	1 (Line) Pt 10	39,01	0,07	0	0,02	10,21	0,19	49,49	0,08	0,22	0,01	0,01	99,31	0,97	0,00	0,00	0,00	0,21	0,00	1,83	0,00	0,00	0,00	0,00	3,03	89,6274
TG12-190	Tongo - Lando	Ol	Rim	2 (Line) Pt 1	40,53	0,04	0,01	0,05	10,5	0,12	47,9	0,03	0,36	0,02	0,01	99,57	1,00	0,00	0,00	0,00	0,22	0,00	1,76	0,00	0,01	0,00	0,00	3,00	89,04972
TG12-190	Tongo - Lando	Ol	Rim	2 (Line) Pt 2	40,52	0,02	0	0,06	10,71	0,12	47,88	0,02	0,37	0,02	0	99,73	1,00	0,00	0,00	0,00	0,22	0,00	1,76	0,00	0,01	0,00	0,00	3,00	88,85099
TG12-190	Tongo - Lando	Ol	Rim	2 (Line) Pt 3	40,63	0,02	0,03	0,06	10,66	0,14	47,65	0,03	0,36	0,03	0,01	99,6	1,00	0,00	0,00	0,00	0,22	0,00	1,76	0,00	0,01	0,00	0,00	3,00	88,84964
TG12-190	Tongo - Lando	Ol	Rim	2 (Line) Pt 4	40,43	0,02	0,01	0,07	10,68	0,13	47,32	0,03	0,3	0,02	0	99,01	1,01	0,00	0,00	0,00	0,22	0,00	1,75	0,00	0,01	0,00	0,00	2,99	88,76192
TG12-190	Tongo - Lando	Ol	Rim	2 (Line) Pt 5	40,54	0,02	0,01	0,09	10,72	0,15	47,82	0,05	0,32	0,02	0,01	99,75	1,00	0,00	0,00	0,00	0,22	0,00	1,76	0,00	0,01	0,00	0,00	3,00	88,8293
TG12-190	Tongo - Lando	Ol	Rim	2 (Line) Pt 6	40,44	0,04	0,01	0,07	10,73	0,15	47,72	0,02	0,29	0,03	0	99,49	1,00	0,00	0,00	0,00	0,22	0,00	1,76	0,00	0,01	0,00	0,00	3,00	88,79925
TG12-190	Tongo - Lando	Ol	Rim	2 (Line) Pt 7	40,29	0,04	0	0,07	10,6	0,15	47,91	0,06	0,27	0,01	0	99,41	1,00	0,00	0,00	0,00	0,22	0,00	1,77	0,00	0,01	0,00	0,00	3,00	88,959
TG12-190	Tongo - Lando	Ol	Rim	2 (Line) Pt 8	40,31	0,07	0,01	0,03	10,63	0,16	47,91	0,06	0,29	0,01	0,01	99,5	1,00	0,00	0,00	0,00	0,22	0,00	1,77	0,00	0,01	0,00	0,00	3,00	88,93121
TG12-190	Tongo - Lando	Ol	Rim	2 (Line) Pt 9	40,16	0,03	0,01	0,04	10,18	0,16	48,22	0,04	0,31	0,02	0,01	99,18	1,00	0,00	0,00	0,00	0,21	0,00	1,78	0,00	0,01	0,00	0,00	3,00	89,4111
TG12-190	Tongo - Lando	Ol	Rim	2 (Line) Pt 10	39,94	0,08	0	0,05	10,33	0,19	48,73	0,09	0,21	0,02	0	99,62	0,99	0,00	0,00	0,00	0,21	0,00	1,80	0,00	0,00	0,00	0,00	3,01	89,37216
TG12-190	Tongo - Lando	Ol	Rim	3 (Line) Pt 1	40,55	0,05	0	0,05	10,55	0,13	47,77	0,04	0,3	0,02	0	99,46	1,00	0,00	0,00	0,00	0,22	0,00	1,76	0,00	0,01	0,00	0,00	3,00	88,97669
TG12-190	Tongo - Lando	Ol	Rim	3 (Line) Pt 2	40,48	0,01	0	0,06	10,77	0,15	47,43	0,05	0,3	0,02	0,01	99,27	1,00	0,00	0,00	0,00	0,22	0,00	1,75	0,00	0,01	0,00	0,00	3,00	88,69701
TG12-190	Tongo - Lando	Ol	Rim	3 (Line) Pt 3	40,63	0,04	0	0,04	10,72	0,15	47,61	0,05	0,29	0,02	0,01	99,56	1,00	0,00	0,00	0,00	0,22	0,00	1,76	0,00	0,01	0,00	0,00	2,99	88,78556
TG12-190	Tongo - Lando	Ol	Rim	3 (Line) Pt 4	40,59	0,03	0,01	0,04	10,64	0,15	47,49	0,05	0,3	0,03	0,01	99,34	1,01	0,00	0,00	0,00	0,22	0,00	1,75	0,00	0,01	0,00	0,00	2,99	88,83492
TG12-190	Tongo - Lando	Ol	Rim	3 (Line) Pt 5	40,6	0,03	0	0,04	10,73	0,13	47,69	0,06	0,28	0,01	0	99,56	1,00	0,00	0,00	0,00	0,22	0,00	1,76	0,00	0,01	0,00	0,00	3,00	88,79299
TG12-190	Tongo - Lando	Ol	Rim	3 (Line) Pt 6	40,74	0,05	0	0,07	10,63	0,16	47,75	0,05	0,29	0,02	0	99,77	1,00	0,00	0,00	0,00	0,22	0,00	1,76	0,00	0,01	0,00	0,00	2,99	88,89824
TG12-190	Tongo - Lando	Ol	Rim	3 (Line) Pt 7	40,55	0,04	0	0,07	10,66	0,12	47,82	0,07	0,29	0,02	0,01	99,64	1,00	0,00	0,00	0,00	0,22	0,00	1,76	0,00	0,01	0,00	0,00	3,00	88,88488
TG12-190	Tongo - Lando	Ol	Rim	3 (Line) Pt 8	40,25	0,04	0,01	0,09	10,52	0,15	48,21	0,08	0,29	0,02	0,01	99,68	0,99	0,00	0,00	0,00	0,22	0,00	1,78	0,00	0,01	0,00	0,00	3,00	89,09399
TG12-190	Tongo - Lando	Ol	Rim	3 (Line) Pt 9	40,22	0,04	0	0,06	10,47	0,15	48,34	0,07	0,33	0,01	0,01	99,71	0,99	0,00	0,00	0,00	0,22	0,00	1,78	0,00	0,01	0,00	0,00	3,01	89,16624
TG12-190	Tongo - Lando	Ol	Rim	3 (Line) Pt 10	40,19	0,06	0,01	0,08	10,37	0,16	48,49	0,1	0,3	0,03	0,05	99,83	0,99	0,00	0,00	0,00	0,21	0,00	1,78	0,00	0,01	0,00	0,00	3,01	89,28827
TG12-190	Tongo - Lando	Ol	Rim	4 (Line) Pt 1	40,43	0,03	0,01	0,02	10,74	0,16	47,69	0,04	0,35	0,02	0	99,49	1,00	0,00	0,00	0,00	0,22	0,00	1,76	0,00	0,01	0,00	0,00	3,00	88,78372
TG12-190	Tongo - Lando	Ol	Rim	4 (Line) Pt 2	40,34	0,03	0,01	0,03	10,69	0,16	47,82	0,02	0,34	0,05	0,05	99,55	1,00	0,00	0,00	0,00	0,22	0,00	1,77	0,00	0,01	0,00	0,00	3,00	88,85708
TG12-190	Tongo - Lando	Ol	Rim	4 (Line) Pt 3	40,6	0,04	0,01	0,04	10,79	0,12	47,64	0,02	0,33	0,02	0,01	99,62	1,00	0,00	0,00	0,00	0,22	0,00	1,76	0,00	0,01	0,00	0,00	3,00	88,72689
TG12-190	Tongo - Lando	Ol	Rim	4 (Line) Pt 4	40,31	0,04	0,01	0,04	10,74	0,14	47,66	0,05	0,35	0,02	0	99,36	1,00	0,00	0,00	0,00	0,22	0,00	1,76	0,00	0,01	0,00	0,00	3,00	88,77745
TG12-190	Tongo - Lando	Ol	Rim	4 (Line) Pt 5	40,64	0,05	0,01	0,03	10,86	0,13	47,54	0,03	0,3	0,01	0	99,61	1,00	0,00	0,00	0,00	0,22	0,00	1,75	0,00	0,01	0,00	0,00	2,99	88,64091
TG12-190	Tongo - Lando	Ol	Rim	4 (Line) Pt 6	40,44	0,04	0	0,05	10,77	0,14	47,62	0,03	0,32	0,01	0	99,41	1,00	0,00	0,00	0,00	0,22	0,00	1,76	0,00	0,01	0,00	0,00	3,00	88,74124
TG12-190	Tongo - Lando	Ol	Rim	4 (Line) Pt 7	40,38	0,05	0,01	0,05	10,82	0,14	47,51	0,06	0,32	0,02	0,01	99,35	1,00	0,00	0,00	0,00	0,22	0,00	1,76	0,00	0,01	0,00	0,00	3,00	88,67167
TG12-190	Tongo - Lando	Ol	Rim	4 (Line) Pt 8	40,42	0,06	0,01	0,04	10,9	0,16	47,61	0,06	0,31	0,02	0,02	99,61	1,00	0,00	0,00	0,00	0,23	0,00	1,76	0,00	0,01	0,00	0,00	3,00	88,61869
TG12-190	Tongo - Lando	Ol	Rim	4 (Line) Pt 9	40,14	0,05	0	0,04	10,9	0,15	47,42	0,07	0,29	0,02	0,02	99,09	1,00	0,00	0,00	0,00	0,23	0,00	1,76	0,00	0,01	0,00	0,00	3,00	88,57829
TG12-190	Tongo - Lando	Ol	Rim	4 (Line) Pt 10	39,91	0,04	0,01	0,05	10,73	0,17	47,21	0,05	0,32	0,02	0,01	98,51	1,00	0,00	0,00	0,00	0,22	0,00	1,76	0,00	0,01	0,00	0,00	3,00	88,69193
TG12-190	Tongo - Lando	Ol	Rim	5 (Line) Pt 1	40,65	0,02	0	0,03	9,8	0,13	48,31	0,01	0,39	0,02	0,02	99,39	1,00	0,00	0,00	0,00	0,20	0,00	1,78	0,00	0,01	0,00	0,00	3,00	89,78303
TG12-190	Tongo - Lando	Ol	Rim	5 (Line) Pt 2	40,68	0,03	0	0,06	9,74	0,14	48,32	0,02	0,35	0,02	0,01	99,38	1,00	0,00	0,00	0,00	0,20	0,00	1,78	0,00	0,01	0,00	0,00	3,00	89,84112
TG12-190	Tongo - Lando	Ol	Rim	5 (Line) Pt 3	40,5	0,03	0,01	0,04	9,77	0,12	48,35	0,02	0,33	0	0	99,19	1,00	0,00	0,00	0,00	0,20	0,00	1,78	0,00	0,01	0,00	0,00	3,00	89,81869
TG12-190	Tongo - Lando	Ol	Rim	5 (Line) Pt 4	40,52	0,05	0	0,03	10,11	0,12	48,04	0,03	0,32	0,03	0,01	99,26	1,00	0,00	0,00	0,00	0,21	0,00	1,77	0,00	0,01	0,00	0,00	3,00	89,44098
TG12-190	Tongo - Lando	Ol	Rim	5 (Line) Pt 5	40,67	0,03	0,01	0,02	10,32	0,14	47,81	0,03	0,33	0,01	0,02	99,38	1,01	0,00	0,00	0,00	0,21	0,00	1,76	0,00	0,01	0,00	0,00	2,99	89,1991
TG12-190	Tongo - Lando	Ol	Rim	5 (Line) Pt 6	40,6	0	0,01	0,01	10,45	0,11	47,75	0,04	0,32	0,01	0	99,3	1,01	0,00	0,00	0,00	0,22	0,00	1,76	0,00	0,01	0,00	0,00	2,99	89,06567
TG12-190	Tongo - Lando	Ol	Rim	5 (Line) Pt 7	40,25	0,04	0	0,03	10,4	0,15	47,84	0,02	0,34	0,01	0	99,08	1,00	0,00	0,00	0,00	0,22	0,00	1,77	0,00	0,01	0,00	0,00	3,00	89,13055
TG12-190	Tongo - Lando	Ol	Rim	5 (Line) Pt 8	40,09	0,05	0	0,04	10,59	0,13	48	0,03	0,36	0,02	0,01	99,32	0,99	0,00	0,00	0,00	0,22	0,00	1,78	0,00	0,01	0,00	0,00	3,00	88,98668
TG12-190	Tongo - Lando	Ol	Rim	5 (Line) Pt 9	40,16	0,03	0,02	0,04	10,81	0,12	47,93	0,04	0,3	0,02	0	99,46	1,00	0,00	0,00	0,00	0,22	0,00	1,77	0,00	0,01	0,00	0,00	3,00	88,769
TG12-190	Tongo - Lando	Ol	Rim	5 (Line) Pt 10	40,15	0,06	0,01	0,02	10,64	0,13	48,19	0,06	0,29	0,02	0	99,56	0,99	0,00	0,00	0,00	0,22	0,00	1,78	0,00	0,01	0,00	0,00	3,01	88,97923
TG12-190	Tongo - Lando	Ol	Rim	6 (Line) Pt 4	40,26	0,04	0	0,02	11,23	0,15	46,96	0,06	0,32	0,03	0,01	99,09	1,00	0,00	0,00	0,00	0,23	0,00	1,74	0,00	0,01	0,00	0,00	3,00	88,17177
TG12-190	Tongo - Lando	Ol	Rim	6 (Line) Pt 5	40,59	0,06	0	0,01	10,64	0,14	47,77	0,03	0,33	0	0	99,57	1,00	0,00	0,00	0,00	0,22	0,00	1,76	0,00	0,01	0,00	0,00	3,00	88,89309
TG12-190	Tongo - Lando	Ol	Rim	6 (Line) Pt 6	40,57	0,04	0,01	0,03	10,58	0,13	47,75	0,03	0,35	0,01	0	99,5	1,00	0,00	0,00	0,00	0,22	0,00	1,76	0,00	0,01	0,00	0,00	3,00	88,94469
TG12-190	Tongo - Lando	Ol	Rim	6 (Line) Pt 7	40,18	0,05	0,01	0,04	10,95	0,16	47,25	0,08	0,28	0,02	0	99,02	1,00	0,00	0,00	0,00	0,23	0,00	1,75	0,00	0,01	0,00	0,00	3,00	88,4954
TG12-190	Tongo - Lando	Ol	Rim	6 (Line) Pt 2	40,58	0,05	0,01	0,05	10,07	0,1	47,89	0,03	0,33	0,02	0,02	99,17	1,00	0,00	0,00	0,00	0,21	0,00	1,77	0,00	0,01	0,00	0,00	2,99	89,44889
TG12-176	Tongo - Lando	Ol	Rim	1 (Line) Pt 3	40,44	0,04	0,02	0,06	10,39	0,12	47,8	0,05	0,33	0,03	0,01	99,28	1,00	0,00	0,00	0,00	0,22	0,00	1,77	0,00	0,01	0,00	0,00	3,00	89,13177
TG12-176	Tongo - Lando	Ol	Rim	1 (Line) Pt 4	40,41	0,03	0	0,05	10,45	0,14	47,79	0,05	0,31	0,02	0	99,25	1,00	0,00	0,00	0,00	0,22	0,00	1,77	0,00	0,01	0,00	0,00	3,00	89,07383
TG12-176	Tongo - Lando	Ol	Rim	1 (Line) Pt 5	40,49	0,01	0,01	0,03	10,22	0,14	47,98	0,06	0,37	0,05	0,01	99,37	1,00	0,00	0,00	0,00	0,21	0,00	1,77	0,00	0,01	0,00	0,00	3,00	89,32644
TG12-176	Tongo - Lando	Ol	Rim	1 (Line) Pt 6	40,72	0,03	0,03	0,04	10,05	0,15	48	0,07	0,33	0,03	0,01	99,46	1,01	0,00	0,00	0,00	0,21	0,00	1,77	0,00	0,01	0,00	0,00	2,99	89,48923
TG12-176	Tongo - Lando	Ol	Rim	1 (Line) Pt 7	40,49	0,06	0,01	0,05	10,46	0,1	47,91	0,08	0,35	0,03	0,01	99,54	1,00	0,00	0,00	0,00	0,22	0,00	1,77	0,00	0,01	0,00	0,00	3,00	89,08892
TG12-176	Tongo - Lando	Ol	Rim	1 (Line) Pt 8	40,56	0,03	0,01	0,04	10,46	0,13	47,78	0,06	0,33	0,03	0,01	99,43	1,00	0,00	0,00	0,00	0,22	0,00	1,76	0,00	0,01	0,00	0,00	3,00	89,06248
TG12-176	Tongo - Lando	Ol	Rim	1 (Line) Pt 9	40,53	0,04	0,01	0,04	10,42	0,14	47,85	0,06	0,33	0,03	0,01	99,46	1,00	0,00	0,00	0,00	0,22	0,00	1,76	0,00	0,01	0,00	0,00	3,00	89,11395
TG12-176	Tongo - Lando	Ol	Rim	1 (Line) Pt 10	40,48	0,03	0	0,05	10,29	0,12	48,21	0,07	0,36	0,05	0	99,67	1,00	0,00	0,00	0,00	0,21	0,00	1,77	0,00	0,01	0,00	0,00	3,00	89,30694
TG12-176	Tongo - Lando	Ol	Rim	2 (Line) Pt 1	40,48	0,04	0,01	0,05	10,43	0,11	47,64	0,03	0,34	0,04	0,01	99,19	1,00	0,00	0,00	0,00	0,22	0,00	1,76	0,00	0,01	0,00	0,00	3,00	89,06187
TG12-176	Tongo - Lando	Ol	Rim	2 (Line) Pt 2	40,44	0,03	0,01	0,04	10,41	0,14	47,88	0,03	0,35	0,04	0,01	99,38	1,00	0,00	0,00	0,00	0,22	0,00	1,77	0,00	0,01	0,00	0,00	3,00	89,12934
TG12-176	Tongo - Lando	Ol	Rim	2 (Line) Pt 3	40,72	0,05	0,02	0,05	10,47	0,12	47,69	0,04	0,3	0,06	0	99,53	1,01	0,00	0,00	0,00	0,22	0,00	1,76	0,00	0,01	0,00	0,00	2,99	89,03477
TG12-176	Tongo - Lando	Ol	Rim	2 (Line) Pt 4	41,15	0,04	0	0,06	10,47	0,12	47,33	0,04	0,32	0,06	0,01	99,6	1,01	0,00	0,00	0,00	0,22	0,00	1,74	0,00	0,01	0,00	0,00	2,99	88,96057
TG12-176	Tongo - Lando	Ol	Rim	2 (Line) Pt 5	40,49	0,06	0	0,04	10,52	0,13	47,65	0,05	0,31	0,05	0	99,31	1,00	0,00	0,00	0,00	0,22	0,00	1,76	0,00	0,01	0,00	0,00	3,00	88,97995
TG12-176	Tongo - Lando	Ol	Rim	2 (Line) Pt 6	40,46	0,03	0,01	0,03	10,14	0,13	47,73	0,05	0,4	0,04	0,01	99,01	1,00	0,00	0,00	0,00	0,21	0,00	1,77	0,00	0,01	0,00	0,00	3,00	89,35153
TG12-176	Tongo - Lando	Ol	Rim	2 (Line) Pt 7	40,64	0,03	0,01	0,06	9,78	0,15	48,13	0,08	0,35	0,06	0	99,28	1,00	0,00	0,00	0,00	0,20	0,00	1,77	0,00	0,01	0,00	0,00	3,00	89,76752
TG12-176	Tongo - Lando	Ol	Rim	2 (Line) Pt 8	40,59	0,04	0,01	0,05	9,5	0,16	48,15	0,18	0,31	0,06	0,07	99,13	1,00	0,00	0,00	0,00	0,20	0,00	1,78	0,00	0,01	0,00	0,00	3,00	90,035
TG12-176	Tongo - Lando	Ol	Rim	2 (Line) Pt 9	40,84	0,04	0,01	0,06	9,62	0,13	48,45	0,1	0,21	0,04	0,01	99,5	1,01	0,00	0,00	0,00	0,20	0,00	1,78	0,00	0,00	0,00	0,00	2,99	89,97796
TG12-176	Tongo - Lando	Ol	Rim	2 (Line) Pt 10	40,83	0,05	0,01	0,02	9,34	0,18	48,25	0,15	0,18	0,03	0,01	99,06	1,01	0,00	0,00	0,00	0,19	0,00	1,78	0,00	0,00	0,00	0,00	2,99	90,20471
TG12-176	Tongo - Lando

SOM Table. Pandebu olivine core EPMA analyses

					Oxide wt%												Cations												
Sample_ID	Location	Grain	Type	Analysis#	SiO2	TiO2	Al2O3	Cr2O3	FeO	MnO	MgO	CaO	NiO	Na2O	K2O	Total	Si	Ti	Al	Cr	Fe	Mn	Mg	Ca	Ni	Na	K	Total	Mg#
TG11-049	Tongo - Pandebu	Ol	Core	1	41,34	0,03	0	0,02	7,98	0,1	49,63	0,02	0,41	0,03	0	99,58	1,01	0,00	0,00	0,00	0,16	0,00	1,81	0,00	0,01	0,00	0,00	2,99	91,72645
TG11-049	Tongo - Pandebu	Ol	Core	2	41,26	0,04	0,02	0,03	7,68	0,09	49,76	0,03	0,43	0,03	0	99,37	1,01	0,00	0,00	0,00	0,16	0,00	1,81	0,00	0,01	0,00	0,00	2,99	92,03185
TG11-049	Tongo - Pandebu	Ol	Core	3	41,92	0	0,02	0,04	5,19	0,06	51,79	0,02	0,34	0,04	0,01	99,44	1,01	0,00	0,00	0,00	0,10	0,00	1,86	0,00	0,01	0,00	0,00	2,99	94,6776
TG11-049	Tongo - Pandebu	Ol	Core	4	41,58	0,02	0,01	0,03	6,63	0,08	51,4	0,01	0,4	0,02	0,01	100,18	1,00	0,00	0,00	0,00	0,13	0,00	1,85	0,00	0,01	0,00	0,00	3,00	93,2524
TG11-049	Tongo - Pandebu	Ol	Core	5	41,19	0,01	0,01	0,02	7,04	0,08	50,45	0,02	0,35	0,03	0,01	99,19	1,00	0,00	0,00	0,00	0,14	0,00	1,84	0,00	0,01	0,00	0,00	3,00	92,7403
TG11-049	Tongo - Pandebu	Ol	Core	6	41,01	0,01	0,04	0,08	9,27	0,09	49,18	0,07	0,38	0,04	0,01	100,19	1,00	0,00	0,00	0,00	0,19	0,00	1,79	0,00	0,01	0,00	0,00	3,00	90,43736
TG11-049	Tongo - Pandebu	Ol	Core	7	41,35	0,03	0,01	0,03	6,91	0,09	50,53	0,01	0,41	0,04	0,01	99,41	1,01	0,00	0,00	0,00	0,14	0,00	1,83	0,00	0,01	0,00	0,00	2,99	92,87528
TG11-049	Tongo - Pandebu	Ol	Core	8	41,76	0	0,01	0,02	6,05	0,08	51,19	0,01	0,42	0,02	0,02	99,56	1,01	0,00	0,00	0,00	0,12	0,00	1,85	0,00	0,01	0,00	0,00	2,99	93,7823
TG11-049	Tongo - Pandebu	Ol	Core	9	41,85	0,02	0,02	0,04	5,54	0,07	51,83	0,02	0,39	0,02	0,02	99,81	1,01	0,00	0,00	0,00	0,11	0,00	1,86	0,00	0,01	0,00	0,00	2,99	94,34311
TG11-049	Tongo - Pandebu	Ol	Core	10	41,37	0	0,02	0,01	7,38	0,09	50,04	0,04	0,39	0,02	0,01	99,38	1,01	0,00	0,00	0,00	0,15	0,00	1,82	0,00	0,01	0,00	0,00	2,99	92,35889
TG11-049	Tongo - Pandebu	Ol	Core	11	41,58	0,07	0	0,04	7,5	0,11	50,01	0,01	0,35	0,03	0,02	99,73	1,01	0,00	0,00	0,00	0,15	0,00	1,81	0,00	0,01	0,00	0,00	2,99	92,23999
TG11-049	Tongo - Pandebu	Ol	Core	12	41,67	0,02	0,01	0,02	6,33	0,09	51,08	0,03	0,33	0,03	0,02	99,62	1,01	0,00	0,00	0,00	0,13	0,00	1,84	0,00	0,01	0,00	0,00	2,99	93,50014
TG11-049	Tongo - Pandebu	Ol	Core	13	41,57	0,04	0,01	0,02	7,37	0,1	50,26	0,01	0,4	0,02	0,01	99,82	1,01	0,00	0,00	0,00	0,15	0,00	1,82	0,00	0,01	0,00	0,00	2,99	92,39932
TG11-049	Tongo - Pandebu	Ol	Core	14	41,67	0,01	0,01	0,04	6,17	0,07	51,39	0,01	0,39	0,03	0,01	99,81	1,01	0,00	0,00	0,00	0,12	0,00	1,85	0,00	0,01	0,00	0,00	2,99	93,68988
TG11-049	Tongo - Pandebu	Ol	Core	15	41,52	0,03	0,02	0,02	6,83	0,07	50,39	0,01	0,41	0,04	0,01	99,35	1,01	0,00	0,00	0,00	0,14	0,00	1,83	0,00	0,01	0,00	0,00	2,99	92,93376

SOM Table. Pandebu olivine rim EPMA analyses

					Oxide wt%												Cations												
Sample_ID	Location	Grain	Type	Analysis#	SiO2	TiO2	Al2O3	Cr2O3	FeO	MnO	MgO	CaO	NiO	Na2O	K2O	Total	Si	Ti	Al	Cr	Fe	Mn	Mg	Ca	Ni	Na	K	Total	Mg#
TG11-049	Tongo - Pandebu	Ol	Rim	1 (Line) Pt 1	40,66	0,04	0	0,07	9,52	0,11	48,69	0,04	0,35	0,03	0	99,52	1,00	0,00	0,00	0,00	0,20	0,00	1,79	0,00	0,01	0,00	0,00	3,00	90,1159
TG11-049	Tongo - Pandebu	Ol	Rim	1 (Line) Pt 2	40,68	0,04	0,01	0,06	10,24	0,13	47,97	0,05	0,35	0,02	0,01	99,55	1,00	0,00	0,00	0,00	0,21	0,00	1,77	0,00	0,01	0,00	0,00	3,00	89,30579
TG11-049	Tongo - Pandebu	Ol	Rim	1 (Line) Pt 3	40,73	0,01	0,01	0,05	9,67	0,14	48,35	0,05	0,39	0,04	0,01	99,44	1,00	0,00	0,00	0,00	0,20	0,00	1,78	0,00	0,01	0,00	0,00	3,00	89,91239
TG11-049	Tongo - Pandebu	Ol	Rim	1 (Line) Pt 4	40,27	0,04	0,01	0,06	9,13	0,17	49,82	0,12	0,21	0,02	0,02	99,87	0,99	0,00	0,00	0,00	0,19	0,00	1,82	0,00	0,00	0,00	0,00	3,01	90,67803
TG11-049	Tongo - Pandebu	Ol	Rim	2 (Line) Pt 4	41,12	0,07	0,02	0,06	10,4	0,15	47,05	0,05	0,33	0,02	0,01	99,29	1,02	0,00	0,00	0,00	0,22	0,00	1,73	0,00	0,01	0,00	0,00	2,98	88,96818
TG11-049	Tongo - Pandebu	Ol	Rim	3 (Line) Pt 3	40,96	0,03	0,01	0,02	10,99	0,12	46,87	0,07	0,34	0,02	0,01	99,45	1,01	0,00	0,00	0,00	0,23	0,00	1,73	0,00	0,01	0,00	0,00	2,99	88,37552
TG11-049	Tongo - Pandebu	Ol	Rim	3 (Line) Pt 4	40,81	0,04	0	0,03	11,05	0,11	46,68	0,08	0,33	0,01	0,02	99,18	1,01	0,00	0,00	0,00	0,23	0,00	1,73	0,00	0,01	0,00	0,00	2,99	88,2775

b) Phlogopite EPMA data

SOM Table. Koidu Phlogopite chemistry for the Koidu and Tongo samples analysed in the current study.

					Oxide wt%														Cations												
Sample_ID	Location	Grain type	Core/ Rim	Grain#	SiO2	TiO2	Al2O3	Cr2O3	FeO	MnO	MgO	CaO	BaO	Na2O	K2O	F	Cl	Total	Si	Ti	Al	Cr	Fe	Mn	Mg	Ca	Ba	Na	K	Total	Mg#
YS770	Koidu	Phl	Core	1	39,9	3,03	12,83	0,65	5,7	0,09	22,44	0,01	0,38	0,13	9,62	0,51	0,01	95,29	5,75	0,33	2,18	0,07	0,69	0,01	4,82	0,00	0,02	0,04	1,77	15,69	87,53
YS770	Koidu	Phl	Core	2	41,49	2,91	11,83	1,26	5,18	0,04	22,47	0,04	0,06	0,17	9,9	0,46	0,03	95,86	5,92	0,31	1,99	0,14	0,62	0,00	4,78	0,01	0,00	0,05	1,80	15,62	88,55
YS770	Koidu	Phl	Core	3	42,69	0,22	12,15	0,1	6,59	0,05	23,65	0,02	0,04	0,12	10,04	0,46	0,05	96,17	6,07	0,02	2,04	0,01	0,78	0,01	5,01	0,00	0,00	0,03	1,82	15,81	86,48
YS770	Koidu	Phl	Core	4	42,4	0,21	11,54	0,01	6,33	0,06	24,13	0,03	0,07	0,11	10,12	0,61	0,04	95,65	6,08	0,02	1,95	0,00	0,76	0,01	5,16	0,00	0,00	0,03	1,85	15,86	87,17
YS770	Koidu	Phl	Core	5	40,95	3,09	12,14	0,99	5,42	0,04	22,32	0,04	0,12	0,18	9,88	0,53	0,01	95,71	5,87	0,33	2,05	0,11	0,65	0,00	4,77	0,01	0,01	0,05	1,81	15,65	88,01
YS770	Koidu	Phl	Rim	1	41,66	0,65	0,25	0,09	14,9	0,13	23,98	0,04	0,07	0,17	9,49	0,71	0,01	92,14	6,57	0,08	0,05	0,01	1,97	0,02	5,64	0,01	0,00	0,05	1,91	16,30	74,15
YS770	Koidu	Phl	Rim	2	41,72	0,96	0,38	0,07	15,82	0,16	23,8	0,14	0,03	0,16	9,74	0,75	0,01	93,72	6,51	0,11	0,07	0,01	2,06	0,02	5,54	0,02	0,00	0,05	1,94	16,33	72,84
YS770	Koidu	Phl	Rim	3	40,14	0,63	0,15	0	17,44	0,14	24,3	0,12	0,02	0,12	8,18	0,48	0,01	91,72	6,40	0,08	0,03	0,00	2,33	0,02	5,78	0,02	0,00	0,04	1,66	16,36	71,30
YS770	Koidu	Phl	Rim	4	41,55	0,59	0,18	0,05	16,49	0,1	23,97	0,04	0,02	0,1	9,33	0,71	0	93,15	6,53	0,07	0,03	0,01	2,17	0,01	5,61	0,01	0,00	0,03	1,87	16,33	72,15
YS770	Koidu	Phl	Rim	5	40,06	0,44	0,11	0	18,21	0,18	23,96	0,06	0,01	0,12	8,59	0,58	0	92,33	6,40	0,05	0,02	0,00	2,43	0,02	5,70	0,01	0,00	0,04	1,75	16,43	70,11
YS774	Koidu	Phl	Core	1	36,53	2,52	13,17	0,02	11,19	0,09	17,81	0,06	0,23	0,38	9,28	0,36	0,01	91,66	5,64	0,29	2,39	0,00	1,44	0,01	4,10	0,01	0,01	0,11	1,83	15,84	73,94
YS774	Koidu	Phl	Core	2	39,32	2,7	12,7	1,14	4,63	0,01	22,04	0,04	0,19	0,34	9,71	0,43	0,04	93,3	5,77	0,30	2,20	0,13	0,57	0,00	4,82	0,01	0,01	0,10	1,82	15,72	89,46
YS774	Koidu	Phl	Core	3	36,68	2,33	14,97	0,06	5,81	0,1	21,73	0,08	1,34	0,27	9,5	0,32	0,01	93,22	5,46	0,26	2,63	0,01	0,72	0,01	4,83	0,01	0,08	0,08	1,81	15,90	86,96
YS774	Koidu	Phl	Core	4	40,06	1,91	12,51	1	4,27	0,02	22,67	0,04	0,08	0,31	9,79	0,33	0,06	93,06	5,86	0,21	2,16	0,12	0,52	0,00	4,95	0,01	0,00	0,09	1,83	15,75	90,44
YS774	Koidu	Phl	Core	5	36,66	2,14	12,31	0,07	5,85	0,1	22,38	0,36	0,7	0,25	8,69	0,45	0,03	89,99	5,63	0,25	2,23	0,01	0,75	0,01	5,13	0,06	0,04	0,07	1,70	15,89	87,21
YS774	Koidu	Phl	Core	6	38,96	3,17	12,07	1,39	4,74	0,04	21,81	0,06	0,1	0,35	9,69	0,42	0,04	92,84	5,76	0,35	2,10	0,16	0,59	0,01	4,81	0,01	0,01	0,10	1,83	15,72	89,13
YS774	Koidu	Phl	Core	7	40,23	2,12	7,45	0	10,01	0,08	22,07	0,06	0,09	0,49	9,44	0,47	0	92,51	6,11	0,24	1,33	0,00	1,27	0,01	5,00	0,01	0,01	0,14	1,83	15,96	79,72
YS774	Koidu	Phl	Core	8	38,85	4,25	8,27	0,02	11,48	0,08	19,17	0,18	0,3	0,56	9	0,28	0,02	92,46	5,95	0,49	1,49	0,00	1,47	0,01	4,38	0,03	0,02	0,17	1,76	15,77	74,85
YS774	Koidu	Phl	Core	9	39,54	2,92	12,57	1,57	4,59	0,02	21,68	0,03	0,08	0,37	9,78	0,34	0,03	93,53	5,78	0,32	2,17	0,18	0,56	0,00	4,73	0,00	0,00	0,10	1,83	15,68	89,38
YS774	Koidu	Phl	Core	10	36,28	3,61	15,13	0,06	6,88	0,04	19,89	0,04	1,06	0,39	9,51	0,29	0,02	93,2	5,42	0,41	2,67	0,01	0,86	0,01	4,43	0,01	0,06	0,11	1,81	15,80	83,75
YS774	Koidu	Phl	Rim	1	36,18	1,74	13,78	0	12,23	0,08	17,18	0,11	0,2	0,4	9,37	0,33	0	91,61	5,61	0,20	2,52	0,00	1,59	0,01	3,97	0,02	0,01	0,12	1,85	15,91	71,46
YS774	Koidu	Phl	Rim	3	37	3,7	15,07	0,12	5,71	0,05	21,35	0,12	1,26	0,31	9,44	0,35	0,01	94,5	5,43	0,41	2,61	0,01	0,70	0,01	4,67	0,02	0,07	0,09	1,77	15,78	86,95
YS774	Koidu	Phl	Rim	6	38,14	3,05	14,15	0,65	5,11	0,07	21,67	0,04	0,57	0,28	9,65	0,34	0,01	93,76	5,59	0,34	2,45	0,08	0,63	0,01	4,74	0,01	0,03	0,08	1,81	15,75	88,32
YS774	Koidu	Phl	Rim	8	37,83	2,17	12,71	0,01	7,02	0,09	21,58	0,57	0,58	0,3	9,22	0,37	0,02	92,46	5,68	0,25	2,25	0,00	0,88	0,01	4,83	0,09	0,03	0,09	1,77	15,88	84,57
YS774	Koidu	Phl	Rim	10	36,9	4,04	15,22	0,09	7,04	0,07	20,08	0,05	1,04	0,35	9,19	0,4	0	94,47	5,43	0,45	2,64	0,01	0,87	0,01	4,41	0,01	0,06	0,10	1,73	15,71	83,56
YS774	Koidu	Phl	Rim	11	37,34	3,33	11,08	0,07	8,44	0,08	20,69	0,2	0,71	0,18	9,48	0,42	0	92,02	5,70	0,38	1,99	0,01	1,08	0,01	4,71	0,03	0,04	0,05	1,85	15,86	81,38

SOM Table. Tongo Phlogopite chemistry for the Koidu and Tongo samples analysed in the current study.

					Oxide wt%														Cations												
Sample_ID	Location	Grain type	Core/ Rim	Grain#	SiO2	TiO2	Al2O3	Cr2O3	FeO	MnO	MgO	CaO	BaO	Na2O	K2O	F	Cl	Total	Si	Ti	Al	Cr	Fe	Mn	Mg	Ca	Ba	Na	K	Total	Mg#
TG11-039A	Tongo - Kundu	Phl	Core	1	38,28	2,29	13,26	0,61	4,74	0,04	22,67	0,01	0,41	0,27	10,1	0,35	0	93,01	5,66	0,25	2,31	0,07	0,59	0,01	5,00	0,00	0,02	0,08	1,90	15,89	89,50
TG11-039A	Tongo - Kundu	Phl	Core	2	38,64	2,19	13,77	0,19	5,83	0,01	22,12	0,03	0,35	0,42	9,47	0,36	0,02	93,40	5,68	0,24	2,39	0,02	0,72	0,00	4,85	0,00	0,02	0,12	1,78	15,82	87,12
TG11-039A	Tongo - Kundu	Phl	Core	3	37,42	1,94	14,45	0	10,15	0,11	19,08	0,04	0,34	0,45	9,55	0,35	0,02	93,88	5,60	0,22	2,55	0,00	1,27	0,01	4,26	0,01	0,02	0,13	1,82	15,88	77,02
TG11-039A	Tongo - Kundu	Phl	Core	4	37,8	2	9,21	0,07	8,07	0,15	24,44	1,38	0,13	0,33	7,09	0,53	0,03	91,24	5,75	0,23	1,65	0,01	1,03	0,02	5,54	0,22	0,01	0,10	1,38	15,93	84,37
TG11-039A	Tongo - Kundu	Phl	Core	5	38,45	2,42	13,22	0,56	4,95	0,04	23,17	0,1	0,35	0,22	9,7	0,43	0,01	93,62	5,64	0,27	2,29	0,06	0,61	0,00	5,07	0,02	0,02	0,06	1,82	15,85	89,30
TG11-039A	Tongo - Kundu	Phl	Core	6	38,58	2,07	11,65	0,1	6,92	0,05	23,35	0,24	0,27	0,32	8,52	0,43	0,02	92,53	5,74	0,23	2,04	0,01	0,86	0,01	5,18	0,04	0,02	0,09	1,62	15,85	85,74
TG11-039A	Tongo - Kundu	Phl	Core	7	37,63	2,46	13,61	0,51	4,85	0,05	22,3	0,03	0,34	0,27	9,73	0,28	0,01	92,06	5,61	0,28	2,39	0,06	0,60	0,01	4,96	0,00	0,02	0,08	1,85	15,85	89,13
TG11-039A	Tongo - Kundu	Phl	Core	8	38,22	1,48	13,73	0,11	6,86	0,08	22,49	0,03	0,4	1	8,15	0,34	0,03	92,92	5,65	0,16	2,39	0,01	0,85	0,01	4,96	0,00	0,02	0,29	1,54	15,89	85,39
TG11-039A	Tongo - Kundu	Phl	Core	10	37,85	1,83	11,23	0,07	6,34	0	25,79	0,12	0,41	0,18	7,52	0,44	0,04	91,81	5,65	0,21	1,98	0,01	0,79	0,00	5,74	0,02	0,02	0,05	1,43	15,89	87,88
TG11-039A	Tongo - Kundu	Phl	Rim	3	38,4	2,11	14,13	0,01	6,08	0,06	21,48	0,63	0,34	0,33	9,03	0,51	0,01	93,11	5,67	0,23	2,46	0,00	0,75	0,01	4,73	0,10	0,02	0,09	1,70	15,76	86,30
TG11-039A	Tongo - Kundu	Phl	Rim	6	38,91	1,61	13,98	0	5,58	0,04	23,65	0,14	0,77	0,21	9,65	0,42	0,02	94,97	5,64	0,18	2,39	0,00	0,68	0,00	5,11	0,02	0,04	0,06	1,78	15,91	88,31
TG11-039A	Tongo - Kundu	Phl	Rim	9	39,34	2,57	13,73	0,06	7,67	0,11	20,86	0,08	0,27	0,34	9,64	0,41	0,01	95,07	5,73	0,28	2,35	0,01	0,93	0,01	4,53	0,01	0,02	0,10	1,79	15,75	82,90
TG11-039A	Tongo - Kundu	Phl	Rim	10	37,85	2,32	14,38	0,29	5,26	0,07	22,19	0,05	0,56	0,21	9,91	0,32	0,01	93,42	5,58	0,26	2,50	0,03	0,65	0,01	4,87	0,01	0,03	0,06	1,86	15,86	88,26
TG12-176	Tongo - Lando	Phl	Rim	1	39,45	0,05	0,42	0	15,23	0,19	26,52	0,02	0,3	0,15	8,76	0,46	0,03	91,58	6,29	0,01	0,08	0,00	2,03	0,03	6,30	0,00	0,02	0,05	1,78	16,58	75,63
TG12-176	Tongo - Lando	Phl	Rim	2	40,4	0,07	0,36	0	14,45	0,18	25,75	0,04	0,46	0,11	9,65	0,47	0,01	91,98	6,41	0,01	0,07	0,00	1,92	0,02	6,09	0,01	0,03	0,03	1,95	16,54	76,06
TG12-176	Tongo - Lando	Phl	Rim	3	40,48	0,1	0,42	0,05	15,23	0,31	25,94	0,11	0,21	0,12	9,26	0,58	0	92,80	6,37	0,01	0,08	0,01	2,00	0,04	6,08	0,02	0,01	0,04	1,86	16,52	75,22
TG12-176	Tongo - Lando	Phl	Rim	4	40,5	0,1	0,52	0,01	14,71	0,28	25,46	0,03	0,33	0,14	9,87	0,8	0,01	92,74	6,40	0,01	0,10	0,00	1,94	0,04	6,00	0,01	0,02	0,04	1,99	16,55	75,52
TG12-176	Tongo - Lando	Phl	Rim	5	40,24	0,07	0,48	0,04	14,89	0,28	25,49	0,15	0,35	0,14	9,8	0,57	0	92,49	6,38	0,01	0,09	0,01	1,97	0,04	6,02	0,03	0,02	0,04	1,98	16,58	75,32
TG12-176	Tongo - Lando	Phl	Rim	6	40,16	0,03	0,76	0,02	15,91	0,25	25,12	0,23	0,29	0,11	9,9	0,61	0	93,38	6,33	0,00	0,14	0,00	2,10	0,03	5,91	0,04	0,02	0,03	1,99	16,60	73,78
TG12-176	Tongo - Lando	Phl	Rim	7	40,6	0,11	0,99	0	15,32	0,23	25,07	0,21	0,14	0,14	9,8	0,54	0,02	93,18	6,37	0,01	0,18	0,00	2,01	0,03	5,87	0,04	0,01	0,04	1,96	16,53	74,47
TG12-176	Tongo - Lando	Phl	Rim	9	40,47	0,08	0,9	0,03	15,21	0,22	25,7	0,23	0,24	0,12	9,61	0,64	0	93,46	6,34	0,01	0,17	0,00	1,99	0,03	6,00	0,04	0,01	0,04	1,92	16,55	75,07
TG12-176	Tongo - Lando	Phl	Rim	10	39,71	0,08	0,96	0,06	15,82	0,27	25,01	0,15	0,17	0,12	9,71	0,57	0,01	92,64	6,30	0,01	0,18	0,01	2,10	0,04	5,92	0,03	0,01	0,04	1,97	16,59	73,81
TG12-176	Tongo - Lando	Phl	Core	1	37,87	2,91	13,27	0,41	5,78	0,02	21,85	0,04	0,49	0,37	9,77	0,24	0,02	93,04	5,62	0,32	2,32	0,05	0,72	0,00	4,83	0,01	0,03	0,11	1,85	15,85	87,08
TG12-176	Tongo - Lando	Phl	Core	2	37,33	3,22	14,91	0,26	6,17	0,05	21,32	0,06	0,69	0,29	9,8	0,27	0,01	94,36	5,47	0,36	2,58	0,03	0,76	0,01	4,66	0,01	0,04	0,08	1,83	15,82	86,03
TG12-176	Tongo - Lando	Phl	Core	3	38,46	2,68	13,46	0,21	6,29	0,08	21,81	0,09	0,46	0,38	9,64	0,33	0,02	93,90	5,65	0,30	2,33	0,02	0,77	0,01	4,78	0,01	0,03	0,11	1,81	15,83	86,07
TG12-176	Tongo - Lando	Phl	Core	4	38,47	2,58	13,1	0,61	5,7	0,1	22,27	0,04	0,42	0,24	9,87	0,34	0,01	93,75	5,66	0,29	2,27	0,07	0,70	0,01	4,89	0,01	0,02	0,07	1,85	15,84	87,44
TG12-176	Tongo - Lando	Phl	Core	5	38,55	2,8	13,52	0,68	5,42	0,03	22,37	0	0,38	0,34	9,69	0,33	0	94,10	5,63	0,31	2,33	0,08	0,66	0,00	4,87	0,00	0,02	0,10	1,81	15,81	88,03
TG12-176	Tongo - Lando	Phl	Core	6	38,24	2,85	13,2	0,28	6,24	0,05	22,4	0,07	0,43	0,26	9,73	0,27	0,03	94,05	5,62	0,31	2,28	0,03	0,77	0,01	4,90	0,01	0,02	0,07	1,82	15,86	86,48
TG12-176	Tongo - Lando	Phl	Core	7	38,41	2,89	13,41	0,33	6,08	0,04	22,19	0,05	0,54	0,37	9,76	0,27	0,03	94,36	5,62	0,32	2,31	0,04	0,74	0,00	4,84	0,01	0,03	0,10	1,82	15,85	86,68
TG12-176	Tongo - Lando	Phl	Core	8	38,09	2,81	14,13	0,44	5,4	0,04	21,8	0,08	0,56	0,36	9,68	0,34	0,02	93,74	5,59	0,31	2,45	0,05	0,66	0,00	4,77	0,01	0,03	0,10	1,81	15,80	87,80
TG12-176	Tongo - Lando	Phl	Core	9	38,18	2,78	13,71	0,71	5,07	0,02	22,46	0,22	0,45	0,35	9,67	0,35	0,01	93,98	5,59	0,31	2,37	0,08	0,62	0,00	4,90	0,03	0,03	0,10	1,81	15,83	88,76
TG12-176	Tongo - Lando	Phl	Core	10	38,83	2,8	13,23	0,67	5,28	0,04	22,36	0,09	0,34	0,31	9,99	0,35	0,01	94,30	5,67	0,31	2,28	0,08	0,64	0,00	4,86	0,01	0,02	0,09	1,86	15,82	88,30
TG12-190	Tongo - Lando	Phl	Rim	1	38,13	2,77	14,85	0,02	5,16	0,05	22,92	0,02	0,9	0,25	9,85	0,42	0,01	95,36	5,51	0,30	2,53	0,00	0,62	0,01	4,94	0,00	0,05	0,07	1,82	15,86	88,79
TG12-190	Tongo - Lando	Phl	Rim	2	39,2	2,61	14,19	0,52	5,06	0,08	22,83	0,04	0,55	0,18	9,87	0,34	0	95,48	5,63	0,28	2,40	0,06	0,61	0,01	4,89	0,01	0,03	0,05	1,81	15,78	88,94
TG12-190	Tongo - Lando	Phl	Rim	3	39,6	1,48	13,63	0,01	6,02	0,08	23,6	0,1	0,86	0,22	9,71	0,36	0,01	95,66	5,71	0,16	2,31	0,00	0,73	0,01	5,07	0,02	0,05	0,06	1,78	15,90	87,48
TG12-190	Tongo - Lando	Phl	Rim	4	37,8	2,38	15,09	0	5,17	0,08	22,62	0,06	1,33	0,21	9,78	0,34	0,01	94,86	5,51	0,26	2,59	0,00	0,63	0,01	4,91	0,01	0,08	0,06	1,82	15,87	88,64
TG12-190	Tongo - Lando	Phl	Rim	5	39,76	2,81	13,39	0,06	6,35	0,05	22,52	0,04	0,39	0,35	9,73	0,38	0,01	95,85	5,71	0,30	2,27	0,01	0,76	0,01	4,82	0,01	0,02	0,10	1,78	15,79	86,34
TG12-190	Tongo - Lando	Phl	Rim	6	39,94	1,29	11,44	0	7,22	0,05	23,45	0,02	0,49	0,21	9,93	0,46	0,01	94,50	5,86	0,14	1,98	0,00	0,89	0,01	5,13	0,00	0,03	0,06	1,86	15,96	85,27
TG12-190	Tongo - Lando	Phl	Rim	7	39,04	2,67	14,06	0,57	4,67	0,04	22,8	0,03	0,63	0,29	9,97	0,37	0,01	95,15	5,63	0,29	2,39	0,07	0,56	0,00	4,90	0,00	0,04	0,08	1,84	15,81	89,69
TG12-190	Tongo - Lando	Phl	Rim	8	38,08	1,65	13,76	0	5,76	0,05	22,36	0,08	1,01	0,15	9,89	0,32	0,02	93,13	5,66	0,18	2,41	0,00	0,72	0,01	4,95	0,01	0,06	0,04	1,87	15,91	87,37
TG12-190	Tongo - Lando	Phl	Rim	9	38,57	1,9	14,91	0,01	5,28	0,09	23,14	0,12	1,32	0,12	9,57	0,29	0,01	95,33	5,57	0,21	2,54	0,00	0,64	0,01	4,99	0,02	0,07	0,03	1,76	15,85	88,65
TG12-190	Tongo - Lando	Phl	Rim	10	38,07	1,97	13,79	0,04	5,81	0,07	22,59	0,03	1,07	0,13	9,57	0,32	0,01	93,46	5,63	0,22	2,40	0,00	0,72	0,01	4,98	0,00	0,06	0,04	1,80	15,87	87,39
TG12-190	Tongo - Lando	Phl	Core	1	39,37	2,14	12,57	0,18	6,05	0,03	22,65	0,02	0,38	0,35	9,85	0,36	0	93,94	5,77	0,24	2,17	0,02	0,74	0,00	4,95	0,00	0,02	0,10	1,84	15,86	86,97
TG12-190	Tongo - Lando	Phl	Core	3	37,23	2,13	17,32	0,04	6,56	0,01	20,19	0,04	0,6	0,79	9,18	0,2	0,02	94,30	5,43	0,23	2,98	0,00	0,80	0,00	4,39	0,01	0,03	0,22	1,71	15,81	84,58
TG12-190	Tongo - Lando	Phl	Core	4	41,84	0,37	11,85	0,22	4,35	0,06	24,45	0,01	0,02	0,22	10,31	0,31	0,08	94,07	6,04	0,04	2,02	0,03	0,53	0,01	5,26	0,00	0,00	0,06	1,90	15,88	90,93
TG12-190	Tongo - Lando	Phl	Core	5	38,06	3,81	13,75	0,03	10,74	0,09	17,71	0,02	0,4	0,63	9,27	0,3	0,02	94,81	5,64	0,42	2,40	0,00	1,33	0,01	3,91	0,00	0,02	0,18	1,75	15,69	74,62
TG12-190	Tongo - Lando	Phl	Core	6	38,1	2,44	14,39	0,09	5,79	0	21,48	0,06	0,44	0,31	9,74	0,42	0,01	93,28	5,62	0,27	2,50	0,01	0,71	0,00	4,73	0,01	0,03	0,09	1,83	15,81	86,86
TG12-190	Tongo - Lando	Phl	Core	7	37,77	2,76	14,97	0,12	5,44	0,03	21,51	0,02	0,69	0,36	9,57	0,3	0,03	93,57	5,55	0,31	2,59	0,01	0,67	0,00	4,71	0,00	0,04	0,10	1,79	15,79	87,58
TG12-190	Tongo - Lando	Phl	Core	8	38,01	2,13	14,17	0,1	5,36	0,03	21,78	0,06	0,41	0,28	9,96	0,37	0	92,66	5,64	0,24	2,48	0,01	0,67	0,00	4,82	0,01	0,02	0,08	1,89	15,86	87,87
TG12-190	Tongo - Lando	Phl	Core	9	38,23	2,43	13,8	0,67	4,6	0	22,73	0	0,49	0,18	10,03	0,3	0,01	93,47	5,61	0,27	2,39	0,08	0,56	0,00	4,98	0,00	0,03	0,05	1,88	15,85	89,80
TG12-190	Tongo - Lando	Phl	Core	10	39,23	2,09	13,15	0,11	6,71	0,08	21,91	0,01	0,31	0,51	9,58	0,26	0,03	93,99	5,75	0,23	2,27	0,01	0,82	0,01	4,79	0,00	0,02	0,14	1,79	15,84	85,34

c) Spinel EPMA data

SOM Table. Spinel chemistry for the Koidu and Tongo samples analysed in the current study.

					Oxide wt%												Cations												
Sample_ID	Location	Grain	Core/ Rim	Analysis#	SiO2	TiO2	Al2O3	Cr2O3	Fe2O3	FeO	MnO	MgO	CaO	NiO	Na2O	K2O	Total	Si	Ti	Al	Cr	Fe3+	Fe	Mn	Mg	Ca	Ni	Na	K	Total
Y5770	Koidu	Spl	Core	1	0,06	8,77	2,43	32,26	17,81	22,15	0,75	9,63	0,53	0,08	0,01	0,00	94,48	0,00	0,24	0,10	0,93	0,49	0,67	0,02	0,52	0,02	0,00	0,00	0,00	3,00
Y5770	Koidu	Spl	Core	2	0,07	19,46	1,70	1,64	30,55	33,15	0,84	9,10	0,34	0,09	0,01	0,02	96,97	0,00	0,53	0,07	0,05	0,83	1,00	0,03	0,49	0,01	0,00	0,00	0,00	3,00
Y5770	Koidu	Spl	Core	3	0,06	18,79	1,75	4,52	30,40	31,91	0,85	9,75	0,36	0,13	0,03	0,02	98,57	0,00	0,50	0,07	0,13	0,81	0,94	0,03	0,51	0,01	0,00	0,00	0,00	3,00
Y5770	Koidu	Spl	Core	4	0,06	18,89	1,85	5,38	28,69	31,67	0,78	10,00	0,29	0,12	0,01	0,01	97,75	0,00	0,50	0,08	0,15	0,76	0,94	0,02	0,53	0,01	0,00	0,00	0,00	3,00
Y5770	Koidu	Spl	Core	5	0,04	20,75	1,75	1,62	28,78	32,76	0,74	10,15	0,27	0,15	0,04	0,01	97,05	0,00	0,56	0,07	0,05	0,77	0,97	0,02	0,54	0,01	0,00	0,00	0,00	3,00
Y5770	Koidu	Spl	Core	6	0,05	20,31	1,75	1,99	29,15	32,94	0,77	9,93	0,14	0,11	0,04	0,00	97,18	0,00	0,54	0,07	0,06	0,78	0,98	0,02	0,53	0,01	0,00	0,00	0,00	3,00
Y5770	Koidu	Spl	Core	7	0,05	18,44	1,73	0,87	33,97	31,75	0,75	9,63	0,08	0,09	0,05	0,01	97,42	0,00	0,50	0,07	0,02	0,91	0,95	0,02	0,51	0,00	0,00	0,00	0,00	3,00
Y5770	Koidu	Spl	Core	8	0,06	18,54	1,74	0,55	34,09	32,15	0,73	9,45	0,31	0,09	0,01	0,01	97,73	0,00	0,50	0,07	0,02	0,91	0,96	0,02	0,50	0,01	0,00	0,00	0,00	3,00
Y5770	Koidu	Spl	Core	9	0,05	5,59	3,41	46,97	9,95	21,34	0,41	9,43	0,32	0,17	0,00	0,03	97,68	0,00	0,15	0,14	1,30	0,26	0,63	0,01	0,49	0,01	0,00	0,00	0,00	3,00
Y5770	Koidu	Spl	Core	10	0,07	5,89	2,70	47,21	9,77	21,57	0,42	9,54	0,11	0,14	0,01	0,01	97,44	0,00	0,16	0,11	1,31	0,26	0,63	0,01	0,50	0,00	0,00	0,00	0,00	3,00
Y5770	Koidu	Spl	Rim	1	0,05	14,00	1,67	0,23	42,70	29,53	0,89	7,95	0,75	0,08	0,02	0,01	97,88	0,00	0,38	0,07	0,01	1,16	0,89	0,03	0,43	0,03	0,00	0,00	0,00	3,00
Y5770	Koidu	Spl	Rim	2	0,47	16,56	1,74	0,99	35,31	32,39	0,86	8,00	0,46	0,13	0,03	0,02	96,96	0,02	0,45	0,07	0,03	0,96	0,98	0,03	0,43	0,02	0,00	0,00	0,00	3,00
Y5770	Koidu	Spl	Rim	3	0,05	8,38	0,69	0,53	53,55	20,07	0,90	8,07	3,34	0,09	0,03	0,03	95,74	0,00	0,23	0,03	0,02	1,49	0,62	0,03	0,44	0,13	0,00	0,00	0,00	3,00
Y5770	Koidu	Spl	Rim	4	0,05	17,40	1,78	0,89	35,14	32,05	0,81	8,67	0,35	0,09	0,00	0,01	97,24	0,00	0,47	0,08	0,03	0,95	0,97	0,02	0,47	0,01	0,00	0,00	0,00	3,00
Y5770	Koidu	Spl	Rim	5	0,06	12,63	2,34	0,11	44,03	29,14	0,65	7,82	0,37	0,06	0,01	0,01	97,23	0,00	0,34	0,10	0,00	1,20	0,89	0,02	0,42	0,01	0,00	0,00	0,00	3,00
Y5770	Koidu	Spl	Rim	6	0,06	9,55	2,65	0,17	49,30	28,16	0,63	6,85	0,30	0,05	0,00	0,00	97,72	0,00	0,26	0,11	0,00	1,35	0,86	0,02	0,37	0,01	0,00	0,00	0,00	3,00
Y5770	Koidu	Spl	Rim	7	0,07	16,91	1,89	0,26	36,89	31,46	0,73	9,02	0,10	0,09	0,01	0,02	97,46	0,00	0,46	0,08	0,01	1,00	0,94	0,02	0,48	0,00	0,00	0,00	0,00	3,00
Y5770	Koidu	Spl	Rim	8	0,05	14,25	2,01	0,13	41,79	29,76	0,69	8,25	0,55	0,02	0,01	0,02	97,54	0,00	0,39	0,09	0,00	1,14	0,90	0,02	0,44	0,02	0,00	0,00	0,00	3,00
Y5770	Koidu	Spl	Rim	9	0,08	18,45	1,72	1,31	32,86	32,27	0,84	8,98	0,40	0,10	0,03	0,02	97,06	0,00	0,50	0,07	0,04	0,89	0,97	0,03	0,48	0,02	0,00	0,00	0,00	3,00
Y5770	Koidu	Spl	Rim	10	0,10	18,15	1,72	2,41	31,61	31,61	1,08	8,94	0,31	0,07	0,04	0,03	96,07	0,00	0,50	0,07	0,07	0,86	0,96	0,03	0,48	0,01	0,00	0,00	0,00	3,00
TG12-189	Tongo - Lando	Spl	Core	1	0,17	16,05	2,85	7,73	31,60	27,26	0,83	10,85	0,55	0,13	0,10	0,08	98,20	0,01	0,42	0,12	0,21	0,83	0,79	0,02	0,56	0,02	0,00	0,01	0,00	3,00
TG12-189	Tongo - Lando	Spl	Core	3	0,06	19,22	2,94	0,28	33,22	28,83	0,71	11,84	0,54	0,09	0,06	0,02	97,81	0,00	0,50	0,12	0,01	0,87	0,84	0,02	0,61	0,02	0,00	0,00	0,00	3,00
TG12-189	Tongo - Lando	Spl	Core	4	0,05	15,01	2,68	0,14	40,39	29,79	0,81	8,87	0,34	0,04	0,04	0,03	98,19	0,00	0,40	0,11	0,00	1,08	0,89	0,02	0,47	0,01	0,00	0,00	0,00	3,00
TG12-189	Tongo - Lando	Spl	Core	5	0,06	17,26	2,40	0,39	36,69	29,98	0,54	10,30	0,26	0,08	0,04	0,01	98,02	0,00	0,46	0,10	0,01	0,97	0,88	0,02	0,54	0,01	0,00	0,00	0,00	3,00
TG12-189	Tongo - Lando	Spl	Core	7	0,13	11,55	2,29	0,47	47,50	26,02	0,78	8,97	0,69	0,11	0,06	0,04	98,61	0,00	0,31	0,10	0,01	1,27	0,77	0,02	0,48	0,03	0,00	0,00	0,00	3,00
TG12-189	Tongo - Lando	Spl	Core	8	0,12	9,96	1,81	0,08	50,26	24,72	0,79	8,26	1,01	0,05	0,04	0,08	97,18	0,00	0,27	0,08	0,00	1,37	0,75	0,02	0,45	0,04	0,00	0,00	0,00	3,00
TG12-189	Tongo - Lando	Spl	Core	9	0,03	0,40	0,78	0,83	63,76	30,13	0,01	0,04	0,04	0,00	0,02	0,01	96,05	0,00	0,01	0,04	0,03	1,91	1,00	0,00	0,00	0,00	0,00	0,00	0,00	3,00
TG12-189	Tongo - Lando	Spl	Core	10	0,06	18,23	3,08	5,52	29,17	27,23	0,66	12,39	0,33	0,12	0,04	0,02	96,85	0,00	0,48	0,13	0,15	0,77	0,79	0,02	0,64	0,01	0,00	0,00	0,00	3,00
TG12-189	Tongo - Lando	Spl	Rim	2	0,13	15,66	2,47	0,34	39,55	27,20	0,74	10,66	0,49	0,09	0,04	0,07	97,44	0,00	0,42	0,10	0,01	1,05	0,80	0,02	0,56	0,02	0,00	0,00	0,00	3,00
TG12-189	Tongo - Lando	Spl	Rim	3	0,06	20,82	2,71	1,58	29,99	30,34	0,81	12,18	0,35	0,11	0,04	0,02	99,01	0,00	0,54	0,11	0,04	0,77	0,87	0,02	0,62	0,01	0,00	0,00	0,00	3,00
TG12-189	Tongo - Lando	Spl	Rim	5	0,17	6,17	1,42	0,08	57,02	14,06	0,71	6,94	8,01	0,05	0,08	0,07	94,78	0,01	0,17	0,06	0,00	1,59	0,44	0,02	0,38	0,32	0,00	0,01	0,00	3,00
TG12-189	Tongo - Lando	Spl	Rim	6	0,06	20,64	2,78	0,58	30,75	29,25	0,72	12,41	0,47	0,09	0,06	0,05	97,86	0,00	0,54	0,11	0,02	0,80	0,85	0,02	0,64	0,02	0,00	0,00	0,00	3,00
TG12-189	Tongo - Lando	Spl	Rim	7	0,08	14,38	3,46	14,62	26,42	24,76	0,58	11,85	0,26	0,14	0,04	0,03	96,62	0,00	0,38	0,14	0,40	0,70	0,72	0,02	0,62	0,01	0,00	0,00	0,00	3,00
TG12-189	Tongo - Lando	Spl	Rim	8	0,09	15,83	2,84	0,16	38,67	26,94	0,69	10,87	0,51	0,07	0,04	0,05	96,75	0,00	0,42	0,12	0,00	1,03	0,80	0,02	0,57	0,02	0,00	0,00	0,00	3,00
TG12-189	Tongo - Lando	Spl	Rim	10	0,05	13,66	3,52	18,94	23,49	24,38	0,47	11,80	0,18	0,21	0,05	0,02	96,77	0,00	0,36	0,14	0,52	0,62	0,71	0,01	0,61	0,01	0,01	0,00	0,00	3,00
TG11-049	Tongo - Pandebu	Spl	Core	1	0,09	10,82	1,25	0,08	49,43	31,01	0,61	5,98	0,13	0,09	0,03	0,03	99,55	0,00	0,30	0,05	0,00	1,35	0,94	0,02	0,32	0,01	0,00	0,00	0,00	3,00
TG11-049	Tongo - Pandebu	Spl	Core	2	0,09	14,71	1,52	0,15	40,53	32,72	0,55	6,84	0,16	0,09	0,03	0,03	97,42	0,00	0,41	0,07	0,00	1,12	1,00	0,02	0,37	0,01	0,00	0,00	0,00	3,00
TG11-049	Tongo - Pandebu	Spl	Core	3	0,07	16,40	1,47	0,19	37,46	33,47	0,60	7,31	0,14	0,13	0,02	0,03	97,28	0,00	0,45	0,06	0,01	1,03	1,02	0,02	0,40	0,01	0,00	0,00	0,00	3,00
TG11-049	Tongo - Pandebu	Spl	Core	5	0,13	18,25	2,06	0,62	30,73	36,45	0,70	6,18	0,19	0,13	0,02	0,01	95,47	0,00	0,51	0,09	0,02	0,86	1,14	0,02	0,34	0,01	0,00	0,00	0,00	3,00
TG11-049	Tongo - Pandebu	Spl	Core	6	0,09	15,09	1,39	0,08	40,79	32,11	0,56	7,49	0,14	0,08	0,05	0,04	97,91	0,00	0,41	0,06	0,00	1,11	0,97	0,02	0,41	0,01	0,00	0,00	0,00	3,00
TG11-049	Tongo - Pandebu	Spl	Rim	2	0,83	8,10	1,08	0,05	50,75	25,44	1,07	5,53	2,64	0,06	0,02	0,06	95,63	0,03	0,23	0,05	0,00	1,43	0,80	0,03	0,31	0,11	0,00	0,00	0,00	3,00
TG11-049	Tongo - Pandebu	Spl	Rim	3	0,15	9,35	1,37	0,07	50,34	29,37	0,74	5,61	0,22	0,08	0,02	0,06	97,38	0,01	0,26	0,06	0,00	1,41	0,91	0,02	0,31	0,01	0,00	0,00	0,00	3,00
TG11-049	Tongo - Pandebu	Spl	Rim	5	0,05	17,59	1,68	0,15	35,14	33,89	0,52	7,79	0,12	0,15	0,03	0,01	97,12	0,00	0,48	0,07	0,00	0,96	1,03	0,02	0,42	0,00	0,00	0,00	0,00	3,00
TG11-049	Tongo - Pandebu	Spl	Rim	6	0,04	18,42	1,52	0,10	33,91	33,65	0,61	8,31	0,16	0,09	0,02	0,03	96,86	0,00	0,50	0,07	0,00	0,93	1,02	0,02	0,45	0,01	0,00	0,00	0,00	3,00
TG11-048	Tongo - Kundu	Spl	Core	1	0,01	0,27	18,03	48,16	2,84	17,04	0,23	11,10	0,00	0,08	0,02	0,00	97,78	0,00	0,01	0,69	1,23	0,07	0,46	0,01	0,54	0,00	0,00	0,00	0,00	3,00
TG11-048	Tongo - Kundu	Spl	Core	2	0,02	15,11	0,21	0,38	37,07	42,49	0,07	0,80	0,04	0,00	0,02	0,02	96,23	0,00	0,44	0,01	0,01	1,09	1,39	0,00	0,05	0,00	0,00	0,00	0,00	3,00
TG11-048	Tongo - Kundu	Spl	Core	3	0,08	5,33	3,60	48,84	9,50	19,71	0,31	10,83	0,06	0,18	0,01	0,01	98,46	0,00	0,14	0,15	1,33	0,25	0,57	0,01	0,56	0,00	0,00	0,00	0,00	3,00
TG11-048	Tongo - Kundu	Spl	Core	4	0,06	17,79	3,23	0,20	35,56	29,41	0,54	11,10	0,25	0,12	0,05	0,01	98,32	0,00	0,47	0,13	0,01	0,93	0,86	0,02	0,58	0,01	0,00	0,00	0,00	3,00
TG11-048	Tongo - Kundu	Spl	Core	5	0,07	11,29	4,41	26,59	19,52	22,66	0,43	11,98	0,10	0,23	0,01	0,02	97,31	0,00	0,29	0,18	0,73	0,51	0,65	0,01	0,62	0,00	0,01	0,00	0,00	3,00
TG11-048	Tongo - Kundu	Spl	Core	6	0,00	0,16	37,50	22,12	6,87	19,16	0,08	11,49	0,01	0,36	0,03	0,00	97,79	0,00	0,00	1,32	0,52	0,15	0,48	0,00	0,51	0,00	0,01	0,00	0,00	3,00
TG11-048	Tongo - Kundu	Spl	Core	7	0,09	4,99	3,88	48,53	9,27	18,63	0,33	10,97	0,06	0,19	0,03	0,02	96,99	0,00	0,13	0,16	1,33	0,24	0,54	0,01	0,57	0,00	0,01	0,00	0,00	3,00
TG11-048	Tongo - Kundu	Spl	Core	8	0,84	14,14	2,89	0,15	40,37	26,37	1,22	10,83	0,33	0,07	0,04	0,02	97,28	0,03	0,37	0,12	0,00	1,07	0,78	0,04	0,57	0,01	0,00	0,00	0,00	3,00
TG11-048	Tongo - Kundu	Spl	Core	9	0,06	14,69	3,37	0,07	40,32	28,90	0,60	9,60	0,13	0,05	0,04	0,01	97,84	0,00	0,39	0,14	0,00	1,07	0,86	0,02	0,51	0,00	0,00	0,00	0,00	3,00
TG11-048	Tongo - Kundu	Spl	Core	10	0,06	15,92	3,50	5,45	32,69	27,64	0,54	11,29	0,05	0,09	0,01	0,00	97,25	0,00	0,42	0,14	0,15	0,86	0,81	0,02	0,59	0,00	0,00	0,00	0,00	3,00
TG11-048	Tongo - Kundu	Spl	Rim	1	0,05	17,21	3,35	0,23	35,90	29,15	0,62	10,84	0,12	0,07	0,05	0,02	97,61	0,00	0,45	0,14	0,01	0,95	0,86	0,02	0,57	0,00	0,00	0,00	0,00	3,00
TG11-048	Tongo - Kundu	Spl	Rim	2	0,07	12,84	3,78	0,03	42,88	27,88	0,55	9,18	0,22	0,05	0,01	0,01	97,50	0,00	0,34	0,16	0,00	1,15	0,83	0,02	0,49	0,01	0,00	0,00	0,00	3,00
TG11-048	Tongo - Kundu	Spl	Rim	3	0,08	11,47	3,50	0,26	46,24	28,16	0,67	8,23	0,26	0,04	0,05	0,01	98,97	0,00	0,31	0,15	0,01	1,23	0,83	0,02	0,43	0,01	0,00	0,00	0,00	3,00
TG11-048	Tongo - Kundu	Spl	Rim	4	0,05	10,62	3,62	0,06	47,88	25,73	0,62	8,99	0,58	0,04	0,03	0,00	98,22	0,00	0,28	0,15	0,00	1,28	0,76	0,02	0,48	0,02	0,00	0,00	0,00	3,00
TG11-048	Tongo - Kundu	Spl	Rim	5	0,08	16,20	3,27	0,22	37,95	27,61	0,65	11,27	0,11	0,06	0,03	0,02	97,47	0,00	0,43	0,14	0,01	1,00	0,81	0,02	0,59	0,00	0,00	0,00	0,00	3,00
TG11-048	Tongo - Kundu	Spl	Rim	6	0,10	15,58	3,44	0,18	39,16	27,46	0,60	11,20	0,13	0,03	0,02	0,01	97,91	0,00	0,41	0,14	0,00	1,03	0,80	0,02	0,58	0,00	0,00	0,00	0,00	3,00
TG11-048	Tongo - Kundu	Spl	Rim	7	0,06	10,03	3,74	0,19	47,24	25,86	0,61	8,54	0,09	0,06	0,03	0,03	96,47	0,00	0,27	0,16	0,01	1,29	0,78	0,02	0,46	0,00	0,00	0,00	0,00	3,00
TG11-048	Tongo - Kundu	Spl	Rim	8	0,07	11,59	3,61	0,07	45,85	25,57	0,72	9,50	0,45	0,06	0,04	0,03	97,56	0,00	0,31	0,15	0,00	1,23	0,76	0,02	0,50	0,02	0,00	0,00	0,00	3,00
TG11-048	Tongo - Kundu	Spl	Rim	9	0,06	7,05	2,39	0,12	53,70	27,35	0,71	5,71	0,15	0,08	0,03	0,01	97,36	0,00	0,20	0,10	0,00	1,50	0,85	0,02	0,32	0,01	0,00	0,00	0,00	3,00
TG11-048	Tongo - Kundu	Spl	Rim	10	0,08	14,49	3,41	0,06	41,19	25,53	0,58	9,60	2,77	0,07	0,05	0,02	97,86	0,00	0,38	0,14	0,00	1,09	0,75	0,02	0,50	0,10	0,00	0,00	0,00	3,00